Stability of X-Ray Irradiated Amorphous Selenium Based Photoconductive Films

A Thesis

Submitted to the College of Graduate and Postdoctoral Studies

In Partial Fulfillment of the Requirements for the Degree of

Master of Science

In the Division of Biomedical Engineering

University of Saskatchewan

By

Ozan Gunes

Saskatoon, Saskatchewan

PERMISSION TO USE

In presenting this thesis in partial fulfillment of the requirements for a Postgraduate degree from the University of Saskatchewan, I agree that the Libraries of this University may make it freely available for inspection. I further agree that permission for copying of this thesis in any manner, while or in part, scholarly purpose may be granted by the professor or professors who supervised my thesis work or, in their absence, by the Chair of the Department or the Dean of the College in which my thesis work was done. It is understood that due recognition shall be given to me and to the University of Saskatchewan in any scholarly use which may be made of any material in my thesis.

Request for permission to copy or to make other use of material in this thesis in whole or part should be addressed to:

College of Graduate and Postdoctoral Studies
110 Science Place
University of Saskatchewan
Saskatoon, Canada, S7N 5C9

And

Chair of the Division of Biomedical Engineering
57 Campus Drive
University of Saskatchewan
Saskatoon, Canada, S7N 5A9

ABSTRACT

Amorphous selenium (a-Se) is a photoconductive material that is used in commercial x-ray imaging flat panels. In this study, the effect of x-ray irradiation on the glass stability of aged vitreous a-Se, a-Se:0.5%As, a-Se:6%As-140 ppm Cs thin films are investigated by using differential scanning calorimetry (DSC). This technique is used to detect characteristic temperatures, such as glass transition, crystallization and melting temperatures of the material in terms of the change in the heat flow in a certain temperature scanning range. To investigate glass stability of a-Se based alloy films, fourteen different glass stability criteria are examined. Initially, the reproducibility of stability criteria is analyzed for unirradiated samples, which also provides confidence in the variation of the characteristic temperatures. The study consists of three main stages of glass stability investigation. In the first stage, the a-Se based alloy film samples are dosed with x-rays at different periods and scanned in DSC afterwards. In the second stage, x-ray irradiated samples are rested for an arbitrary period of five hours at laboratory ambient temperature of 295 K. Further, the effect of five hour-annealing on x-ray irradiated samples is analyzed at annealing temperatures of 308 K and 328 K. In the third stage, various annealing periods are inspected for equally x-ray irradiated films that are rested at 308 K and 328 K. Results show that under high x-ray irradiation, the characteristic onset temperatures of a-Se based alloy films have not shown significant instability. On the other hand, least stable case was obtained for the films rested at 328 K after irradiation. The investigation on various resting periods of equally irradiated samples showed that higher stability was achieved at 308 K. In addition, ΔT_{xg}, K_H and K_W were found to be the most useful criteria in analyzing the stability of a-Se based alloy films.

ACKNOWLEDGEMENTS

I would like to declare my deepest gratitude and respect to my supervisor, Dr. Safa O. Kasap, for his instruction, patience and leadership throughout the course of this work. I would like to present my appreciation to Dr. George Belev for preparing the samples and discussing possible experimental outcomes of the work. I would like to thank Dr. Dancho Tonchev, Dr. Cyril Koughia, Dr. Robert E. Johanson for their instruction on various instruments and technical advice. I would like to thank University of Saskatchewan, Analogic Corporation Canada and NSERC for providing financial support. I would like to thank Farley Chicilo and Junyi Yang for their scientific discussions and friendship. Certainly, I would like to thank my mother, my father and my sister who have provided me with endless support and motivation throughout the years.

TABLE OF CONTENTS

LIST OF TABLES

LIST OF FIGURES

LIST OF ABBREVIATIONS

AMA	Active Matrix Array
BMG	Bulk Metallic Glass
DSC	Differential Scanning Calorimetry
DTA	Differential Thermal Analysis
EHP	Electron-Hole Pair
GFA	Glass Forming Ability
H-C-H	Heat-Cool-Heat
IVAP	Intimate Valence Alternation Pairs
VAP	Valence Alternation Pairs
TFT	Thin Film Transistor

1. INTRODUCTION

1.1 Introduction

X-ray imaging is a well developed technique in clinical research. Many techniques of imaging have been developed to date in various fields such as computed tomography, radiography, ultrasound, magnetic resonance and nuclear medicine. X-ray imaging flat panels are used in digital imaging technology for radiography applications. One of the advantages of this technique is to provide a high image quality. One of the high-quality image detector systems is based on direct conversion x-ray imaging. Amorphous selenium (a-Se) based alloys are used as photoconductive materials in direct conversion x-ray flat panels, which are commonly preferred devices in mammography, though they are also used in chest radiology and fluoroscopy. It has distinct advantages over other photoconductors especially for its electronic properties such as producing low dark current, having controllable charge carrier mobility and trapping lifetime.

a-Se is alloyed with arsenic (As) to prevent crystallization, and doped with chlorine (Cl) or cesium (Cs) to control its charge transport properties. One of the recent concerns on the efficiency of a-Se based alloys is whether they become affected by exposure to doses of x-ray irradiation. This problem can be approached from optical, electronic and thermal aspects. The thermal aspect mainly considers the glass stability which is conventionally defined by the glass transition, crystallization and melting regions of the material. Possible changes in glass stability may be during or after x-ray irradiation. Thus, concentrating on the effect of x-ray irradiation on the glass stability of a-Se based alloy films can be appreciated as a necessary investigation that is able to provide valuable limits on operating conditions.

1.2 Amorphous Selenium as a Photoconductive Material

a-Se is a well known photoconductive material used in direct conversion x-ray imaging flat panels. Its performance in producing high resolution images gives a-Se detectors a distinct advantage over indirect conversion imaging systems such as those that are based on caesium-indium (CsI) columnar scintillators. An -ray flat panel consists of an active-matrix array (AMA) of thin film transistors (TFT) that is coated with an a-Se layer. The operation of an x-ray flat panel is based on photogenerating charges in the photoconductor that can be drifted and collected. The charge in each pixel of the AMA represents the incident X-ray intensity on that pixel. The electrical charge distribution is then collected and harvested to create a digital image.

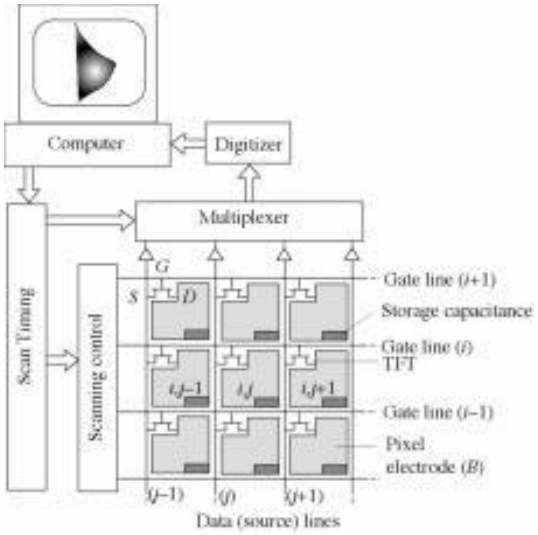

Figure 1.1 Schematic diagram of x-ray imaging system with TFT AMA x-ray flat panel. After Kasap and Rowlands [1].

The basic operation of image production begins with the absorption of x-rays in the photoconductive layer. The x-ray photogeneration processes creates electron-hole pairs (EHPs) in the photoconductor. An electrical field is applied to the photoconductor by an electrode mounted on the a-Se layer. The field drifts the photo-generated carriers. The charge that has the same polarity as the radiation receiving electrode is then collected on the storage capacitors in the pixels. The charge collected by each pixel is proportional to the x-ray dose absorbed by the a-Se layer above that pixel. The charge distribution of each row of the AMA is scanned by a multiplexer. The

analog information is converted to digital information by the use of a digitizer. This information is accumulated in a computer to form the overall image.

a-Se has an EHP creation energy, that is ionization energy, $W_{\pm}$ that depends on the electric field. $W_{\pm}$ can be reduced by applying higher electrical fields to the photoconductive layer [2]. The smaller the EHP creation energy, the greater is the collectable charge from the a-Se layer. Further, in a-Se, both electrons and holes are mobile, and in high quality a-Se layers, both electron and hole Schubwegs are much longer than the photoconductor thickness, which means that the sensitivity is not limited by charge carrier effects. [1] Nevertheless, a-Se confronts challenges in electronic sensitivity due to high x-ray dose absorption. Predictions foresee the effect of high x-ray exposure to cause an increase in dark current and drop in charge carrier lifetimes, moreover induce nucleation to induce crystallization of the material.

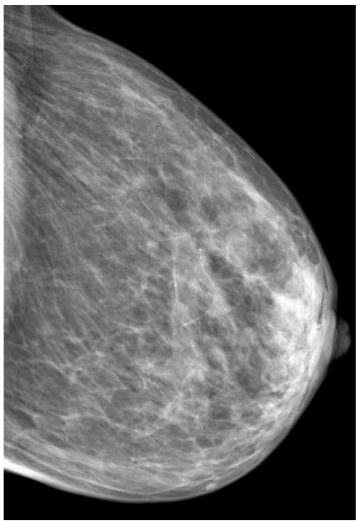

Figure 1.2 Mammography image acquired by a-Se based flat panel x-ray detector. After Kasap et al [3].

Research conducted on investigating the effect of x-ray irradiation on the electronic properties of a-Se:0.3%As-5ppmCl indicate certain dependencies of carrier-trapping lifetime to absorbed x-ray dose and ambient storage temperature. [4] It is observed that as the absorbed x-ray dose by the examined films increase, the carrier-trapping lifetime decreases. Considering equally dosed films, it is found that the elevation of ambient storage temperature during x-ray irradiation

shortens carrier-trapping lifetime. Moreover, it has been observed elevating ambient storage temperature from 283 K to 308.65 K the structural relaxation time falls for equally dosed films. The significant effect of x-ray irradiation motivates conducting thermal analysis to examine glass stability of x-ray irradiated a-Se based alloy films at various storage conditions.

1.3 Thermal Properties of Amorphous Selenium

Thermal properties of a-Se is investigated by differential thermal analysis. Investigations concentrate on glass transition and crystallization kinetics of a-Se alloys in bulk and thin film forms. In fact, these investigations illuminate the nature of glass stability in a-Se based materials. Glass stability is studied in aspects related to kinetic, thermodynamic and structural treatments. Numerous glass stability criteria are established as an indicator of glass forming ability in specific alloy systems. Limitation in all the criteria occurs when they are tested in alloy systems other than the materials which they originally define glass stability. Nevertheless, fundamental criteria which define temperature region intervals between glass transition, crystallization and melting temperatures are reliable to assess glass stability of amorphous materials. The glass stability is a continuous dynamic process which changes with factors such as glass age and ambient temperature. [5, 6] Glass stability can be studied in various methods. One practical tool is differential scanning calorimetry (DSC). This instrument applies heating rate to measure the enthalpy change within a specific temperature range. This enables to detect representative (characteristic) temperatures of glass transition, crystallization and melting phases. The glass transition, crystallization and melting temperatures are unique to a given material. Under DSC experiments, the characteristic temperatures are stable at nearly constant thermal history and heating rate. However, these temperatures can be altered by external effects. Such effects may be irradiation, humidity and pressure among other factors.

1.4 Objective of Research

The aim of this work is to study the effect of x-ray irradiation on the glass stability of aged a-Se based thin film alloys by using differential scanning calorimetry (DSC). This work also

focuses on investigating the usefulness of fourteen selected glass stability criteria that are found in the literature. For the purpose of investigating the glass stability, characteristic onset temperatures and stability criteria of x-ray irradiated pure a-Se, a-Se:0.5%As and a-Se:6%As-140 ppm Cs film samples are analyzed. A preliminary investigation is conducted to study the reproducibility of characteristic onset temperatures and glass stability criteria. In the first main stage of experiments, a set of films are irradiated for various x-ray exposure times and DSC scanned for glass stability analysis. In the second main stage, post irradiation resting period is applied to x-ray irradiated samples. The aim is to observe a change in the characteristic onset temperature of crystallization due to possible induction of nucleation and crystal growth. This investigation is conducted for a resting period of five hours and at three different annealing temperatures which are 295 K, 308 K and 328 K. It is predicted that elevation of the annealing temperature will lead to a change in the glass stability. In the third main stage, extended resting periods are applied for equally irradiated samples at elevated annealing temperatures, 308 K and 328 K. It is proposed that the glass stability would undergo change due to the kinetic factors which may arise from elongated relaxation periods. Further, the behaviour of characteristic temperatures and glass stability criteria obtained from the experimental stages are compared to determine the best stability conditions of x-ray irradiated films. In addition, criteria ordering is conducted to figure the most variant criteria in terms of their nominal values. This analysis is conducted to provide more insight to determine the most useful criteria for glass stability of a-Se based alloy films.

1.5 Content of the Thesis

This thesis consists of six chapters. The first chapter includes introductive information on the use of a-Se based alloys in x-ray imaging technology and electronic and thermal properties. The second chapter provides theoretical background related to the study of glass stability of x-ray irradiated a-Se based alloy films. The third chapter covers the instrumentation and experimental stages applied to the examined materials. In the fourth chapter, the experimental results are presented and analyzed. In the fifth chapter, characteristic temperatures and glass stability criteria are subjected to comprehensive comparisons and discussions. In the last chapter, conclusions and recommendations for future studies are presented.

2. BACKGROUND AND REVIEW

2.1 Introduction

Doped a-Se alloys are commonly used in x-ray imaging flat panels in multilayer structures. Under high x-ray irradiation, electrical properties of a-Se based materials are modified. Glass stability is an important factor in the lifetime of the a-Se based devices. At present, we do not have any systematic studies on how x-ray irradiation affects the glass stability. In this work, glass stability investigations have been conducted by differential thermal analysis (DTA). This analysis consists of quantitative evaluation of characteristic temperatures related to glass transition, crystallization and melting regions of a given glass. There are many glass stability criteria established for specific materials such as bulk metal glasses, polymers, chalcogenide glasses etc. Unfortunately, a uniform criterion which successfully combines all aspects related to glass stability has not been established. This drawback originates from the unresolved nature of glass transition. Thus, analyzing a collection of glass stability criteria in various materials is important in providing knowledge about their usefulness. Particularly, this study covers fourteen criteria to investigate the glass stability of a-Se based alloy films. This chapter starts with a short review of Se rich chalcogenide glasses. Then, the structure of a-Se described briefly. Afterwards, concise information on glass forming ability, glass transition and crystallization in a-Se based alloys is covered. Subsequently, a review of glass stability criteria selected for this study is given. In addition, the theory of x-ray absorption is explained. Finally, differential thermal analysis technique used for the study glass stability is introduced.

2.2 Structure of Amorphous Selenium (a-Se)

Group VI elements other than oxygen (O) are known to be chalcogens, which are basically sulphur (S), selenium (Se) and tellurium (Te). These elements form compositions with other group

elements to form chalcogenides. Some of the chalcogens can be prepared as glasses. Some of the glasses, such as As_2Se_3, are very good glass formers. Selenium can also be prepared as a glass, but it has a tendency to crystallize over time. Vitreous (glassy) selenium can be prepared by quenching molten selenium to solid phase temperatures. It can also be prepared by vacuum deposition as to be described in Chapter 3.

Structurally, it is believed that a-Se consists of chain and ring fragments. [7] These chain and ring fragments may vary under different melt quench temperatures. Generally, random chain model of a-Se structure is more favorable, in which it is accepted that Se_n, Se_6 and Se_8 rings are assorted together within the structure. The atoms that form the chain-like structures are bonded with a certain dihedral angel, which is a function of bond length and angle. The spiral orientation of the chains is explained by + or – configuration of the dihedral angle which indicates the relative phase between adjacent bonding planes. An outstanding aspect of chalcogenide glasses is that they contain valence alternation pairs (VAP). The VAP model suggests that Se_1 and Se_3 pairs are more probable to be formed in a-Se, due to their diamagnetic stability. If these pairs are located at a very close distance, intimate valence alternation pair (IVAP) is formed. More detailed information on the amorphous structure can be found in the literature [8, 9, 10, 11, 12]. An illustration of the structure of a-Se is given in Figure 2.1.

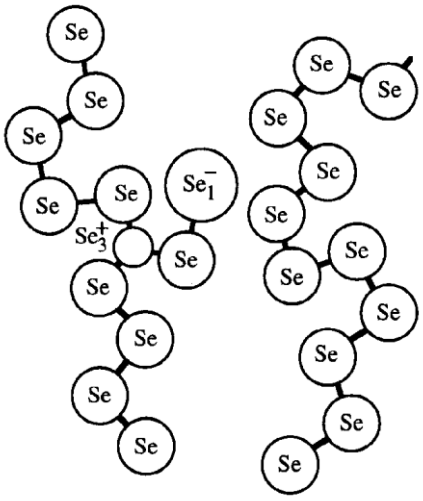

Figure 2.1 Schematic of a-Se with Se_3^+ and Se_1^- defects. After Kasap [7].

Glass transition and crystallization depend on the preparation of glasses. Not only the preparation technique itself, but also the form prepared may have different glass characteristics. Factors related to vacuum deposition technique can induce structural changes in thin films. Such changes may be related to the difference in the substrate temperature or adsorption rate during the deposition process, among other factors. A comprehensive review of thin film crystallization is given by Venables et al [13] which includes the effects of substrate temperature adsorption rates, evaporation rates etc.

2.3 Characteristics of Glass Formation

Glass formation is achieved by undercooling of the liquid phase to low temperatures. The principal requirement is to undercool the melt at a critical rate to overcome the crystallization dynamics. When a melt of a material is undercooled at a certain cooling rate down to a temperature below the melting temperature it becomes glass. The cooling rate required to form a glass should be fast enough to supress the nucleation and crystal growth, which are the key factors for crystallization. The minimum amount of cooling rate required to form glass is described as the critical cooling rate. The process of forming glass from a melt is also expressed as supercooling. As the melt is supercooled, the viscosity of the material drops rapidly. The viscosity (η) of the liquid phase for many chalcogenides and glassy polymers follows an empirical equation, also known as Fulcher [14] equation, which can be expressed in Equation 2.1:

$$\eta = A\exp\left[B/(T_{\text{liquid}} - T_{\text{supercool}})\right] \tag{2.1}$$

where A is a constant that includes the entropy of the material and B is related to the free volume of the cooled melt. $T_{\text{liquid}} - T_{\text{supercoo}}$, is the supercooled temperature range.

When the viscosity is sufficiently low at high temperatures, the medium has liquid-like characteristics. At low temperature, the viscosity is sufficiently high to impart solid-like behaviour to medium. In the viscosity vs. temperature relation that had been obtained by Wong and Angell [15], the viscosity of supercooled melts shows an Arrhenius-type behaviour for temperatures close to glass transition region. The glass transition region in terms of viscosity is around 10^{13} poise.

Glass forming ability (GFA) is conceptualized in three independent views. These views consider the structural, bond-strength and kinetic treatment of the phenomenon. The structural treatment focuses on correlation between GFA and relative ionic radii which exist in binary ionic glass formers, such as oxide, halide and chalcogenide glasses. Historically, fundamental propositions of the treatment estimate the ratio of cation radius (R_c) to anion radius (R_a) present in the glass is limited to $0.2< (R_c/R_a) <0.4$. [16] More advanced treatments combine different geometric orientations of atomic structure in metal alloys. [17] Although the treatments on the structural view of glass formation have been given qualitative assessments to explain the nature of glass formation quite adequately, the view has limitations regarding complex groups and mixture systems to establish an empirical theorem. An alternative atomic scale treatment suggests that a certain correlation exists between interatomic bond-strength to crystallization of amorphous materials. A criterion proposed for this treatment defines a characteristic ratio of bond-strength to kinetic energy barrier at melting temperature ($k_B T_m$) as an indicator of GFA. [18] This criterion enables the classification of glasses that have a high crystallization tendency. Unfortunately, the atomic scale treatment fails in specifying the necessary conditions for glass vitrification.

The kinetic treatment of GFA provides a more comprehensive approach on the phenomenon. It is already known that the crystallization process involves both nucleation (I) and crystal growth (G). It has been suggested that these processes are the main factors involved in glass formation. [19] Accordingly, the likelihood of glass formation depends on the crystal growth and nucleation rates of an undercooled melt. The separation of crystal growth and nucleation rates during undercooling determines whether the melt becomes crystalline or forms glass. Slower cooling rates lead to a high possibility of crystallization, whereas faster the cooling will minimize or prevent the process of nucleation and crystal growth. In addition, the nucleation process has an incubation period (time lag). If the nucleation starts early during cooling, it is likely that the growth and hence crystallization will follow, and the cooled sample may be either fully or partially crystallize. [20] Thus, the GFA depends on crystallization rate, and in a way, on the three factors that control crystallization.

$$\text{GFA} \propto \alpha_c(I, G, \tau) \tag{2.2}$$

where α_c is crystallization rate, and it is a function of nucleation (I), crystal growth (G) and time lag (τ).

Specific models are developed to explain GFA of chalcogenide glasses. One of the quantitative explanations is achieved by Sun-Rawson-Minaev (SRM) model. [21] This model applies for pure substances. The criterion relates the GFA to the melting temperature (T_m) of substance and the covalence-ion bonding energy ratio. [22] Amongst the chalcogenide group elements, Se possesses highest GFA. However, limits in the SRM criterion appear in quantifying the GFA of multi-component glasses, including heterogeneous chalcogenide systems.

2.4 Characteristics of Glass Transition

Glasses exhibit glass transition behaviour upon heating or cooling. The glass transition can be detected by DTA, such as differential scanning calorimetry (DSC), where the sample is continuously heated. This phenomenon is observed in a specific temperature range which is referred as glass transition region.

The glass transition occurs as the heat flow of the glass changes with increasing temperature. During glass transition the material becomes less viscous, transforming glass into a liquid-like mesophase. [23] A characteristic temperature is assigned for the glass transition region. According to discussions covered in Seyler [24], there are two different views on assigning this temperature. In the discussion, one view accepts the definition of glass transition temperature (T_g) as "*the midpoint of the temperature region over which the glass transition takes place*". The temperature obtained according to this definition is defined as the *peak temperature*. The other view that has been introduced defines T_g as the temperature assigned to the intersection between the baseline of the heat flow and the tangent drawn from midpoint of the endothermic peak of the glass transition. This temperature is called the *onset temperature*. Until the present, the peak and the onset temperatures are used to assign glass transition temperature. Nevertheless, in stability investigations for chalcogenide glasses such as a-Se, onset temperature values are considered. The assignment of onset and peak values of glass transition temperature (T_g) can be seen in Figure 2.2.

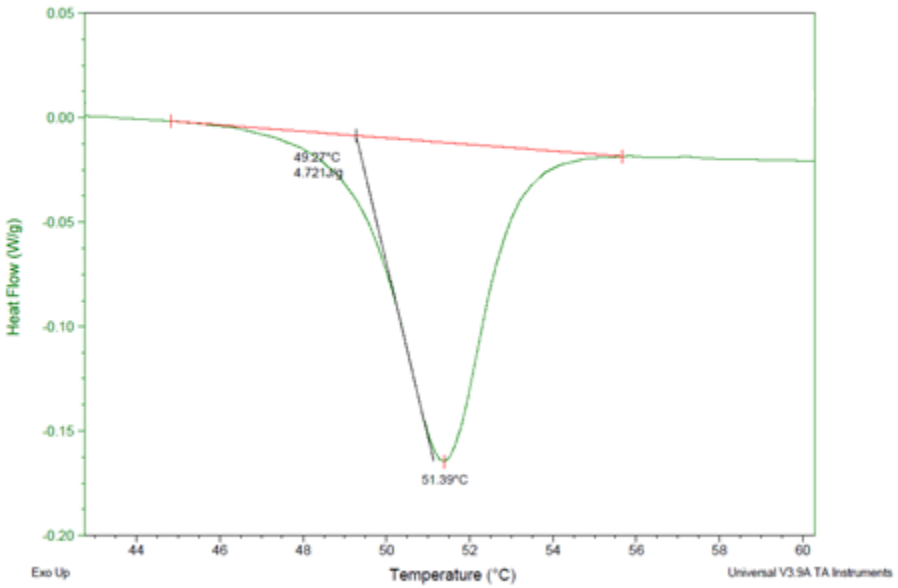

Figure 2.2 Onset and peak temperatures of glass transition region of pure a-Se thin film sample aged at 295 K ∓ 0.5. The software also estimates the enthalpy (J/g) of the selected region. Taken from Universal V3.9A software of TA instruments.

The glass transition observed during a DTA heating experiment depends on two main factors, which are the thermal history of the sample and heating rate applied on the glass. Thermal history of a glass depends on the temperature-time schedule that had been imposed, prior to DTA experiments. One of the main components of thermal history is the sample storage (annealing) temperature. Samples stored at different storage temperatures display different glass transition temperatures. For a-Se, as the storage temperature increases, the glass transition temperature drops. [6] Also, different heating rates applied on identical samples of a glass produce a shift in the glass transition region and in crystallization region. [25] DSC characterization of Se-Te thin films have shown that as heating rate applied on the glass sample increases, its T_g drops to lower temperatures. [26]

Glass transition has not yet been fully understood to establish a unified empirical formulation. Indeed, this phenomenon is examined in various aspects. One of the treatments is based on thermodynamic parameters, such as volume, entropy and enthalpy and differential quantities such as thermal expansion coefficient (α_T), heat capacity (C_P) and bulk compressibility

(κ_T). [27] In the view related to thermodynamic aspects, it is argued that the glass transition is a second order transition. During this type of transition, first-order thermodynamic properties such as entropy is supposed to be continuous. Correspondingly, the changes in volume and pressure during transition must satisfy the equilibrium of entropy before and after the transition. Thus, under these circumstances, the glass transition temperature can be determined in terms of thermodynamic parameters which are derived from Maxwell's thermodynamic relations. This determination can be expressed in Equation 2.3.

$$\frac{dT_g}{dp} = \frac{\Delta\kappa_T}{\Delta\alpha_T} = TV\frac{\Delta\alpha_T}{\Delta C_P} \tag{2.3}$$

In a typical second order transition, the change in isothermal compressibility (κ_T) with respect to coefficient of thermal expansion ($\Delta\alpha_T$) is expected to be the equal to the change in the $\Delta\alpha_T$ with respect to the heat flow at constant pressure (C_p). However, for glasses, Prigogine and Defay [28] have shown that the ratio of $\frac{\Delta\kappa_T}{\Delta\alpha_T}$ to $TV\frac{\Delta\alpha_T}{\Delta C_P}$ is greater than unity (1). Thus, it can be understood that the glass transition isn't a simple second-order transition.

A more theoretical approach considers the continuity of entropy at glass transition, crystallization and liquid regions. Pioneered by Kauzmann [29], this view states that under thermodynamic equilibrium, the glass transition temperature has a lower limit. This limit is defined as Kauzmann's temperature (T_K) in which the glass and the crystalline states have the same entropy. The glass transition temperature can neither fall below the limit, which would cause the liquid entropy region to fall in crystallization entropy region, nor display different entropy than the liquid region. This idea has been disproved for lithium acetate ionic system, where heat capacities and entropy vary in three characteristic phases with respect to temperature. [15] The drawback of this view is that, it is impossible to assume that the material would exhibit no residual entropy during glass transition, since heat flow near glass transition temperature changes sharply. This inconsistency is also known as the Kauzmann paradox. Detailed discussions related to this paradox are covered in Stillinger [30].

An alternative treatment focuses on the relaxation phenomenon. This treatment aims to explain glass formation and respectively glass transition by the relaxation of glass. In this view, as the temperature decreases, the viscosity and the structure relaxation time (τ_r) increase. If τ_r is much

shorter than the experimental time scale (Δt_{exp}) the material is considered to be in the liquid state. If τ_r is much greater than Δt_{exp}, then the material exhibits solid-like behaviour, that is, it is in the glass transition region. In which $\tau_r \approx \Delta t_{exp}$ is defined as the glass transition region. [27]

An elementary approach on the structural aspect of glass considers the concept of free volume. It is considered that the total volume of glass consists of the volume occupied by the atoms, assuming spheres, and a free volume that exists between the atomic arrangements. [31] In this aspect, the spatial motion of the atoms during thermal expansion is simply considered as one-dimensional (linear). This model is defined for metallic glass formers, which possess non-directional chemical bonding. When the liquid is cooled down, changes in the atomic configuration causes decrease in the free volume. The model states that, during the undercooling process, the volume reaches a critical limit which prevents configurational atomic freedom. [32] At the point where redistribution of the free volume no longer exists, glass formation occurs. This simple concept is valid in structural analyses of many glass systems including chalcogenide glasses. Doolittle's work [33] related to free volume model, have proven that the viscosity of supercooled melt obeys Equation 2.1. One of the drawbacks of this model is that it considers linear thermal expansion in volume at temperatures close to T_g. Another drawback is that the free-volume model does not apply for glass system with strong covalent bonds (directed bonds) at temperatures over T_g.

Arsenic (As) is a mainly preferred group V member element to combine with Se to form chalcogenide glasses. In Borisova [34], it has been shown that As can be mixed at various atomic percentages up to 67%. Investigation on impurity doping show that the T_g As-Se compositions increase until percentage of As reaches 40%, which then displays a drop as the percentage is added up to 60%. Remarkably, similar trend is followed by the average bond energy with respect to As percentage.

2.5 Characteristics of Crystallization in a-Se

Most amorphous solids undergo crystallization when heated. This phenomenon takes place due to nucleation and crystal growth. Nucleation can be induced by external factors including mechanical, electrical and magnetic forces, and even by high-energy light. More prominent effect

to enhance nucleation is to collapse atomic scale cavities within the material, which can be achieved by applying high pressures (~10^5 bar) to a melt.

In general, the nucleation process can be classified in two ways. The primary type can either occur spontaneously in a homogeneous material or can be initiated by an external particle in a heterogeneous system. As mentioned in Mullin [35], homogeneous type of nucleation can be achieved by condensing oversaturated vapor compositions to liquid state in an ideally isolated system. A more realistic form of nucleation considers impurities which are captured within the cooling of a melt. This causes heterogeneous nucleation. Melts with greater volume bear more impurities, which lead to an increase in heterogeneous nucleation sites throughout the surface and interface of the melt. Additionally, secondary nucleation may take place by applying or controlling nuclei to less saturated substances which are already nucleated.

Crystallization can appear under isothermal and non-isothermal conditions. Specifically, Kolmogoroff model [36] is developed to study crystallization under non-isothermal conditions, such as heating sample with constant heating rate. As mentioned in Kasap and Juhasz [37], the model describes crystallization of a given glass in terms of nucleation (I_v) and growth rates (u). This model is used to calculate the so-called extended volume fraction V_{ex} of crystallized material, when heated with constant heating rate. By considering that the nuclei generated, $I_v dt$, in the time interval dt' grow with a velocity u. The growth dimensionality is m and the nuclei geometric factor is g. The extended volume is then given in Equation 2.5.

$$V_{ex}(t) = g\int_0^t I_v\left[\int_{t'}^{t} u \cdot dt\right]^m dt' \tag{2.4}$$

Structural investigations conducted on the crystallization of pure a-Se thin films show that crystallization in a-Se commonly occurs by growth of surface and interface cylindrites. [38] Study held by Kim and Turnbull [39] on the morphology of crystallization in a-Se films, indicate that the nucleation and growth become more regular as the isothermal annealing temperature is increased from 303 K to 373 K. Nevertheless, the thermal analysis conducted in this study had shown that the crystallization temperature is independent of ambient annealing temperature and film thickness. Progressive examination of pure a-Se based thin films has shown that interface cylindrites can be increased by photoillumination. [40] It has been observed that not only the number density of

surface cylindrites increase but also the crystallization morphology appears to be different. Moreover, significant changes in surface structure have been also observed in As doped a-Se films. However, it has been found that the crystal growth rate drops, which causes the material not to crystallize. As the atomic percentage of As is increased from 1% to 5%, it has been observed that films do not experience crystallization, even when they are illuminated for three days at high ambient surface temperature of 303 and 373 K.

Amongst the two views of assigning characteristic temperature in DTA, onset temperature is the most commonly preferred to assign the T_x. This is due to the fact that the actual shape and the peak of the crystallization exotherm can vary widely between samples. The peak temperature of the exotherm depends on a number of factors such as the geometry of nuclei and crystallites, the sample dimensionality or shape, and whether the nucleation is homogenous or heterogeneous. On the other hand, the onset temperature is less dependent on grain impingement, and the sample geometry. [37] Thus, onset temperature of crystallization is widely considered in glass stability analysis.

2.6 Glass Stability Criteria

The stability of glasses is investigated by considering three characteristic temperatures: the glass transition (T_g), crystallization (T_x) and melting temperatures (T_m). Many works have suggested that glass stability of materials can be quantified by establishing a proper algebraic relation between these characteristic temperatures. Fundamental arguments are based on setting the norms of stability on the temperature intervals between the characteristic temperatures. Also, reduced temperature representation of one characteristic temperature with respect to another, more preferably to T_m, can be considered as a fundamental criterion to study glass stability. More advanced criteria are formed to provide a dimensionless value which rationalize the relation between the temperatures. In general, glass stability criteria are developed for specific materials to relate characteristic temperatures to GFA. Depending on the interest of study and the material, characteristic temperatures may be defined in terms of onset or peak value observed during the critical transitions. Nevertheless, practically most of the research that involve glass stability considers onset values.

In general, the definitions of glass stability are based on how the critical regions of glassy materials are separated from each other. However, no single general rule has been accepted to quantify glass stability. Various glass stability criteria have been defined for different glasses, which in certain circumstances are found to be applicable to specific group of materials. Basically, these advanced glass stability criteria associate characteristic temperatures with the GFA. However, the usefulness and the basis of establishing a promising criterion depends on both correlation with the critical cooling rate specific to the glass, and the GFA of the material. The advanced glass stability criteria, including fundamental criteria that defines reduced temperature of critical regions, are typically named after founding scientists. Most common stability criteria are summarized in Table 2.1.

Table 2.1 Glass Stability Criteria.

Glass Stability Criterion	Symbol	Formula	Equation
Supercooled Region Interval	ΔT_{xg}	$T_x - T_g$	(2.5)
Liquid Region Interval	ΔT_{mg}	$T_m - T_g$	(2.6)
Wakasugi	α	$\frac{T_x}{T_m}$	(2.7)
Turnbull	K_T	$\frac{T_g}{T_m}$	(2.8)
Hruby	K_H	$\frac{T_x - T_g}{T_m - T_x}$	(2.9)
Weinberg	K_W	$\frac{T_x - T_g}{T_m}$	(2.10)
Lu-Liu	K_{LL}	$\frac{T_x}{T_g + T_m}$	(2.11)
Long	ω	$\frac{T_g}{T_x} - \frac{2T_g}{(T_g + T_m)}$	(2.12)
Mondal	β'	$\frac{T_x}{T_g} + \frac{T_g}{T_m}$	(2.13)
Fan	ϕ	$\left(\frac{T_x - T_g}{T_m - T_g}\right)\left(\frac{T_x}{T_g} - 1\right)^{0.143}$	(2.14)

Zhang	ω_2	$\frac{T_g}{2(T_x - T_g)} - \frac{T_g}{T_m}$	(2.15)
Yuan	β	$\frac{T_x T_g}{(T_m - T_g)^2}$	(2.16)
Du	ξ	$\frac{T_x - T_g}{T_x} + \frac{T_g}{T_m}$	(2.17)
2nd Du	γ_m	$\frac{2T_x - T_g}{T_m}$	(2.18)

2.6.1 Fundamental Glass Stability Criteria

Fundamentally, several criteria had been stated considered to set a preliminary approach to analyze stability. One of the measures of glass stability is defined as the difference of crystallization temperature to glass transition temperature. This temperature region is defined as the supercooled region interval (ΔT_{xg}). Another criterion is defined as the liquid region interval (ΔT_{mg}), which is the separation between melting and glass transition temperatures.

One of the most fundamental criteria was established by Turnbull [41]. In the related work, a reduced temperature (T_r) had been defined to represent the ratio of glass transition temperature (T_g) to melting temperature (T_m). Also, it had been argued that rate of crystallization is dependent on this reduced temperature. As an alternative reduced temperature criterion, Wakasugi et al [42] had proposed a reduced temperature criterion by investigating GFA in Na_2O-B_2O_3 and Na_2O-B_2O_3-Al_2O_3 systems. As a result, it had been stated that the reduced temperature of crystallization signified the GFA. The usefulness of this criterion has been proven to be valid for the specific systems, according to the correlation between the criterion and critical cooling rate. However, depending on the material, it has been expressed that this correlation may be direct or inverse. In summary, Turnbull's criterion (K_T) and Wakasugi criterion (α) are based on relating glass stability to the reduced temperature representations of T_g and T_x with respect to T_m.

2.6.2 Advanced Glass Stability Criteria

Plenty of criteria that involve more sophisticated analysis of glass stability in different glass material systems are developed. In common, these criteria evaluate the glass stability by producing a dimensionless quantity from a defined algebraic relation. Some of these criteria are related to the fundamental criteria indicated above. These so called advanced criteria are mentioned individually. Their relation to the GFA in certain materials is also mentioned.

Initially, the Hruby (K_H) criterion can be introduced. As many other criteria, the evolution of K_H criterion lies in the investigation of GFA. The essential study done by Hruby [43] is based on DTA of the glass stability of Si doped As_2Te_3 chalcogenides. It has been stated that the supercooled region (ΔT_{xg}) and liquid interval regions (ΔT_{mg}) are related to the GFA. It is indicated that a direct proportionality exists between ΔT_{xg} and GFA, where this relation with ΔT_{mg} has an inverse proportionality. Hence, the ratio of ΔT_{xg} to ΔT_{mg} is defined as the Hruby (K_H) criterion. It is important to mention that this criterion is known to be a good quantitative representation of GFA. This criterion has proven to be one of the best glass stability indicators for a wide range of materials, including oxide glasses [44]. The usefulness of this criterion is verified by further investigations in terms of reduced temperatures ($\frac{T_g}{T_m}$, $\frac{T_x}{T_m}$) and sensitivity analysis, which consider the derivation of glass stability criteria with respect to the reduced temperatures. K_H displays a consistent behaviour relative to other criteria, which has proven to be a good indicator of GFA and glass stability in different families of materials. [45] This criterion is commonly used in glass stability analysis of a-Se based glasses. [6, 25, 26]

Weinberg (K_W) criterion has been formulated based on DTA-DSC analysis of several previously proposed stability criteria that include the fundamental stability criterion of supercooled region interval ($T_x - T_g$) and its variants: $(T_x - T_g)/T_g$, and $(T_x - T_g)(T_p - T_x)/T_g$, in which T_p represents the crystallization peak value. [46] The main purpose of focusing on the crystallization peak temperature is to compose a relation to crystal growth rate and nucleation in simple glass forming systems. In the investigation of the glass stability of some glasses, the standard K_W have been expressed with the onset temperature instead of the peak temperature, that is T_x instead of T_p as observed in Equation 2.10.

Lu and Liu [47] have established a criterion for Mg, Zr, La, Pd, Nd, Cu, Ti based bulk metallic glass alloys. Also denoted as γ, the Lu-Liu (K_{LL}) criterion is developed with respect to the direct relation of fundamental criteria formulated by Turnbull and Wakasugi, $\left(\frac{T_g}{T_m}\right)$ and $\left(\frac{T_x}{T_m}\right)$. Giving a high coefficient of determination (R^2=0.91) in the statistical analyses, this criterion offers reliability for the glass stability of examined alloys. The usefulness of this criterion is confirmed in a statistical study on oxide glasses and cryoprotectants. [48] It is concluded that this criterion properly associates GFA to glass stability, which has been given high correlation for oxides, cryoprotectants and metallic glasses.

Another glass stability criterion established from analyses of bulk metallic glasses is carried out by Long et al [49]. The usefulness of this criterion has been tested by using thermal properties of Au, Ca, Ce, Cu, Fe, La, Mg, Ni, Pd, Pr, Ti, Zr based bulk metallic glasses which are obtained from the previous work of Lu et al [50]. It is reassured that analysis of critical cooling rate is important in the evaluation of the GFA. The usefulness of Long (ω) criterion has been studied along with various other criteria (α, β, β', K_{LL}, ϕ, γ_m etc.). This glass stability criterion has shown the highest coefficient of determination (R^2) with the thermal properties of metallic glasses and cryoprotective solutions whereas the α criterion has the highest reliability for glassy oxides.

Mondal and Murty [51] have proposed a criterion that is particularly formulated to investigate the GFA in liquids. As a conclusion of their work, it has been stated that better glass formers have high supercooled region interval (ΔT_{xg}), which means higher glass stability. The Mondal (β') criterion is identified as a summation of two reduced temperatures, which is connected to reduced temperature representations, known as Turnbull (K_T) and Wakasugi (α) criteria.

Another dimensionless criterion has been introduced by Fan et al [52] to correlate the characteristic temperatures to the GFA in various liquid metallic and molecular glasses and networks. The criterion is established from the basis of high viscosity and nucleation theory to produce a model related to the GFA. This sophisticated criterion can be reintroduced below:

$$\phi = \left(\frac{T_x - T_g}{T_m - T_g}\right)\left(\frac{T_x}{T_g} - 1\right)^{0.143} \tag{2.14}$$

The first multiplying term on the right-hand side of Equation 2.14 can be recognized as the ratio of the two fundamental glass stability criteria, ΔT_{xg} and ΔT_{mg}. The second term includes a reduced crystallization temperature ratio, $T_{rg}=\frac{T_x}{T_g}$, that is subtracted from 1. The power 0.143 is set to give very good correlation between critical cooling rate and the criterion. Fan has stated that the GFA is not only determined by the reduced crystallization temperature, but also by the differentiation of viscosity around glass transition. In other words, GFA is quantitatively related to glass stability in terms of the supercooled region interval ΔT_{xg}.

Zhang et al [53] have proposed a criterion that contrasts with other criteria developed for the stability of bulk metallic glasses (BMGs). The relations between characteristic temperatures and critical cooling rate were considered to form this criterion. Uniquely, the negative value of reduced glass transition temperature with respect to crystallization temperature ($-\frac{T_g}{T_x}$) is correlated with the critical cooling rate. To study the glass stability of substances that display variations in the T_g, the criterion is the sum of the above mentioned reduced temperature and T_g normalized by the supercooled region interval (ΔT_{xg}). These two normalized terms of T_g is stated to be directly related to the GFA. The usefulness test of this criterion on BMGs based on Au, Ca, Ce, Fe, La, Mg, Ni, Pd, Pr, Ti, and Zr show the highest coefficient of determination (R^2) for ω_2, compared to other criteria, including α, β, ϕ, γ_m and ξ.

Yuan et al [54] has developed a criterion that is proven to indicate GFA in bulk metallic systems. The new criterion is defined to be dimensionless and is related to the product of reduced crystallization temperature and glass transition temperature with respect to the liquid region interval (ΔT_{mg}). This criterion is proposed to reflect the viscosity, nucleation and crystal growth of the substance. An extensive statistical analysis of 214 different bulk metallic alloys, based on Cu, Ca, Pd, Ti, Pr, Y and Co, has shown that the glass stability criterion established from this work has proven to have more sensitivity in reflecting GFA in BMGs compared to other criteria developed for bulk metals.

Du and Huang [55] obtained two factors that are related to the GFA of supercooled liquids. The aim of investigation is to establish a criterion that reflects the GFA not only in metallic alloys but also in oxides and cryoprotectants. The algebraic summation of these two factors is indicated as a quantitative representation of glass stability. The criterion can be restated:

$$\xi = \frac{T_x - T_g}{T_x} + \frac{T_g}{T_m} \tag{2.17}$$

The first term represents the resistance to crystallization. The second term is a normalized representation of the liquid region interval ($\Delta T_{mg} = T_m - T_g$) which is related to the GFA by the critical cooling rate. This relation is commonly satisfied in metallic glasses. Further, linear regression analysis on the characteristic temperatures and critical cooling rates of certain metallic glasses confirm that this criterion has the highest correlation to GFA. Usefulness analysis of this criterion with respect to critical cooling rate shows high correlation with the GFA of metallic glasses, glassy oxides and cryoprotective agents. Specifically, results give $R^2 = 0.90$ for metallic glasses and cryoprotectants, where for glassy oxides $R^2 = 0.85$ is obtained. This criterion promises the best usefulness as a GFA indicator of the examined materials.

Du et al [56] has established an additional criterion for metallic glasses which indicates the dependence of glass stability on both crystallization and supercooled region interval, ($\Delta T_{xg} = T_x - T_g$). This criterion focuses on the direct relation between the ΔT_{xg} and the GFA. Also, it is stated that the melting temperature has an inverse relation to GFA in metallic glasses. Moreover, the T_x is predicted to have a direct relation to stability. It is suggested that higher T_x contributes to higher resistance to crystallization. This increases the tendency of the melt to form a glass. The dependence of GFA on T_x can be expressed as reduced temperature with respect to T_m. The accumulation of the characteristic temperature relations defines the second (2^{nd}) Du criterion.

$$\gamma_m = \frac{2T_x - T_g}{T_m} \tag{2.18}$$

The examination of this criterion using data on BMGs taken from earlier works of Lu and Liu [47, 57] shows very high correlation to the critical cooling rate, giving a high coefficient of determination, $R^2 = 0.931$ for BMGs.

2.7 X-Ray Generation and Absorption

2.7.1 X-ray Generation

X-rays are high photon energy electromagnetic (EM) radiation, which lies within the energy range between 124 eV to 124 keV. The x-rays possessing energy below the keV range are referred as soft x-rays, where x-rays generated in keV range are known as hard x-rays. Fundamentally, x-radiation is generated by x-ray tubes. The operation principle of this instrument is based on the photoelectric effect. In principle, this instrument consists of an anode and cathode assembly contained in a vacuum tube. The cathode part includes a tungsten filament that is heated to a high temperature for thermionic emission. Under an applied voltage, there is a thermionic emission current from the heated filament. A focusing cup is used to impinge high density of electrons through the anode end, which consists of a tungsten target. This target is fixed at a certain angle. High energy electrons that strike the target are scattered at different angles, producing a spectrum of x-radiation, known as Bremsstrahlung. The generated rays will form a cone emanating from the target as shown in Figure 2.3.

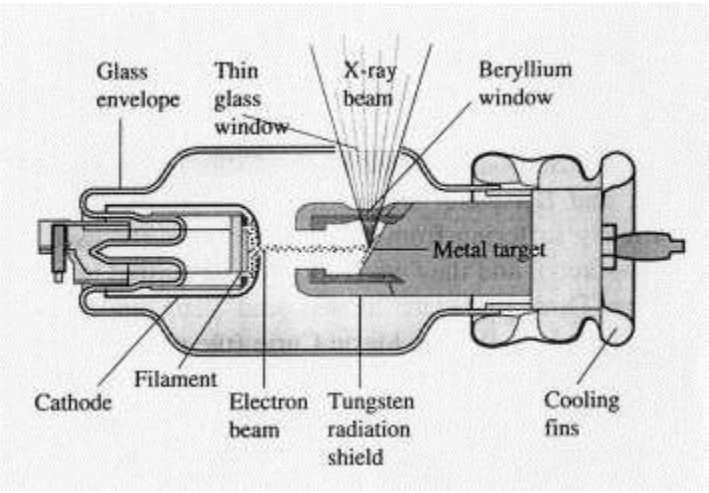

Figure 2.3 Schematic of an x-ray tube. Produced x-rays pass through a beryllium (Be) window. After http://physik.uibk.ac.at/museum/en/details/tubes/roentgen.html (retrieved December 19, 2017)

2.7.2 X-Ray Absorption

X-rays generated from an x-ray tube interact with the objects along the propagation cone. The high-energy rays are absorbed within the volume of encountered medium. The total energy of x-rays is attenuated as x-rays propagate within the medium. A quantitative description of the energy lost per unit distance along the direction of propagation is represented by the linear attenuation coefficient. The attenuation of x-rays is related to a number of possible physical interactions of photons with matter. These interactions can be identified with the photoelectric effect (τ'), Compton scattering (σ_C), Rayleigh scattering (σ_R), pair (π) and/or triplet (γ') production.

In photoelectric absorption, photons strike inner electron shells of atoms present in the medium. The energy of an x-ray photon is transferred to one of these core electrons to excite it from the inner shell to the conduction band, where the electron is free with a certain amount of kinetic energy. The second possibility is Compton scattering, in which an x-ray photon can free or excite electron from an atom by transferring a portion of its energy. After the inelastic impact, the photons are scattered in different directions. Rayleigh scattering is the third possible interaction between x-ray photons with the atoms in the medium. In this situation, the majority of photons are scattered elastically from the host atoms, leaving them unexcited. Furthermore, a high energy photon may impinge on a nucleus or free electron, transferring the electromagnetic energy into kinetic energy to create an electron-positron pair or electron-electron-positron triplet. Consequently, the mass attenuation coefficient of a medium is the summation of these processes expressed as

$$\left(\frac{\mu}{\rho}\right)_{\text{mac}} = \frac{\tau'}{\rho} + \frac{\sigma_C}{\rho} + \frac{\sigma_R}{\rho} + \frac{\pi}{\rho} + \frac{\gamma'}{\rho} \tag{2.19}$$

The transferred energy by bremsstrahlung radiation is also attenuated as the x-ray beam propagates in the medium. Some amount of the x-ray energy is deposited in the medium and the rest of the energy is carried through scattered or uninterrupted x-rays. The energy absorbed in unit density of medium is defined as energy absorption coefficient,

$$\left(\frac{\mu}{\rho}\right)_{\text{eac}} = \left(\frac{\mu}{\rho}\right)_{\Sigma} (1-g) \tag{2.20}$$

The factor-*g* is the fraction of the kinetic energy of all charged particles produced by absorbed photons that is lost as radiation as the charges decelerate. The absorbed energy by the medium per photon is the multiplication of photon energy with the ratio of the energy absorption to mass attenuation coefficient,

$$E_{\text{absorbed}} = E_{\Sigma}\left(\frac{\mu}{\rho}\right)_{\text{eac}} \Big/ \left(\frac{\mu}{\rho}\right)_{\text{mac}} \tag{2.21}$$

The energy absorbed in a medium or material can be found from the incident photon flux Φ, provided we know the energy distribution of this flux, Φ(*E*)

$$E_{\text{abs}} = \int_{0}^{E_{\max}} \Phi(E) E \frac{(\mu/\rho)_{\text{eac}}}{(\mu/\rho)_{\text{mac}}} \left[1 - \exp(-\mu(E)_{\text{mac}} L_{\text{m}})\right] dE \tag{2.22}$$

where ρ_m is the density and L_m is the thickness of the medium. The energy absorbed in the material per unit mass gives the absorbed dose (*D*) of radiation. Thus, for an x-ray exposed material, the absorbed dose can be found from

$$D_{\text{mat}} = \frac{E_{\text{abs}}}{A_{\text{m}} t_{\text{m}} \rho_{\text{m}}} \tag{2.23}$$

where the multiplication of the area (A_m), the thickness (t_m) and the density (ρ_m) of the volume gives the mass of the material.

2.8 Differential Scanning Calorimetry (DSC)

Differential scanning calorimetry (DSC) is a calorimetric technique that has been developed to obtain precise measurements of heat flow and characteristic temperatures associated with in phase transitions, chemical reactions and other processes in which heat exchange is involved. DSC has now become one of the most important tools in the study of thermal properties of materials. [58] In the present work, DSC has been used to examine glass transition, crystallization and melting phenomena.

Most DSC experiments normally require a constant heating rate throughout a certain temperature range. Under a linearly increasing temperature, DSC monitors the sample temperature and the temperature of a reference inert material and measures the temperature difference (ΔT). The rate of differential heat flow Q' is determined regarding to the Fourier's law of heat conduction. [59]

$$Q' = \frac{\Delta T}{R} \tag{2.24}$$

where R is the effective thermal resistance between sample and reference pans.

The DSC experiments take place in a DSC cell. As it can be seen in Figure 2.4, this cell consists of several parts. The sample to be tested is encapsulated in an aluminum pan. The reference is usually an empty pan. Concisely, the reference and sample pans are placed on the top of two disks which are on a heating block. Reference pan is located on the chromel disk where the sample pan is located on the constantan disk. These disks are connected to alumel and chromel wires which form the arms of a thermocouple.

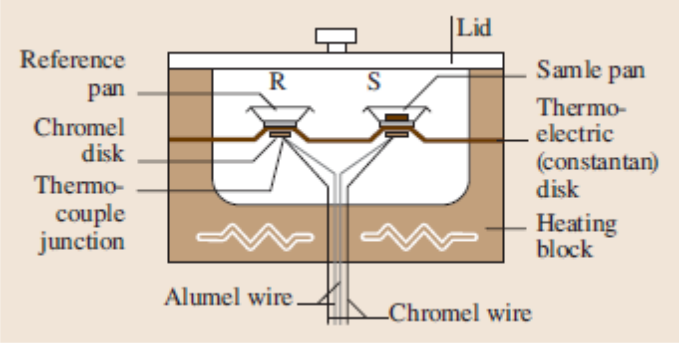

Figure 2.4 A heat-flux DSC Cell containing reference (R) and sample (S) platforms. After Kasap, Malek and Svoboda [59].

During a typical experiment, the DSC cell is heated so that the temperature is ramped with a certain heating rate. The temperature difference between the sample and the reference is measured and converted into a different heat flow. The individual thermocouples on the disk allow the sample and reference temperatures to be measured. The differential heat flow (Q') is measured and plotted against the sample temperature under a constant heating rate. The result of a typical DSC heating

scan is therefore the differential heat flow vs temperature for a given sample, which is called a thermogram. Figure 2.5 shows a thermogram of a Se-Te alloy glass obtained from DSC heating scan.

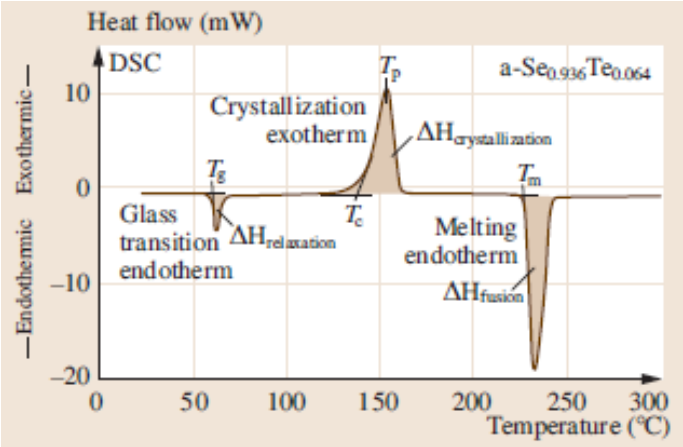

Figure 2.5 A thermogram of Se-Te alloy glass obtained from a DSC heating scan. Here, the crystallization onset temperature is denoted as T_c. After Kasap et al [59].

2.9 Summary

This chapter covers the theoretical background of this thesis. Initially, brief information on the structure of a-Se, a glass forming chalcogen, was introduced. Then, fundamental concepts of glass forming ability (GFA) were mentioned. Then, the phenomenon of glass transition was introduced. Primarily, the onset and peak definitions of the assignment of the glass transition temperature was mentioned. The advantage of onset temperature was pointed out. Subsequently, various views that were introduced to explain the nature of glass transition were discussed. Unfortunately, none of these views have been completely valid to explain this phenomenon. On the other hand, fundamentals of and quantification of the crystallization in a-Se were explained. Also, the advantage of the onset temperature assignment of crystallization phase for glass stability studies was mentioned. Afterwards, the concept of glass stability was described. Fourteen different glass stability criteria established independently, from the glass stability investigations of different glass forming materials were presented. Further, the theory of x-ray absorption was introduced. Finally, differential scanning calorimetry (DSC), the technique used for differential thermal analysis (DTA) of x-ray induced effects in the glass stability of a-Se based alloy films was

introduced. All in all, the experimental procedure and analysis of the results for glass stability analysis of a-Se based alloy films is executed under the scope of the concepts given in this chapter.

3. EXPERIMENTAL PROCEDURE

3.1 Introduction

This chapter covers the experimental procedure that is used in the study of x-ray irradiation effect on glass stability of pure a-Se, a-Se:0.5%As and a-Se:6%As- 140 ppm Cs films. Initially, the instruments that are used to conduct the experiments are introduced. These instruments consist of a vacuum deposition system, an x-ray source, a differential scanning calorimeter (DSC) and an isothermal annealing temperature. Afterwards, four different experimental stages conducted to examine the effect of x-ray irradiation on the glass stability of above mentioned materials are presented.

3.2 Thin Film Deposition

Thin films have been prepared by a conventional vacuum coating system. Pure a-Se, a-Se:0.5%As and a-Se:6%As-140 ppm Cs thin films are coated onto the inside of aluminum (Al) hermetic pans, which are needed for DSC experiments. The vacuum coating system used to produce thin films samples is presented in Figure 3.1. The process of thin film deposition consists of several parts. Initially, a certain number of pellets (vitreous Se-alloy shots) of the material is loaded into a molybdenum (Mo) boat. The film thickness depends on the total weight of pellets that are loaded into the boat. Depending on the desired film thickness, the weight of the pellets can be adjusted. There is a mechanical shutter between the boat and the substrate. Schematic diagram of deposition chamber can be observed in Figure 3.2.

Figure 3.1 NRC 3117 Stainless thermal evaporation system.

Experimental vacuum condition is achieved by evacuating chamber down to nearly 10^{-6} torr by the use of a vacuum pump. Initially a mechanical (rotary) pump is used to reduce the pressure and then a diffusion pump is used to reach down to 10^{-6} torr, following conventional diffusion pump procedures. The Mo boat is heated by passing a large AC current from a transformer. The Mo boat is heated to 523 K (250 °C), which is above the melting temperature of Se, T_m = 490 K (217 °C).

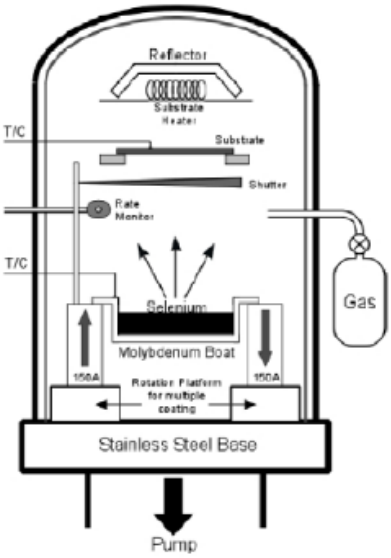

Figure 3.2 Schematic diagram of thin film deposition in NRC 3117 system. After Fogal [60].

The evaporation rate is controlled by the boat temperature. The shutter is opened to allow the evaporation to reach the substrate. A substrate mask holds a set of Al hermetic pans. The mask temperature, and hence the substrate temperature, is stabilized around 333 K (60 °C), above the glass transition temperature of a-Se. The vapor from the boat condenses on the substrate to form the thin film. A group of Al hermetic pans coated with Se can be observed in Figure 3.3.

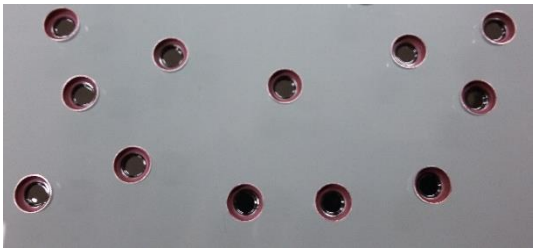

Figure 3.3 Thin film coating on the inner surface of Al-pans.

The thicknesses of the produced pure a-Se, a-Se:0.5%As and a-Se6%As-140 ppm Cs sample sets lies between 50 μm and 150 μm. The thickness of the samples produced in a set varies roughly by $\mp$ 1 μm.

3.3 X-Ray Irradiation

X-ray exposure measurements are conducted in a Faxitron x-ray cabinet system. This system consists of a self-rectified thermionic x-ray generator with control circuitry and radiation-shielded cabinet. The self-rectifying x-ray tube includes a beryllium (Be) window which enables full spectrum of soft x-rays to pass through. The focus of the x-ray tube is 0.5 mm and the maximum tube voltage is 110 kVp. The control panel of the system allows the adjustment of the tube voltage and exposure time. Figure 3.4 shows the outlook of the system.

Figure 3.4 Faxitron® Model 43855D x-ray cabinet system, 71 cm maximum focal distance. Tube voltage selection from 10 to 110 kVp, continuous 3 mA-tube current, 0.76 mm- Be window, operating at 117 V and 60 Hz.

The x-ray irradiation procedure involves two steps. Initially, the x-ray tube is warmed up by increasing the tube voltage first up to 60 kVp for five minutes. The film sample sealed in the Al-pan is placed on top of a 35 cm-long metal rod. The rubber end of the rod holds the sample in an immovable position. After the x-ray tube is warmed up, the metal rod is placed as close as possible to the Be window. The bottom of the metal rod is fixed on a platform which is located at 46 cm from the x-ray source, which gives sample distance to source of around 10 cm. After fixing the sample, the cabinet door is closed. The tube voltage is set to 70 kVp, and the desired exposure time is adjusted on the set-up panel, and irradiation is activated.

X-ray exposure measurements are conducted using a dosimeter with an ionization chamber. The dosimeter is connected to Fluke voltmeter, which is used for the voltage rate reading. Initially, the ionization chamber is connected to the dosimeter by a coaxial cable. The output of the dosimeter is connected to the input of the voltmeter to obtain a voltage rate reading. Aluminum (Al) shielding on the ionization chamber is used to reduce the x-ray flux so that voltage rate measurements do not saturate when the ion chamber is very close to the source. The calibration factor of shielding is multiplied with the voltage reading obtained. This gives an estimate of the bare voltage rate. Consequently, the exposure and dose rates are calculated using conversion factors of 0.7 R/V and

0.00877 Gy/R. The measured voltage rates and associated exposure rate and dose rates for different distances to x-ray source can be observed in Table 3.1.

Table 3.1 Voltage rates with end exposure and dose rates.

Distance to X-ray Source (cm)	Voltage Reading with Al Shielding (V/min)	Estimated Bare Voltage Rate (V/min)	Exposure Rate (R/min)	Dose Rate (Gy/min)
31	10.75	369.4	258.6	2.27
36	7.61	261.5	183.1	1.61
41	6.2	213.1	149.1	1.31
46	4.93	169.4	118.6	1.04
51	4.05	139.2	97.4	0.85
56	3.33	114.4	80.1	0.70
61	2.86	98.3	68.8	0.60
66	2.59	89.0	62.3	0.55

Absorbed dose in the sample is calculated by referring to the air dose rate measurements. Considering 70 kVp tube voltage, 0.076 cm beryllium window and 0.0075 cm Al lid shielding of thin film samples, photon fluence vs. x-ray energy spectrum simulation is obtained from Siemens' website [61], which can be observed in Figure 3.5.

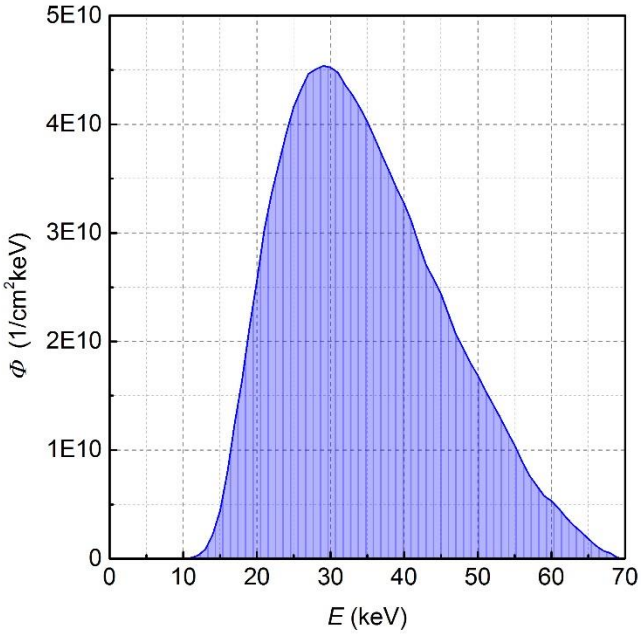

Figure 3.5 Photon fluence with respect to energy spectrum generated at 70 kVp-tube voltage. Data taken from web simulation program of Siemens [61]. This spectrum is for 1 Gy air kerma. The average energy is 34.7 keV.

The mass and energy absorption coefficients of dry air, pure Se, Se:0.5%As, Se:6%As-140 ppm Cs are obtained from NIST[1]. The absorbed energy for each x-ray photon energy interval in the medium is calculated by Equation 2.23.

As an example, we can consider a 150 μm pure a-Se sample located at 9.7 cm distance to the x-ray source, and it is irradiated at 70 kVp for 4 minutes and 34 seconds. First, the energy absorbed by the sample is calculated as 5.21×10^{-6} J/R. The estimated exposure rate time from the distance of 9.7 cm from sample to source is 2419.4 R/min. To calculate the absorbed dose rate by the sample, dose equation is used. Exposure rate and exposure time are included to the right-hand side of the equation as multipliers. The area of the sample is 0.16 cm^2 and the density is 4.28 g/cm^3. Thus, the absorbed dose is estimated as 5.61 kGy.

[1] See Appendix A.

As it occurs, the absorbed dose is quite high. This is due to the small sample-to-source distance, thickness in terms of microns (50 – 150 μm) and small surface area. Correspondingly, high energy is deposited on a very small sample mass, roughly 1.03×10^{-5} kg. Hence, very high exposure rate and times give high absorbed doses of x-rays. The exposure rate at 9.7 cm distance is estimated by extrapolating the obtained data from the dosimeter measurements. The possibility of this value shifting $\pm$ 100 R/min, will approximately give $\pm$ 200 Gy/min in the sample. Thus, the possible error in the estimated dose of 5.61 kGy is about 4%, which is not a significant factor in present measurements that involve very high doses.

3.4 Stability Analysis with Differential Scanning Calorimeter (DSC)

Differential scanning calorimeters (DSC) are instruments which operate with respect to the principles of differential scanning calorimetry. This instrumentation consists of three main parts, which are the DSC cell, refrigerated cooling system and software control system. The DSC cell is the part where the experiment takes place. A DSC can be observed in Figure 3.6.

Figure 3.6 DSC 2910 (TA Ins.) with Refrigerated Cooling System (RCS). Refrigerated cooling system is used to apply constant cooling rate to the cell in multiple cycle operations. For the cases of heat-cool-heat (H-C-H) scanning, the use of this unit is vital.

As explained in Chapter 2, the differential heat flow (Q') and the temperature difference (ΔT) between the sample and the reference is acquired by the software and plotted in a thermogram during the assigned DSC cycle. The data are plotted in terms of heat flow vs temperature during temperature ramping. A possible observation of characteristic regions of an a-Se:0.5%As thin film alloy can be obtained in a thermogram in Figure 3.7.

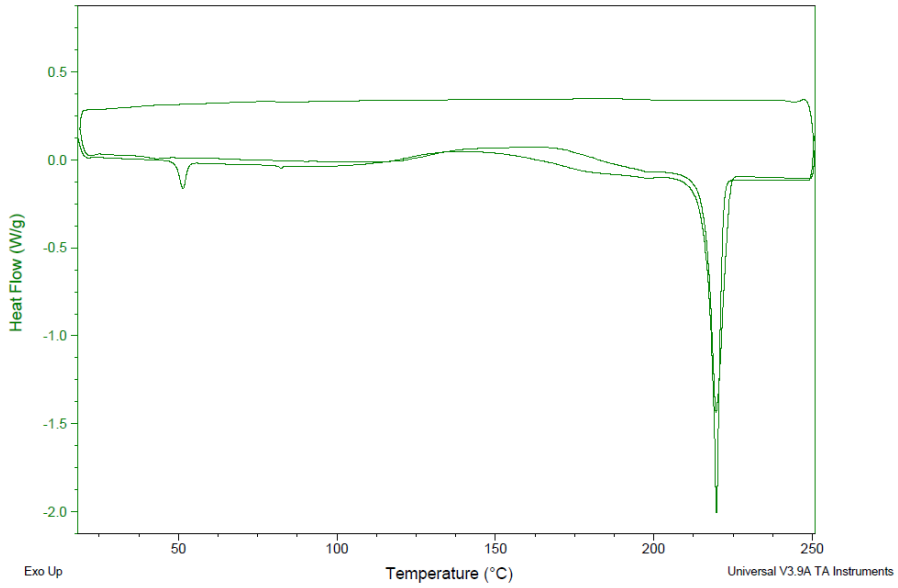

Figure 3.7 Thermogram of a-Se:0.5%As thin film sample aged-stabilized at 295 K. Glass transition, crystallization and melting regions are visible for both the heating scans of H-C-H procedure.

Typically, the assigned DSC procedure consists of a heat-cool-heat scan. In the first part, the samples are heated up from 293 K (20 ºC) to 523 K (250 ºC) with a 5 K/min (ºC/min) heating rate. After reaching the 523 K, the DSC cell is kept isothermally for 1 minute. Afterwards, cooling rate of 5 K/min is applied to the cell by use of the refrigerated cooling system (RCS), and samples are cooled down to 293 K. At the time the cell temperature reaches 293 K, the cell is kept isothermally for 1 minute. A second heating scan is conducted by ramping the cell temperature at constant heating rate of 5 K/min. After the second heating scan, the system is automatically shot off and the DSC cell is left to cool down.

A second heating process is applied to analyze the glass transition and crystallization regions, which in this case would be independent of thermal history. The related conventional DSC procedure for this study is presented in Figure 3.8.

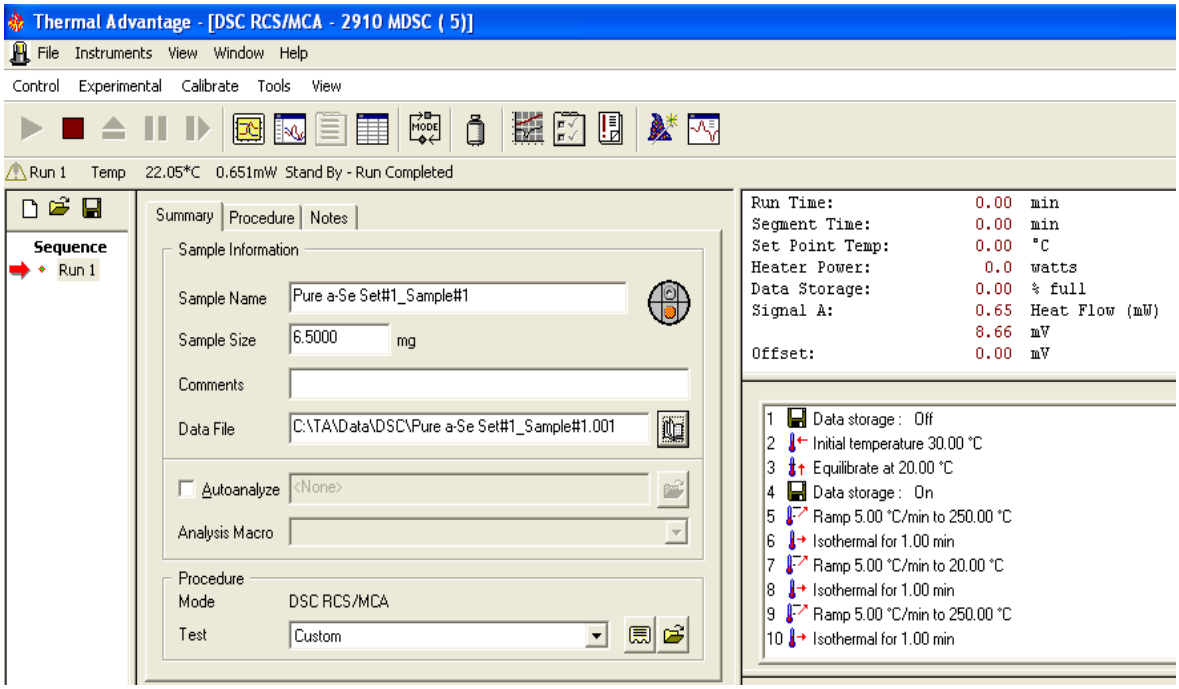

Figure 3.8 Thermal Advantage (TA) Ins. Software. Sample information is typed in the Summary section. The procedure of the DSC measurement is found in the bottom right window, where heat-cool-heat (H-C-H) cycle is set. Each heating and cooling scan is ramped by 5 K/min.

The heating/cooling rate of 5 K/min is taken as standard to form a basis with previous studies and data related to collaborative research[2] in stability investigations of a-Se based alloys. This rate is adequate to capture and distinguish the characteristic thermal regions in a typical thermogram of a-Se.

Different information can be acquired on the thermal behaviour of a-Se in DSC heat-cool-heat (H-C-H) scans. In the first heating process, the characteristic temperatures that are extracted depend on thermal history, which is a convolution of aging time and aging temperature. Since the samples are kept in a laboratory ambient temperature, which varies within $\mp$ 0.5 K (°C), the effect of aging can be easily analyzed. However, in this study, the samples have been aged for a sufficiently long time to achieve structural stability and thermal equilibrium with the ambient temperature. Long aging times are preferred so that the thin film samples have reached thermally stable structure and the difference in DSC measurements before and after x-ray irradiation are not

[2] Analogic Corporation Canada.

due to aging effects. Thus, the main intention is to exclude the aging effect and analyze the effect of x-ray irradiation and post x-ray irradiation conditions on the glass stability of a-Se based alloy films.

The second heating is usually examined to see inherent properties of an individual sample with erased thermal history. According to the DSC procedure, when the glass is melted during the first scan, it is highly predicted that externally induced defects would diminish. The lack of significant changes in the characteristic regions obtained from the first heating scan makes it pointless to analyze the second heating scan. As to be restated, the main intention is to analyze the primary effects of x-ray irradiation on the characteristic regions of samples, which would be only observed during the first heating scan. Hence, analysis of second heating is outside the scope of this study.

3.5 Isothermal Annealing

Isothermal annealing has been carried out post irradiation, to relax the a-Se structure to its original state, that is, to anneal out x-ray induced defects, if any. FTS® 29 ATC-40 isothermal temperature chamber is used to anneal the x-ray irradiated films at elevated temperatures, 308 K (35 °C) and 328 K (55 °C). Technically, the inner surface of this chamber is covered with an isothermal material. The temperature of the chamber is adjusted from its external control panel. Either cooling or heating is possible. After setting the desired ambient temperature, a fan inside the chamber is triggered to provide air circulation so that the temperature in the chamber is relatively uniform. The chamber temperature set for annealing was within $\mp$ 0.3 K (°C). The temperature of the chamber is measured by a type-K thermocouple (Omega® microcomputer thermometer, model HH-71 K2) as can be observed in Figure 3.9. The reason for choosing these annealing temperatures is explained below in Section 3.2.3.

Figure 3.9 FTS® 29 ATC-40 temperature chamber.

3.6 Experimental Stages

Experiments consist of four stages. Initially, statistical analysis of the characteristic temperatures and glass stability criteria are conducted. Preliminary method investigates the reproducibility of glass stability criteria of unirradiated pure a-Se, a-Se:0.5%As and a-Se:6%As-140 ppm Cs films. Next, the effect of x-ray irradiation on glass stability is examined with various x-ray dose applications delivered into the films. In the second step of x-ray experiments, the effect of post irradiation relaxation (resting) period at laboratory ambient temperature is studied. This stage is repeated at elevated annealing temperatures using the isothermal chamber described in Section 3.2.3. Furthermore, the effect of extended post irradiation resting periods on glass stability at elevated annealing temperatures is analyzed.

3.6.1 Reproducibility of Characteristic Temperatures and Glass Stability Criteria

In this preliminary stage, the aim is to conduct DSC measurements for a set of pure a-Se, a-Se:0.5%As and a-Se:6%As-140 ppm Cs film samples which have nearly equal thermal history. The objective of the investigation is to obtain possible variance of characteristic temperatures. Correspondingly, the glass stability criteria of each sample are analyzed. An additional intention is

to compare the characteristic temperatures of pure a-Se, a-Se:0.5%As and a-Se:6%As-140 ppm Cs samples.

To conduct the statistical analyses, the samples aged at room temperature 295 K (22 ºC) ∓ 0.5 from each a-Se alloy set scanned in DSC heating experiment. The measurements are conducted in short duration to eliminate possible shift in characteristic temperatures of the film due to structural relaxation (aging). Table 3.2 summarizes the thermal history of the thin film sample set that are used in reproducibility measurements, where the sample age, sample thickness and duration of measurement for the composition sets are included.

Table 3.2 Thermal history of a-Se based alloy sample sets.

Material	Age (days)	Ambient Temperature of Aging (K), ∓ 0.5	Duration of Measurements (days)
Pure a-Se	54	295	2
a-Se:0.5%As	65	295	3
a-Se6%As-140 ppm Cs	34	295	14

3.6.2 Investigation of X-ray Irradiation Induced Effects on Glass Stability

This experimental stage aims to examine the effects of x-ray irradiation on a certain number of films from each composition. Each thin film sample has been exposed to a different amount of x-ray irradiation. A correlation has been predicted between the characteristic temperatures and the glass stability criteria and the amount of absorbed x-ray dose.

Samples of pure a-Se, a-Se:0.5%As and a-Se:6%As-140 ppm Cs are aged at laboratory temperature of 295 K (22ºC) ∓ 0.5. Since the main objective is to study the effect of x-ray irradiation, samples from the same production set of each material have been considered. Thus, the effect of various x-ray doses can be studied properly with samples of equal thermal history.

Initially, six samples from the same production set have been exposed to x-ray irradiation for different durations, which lie in the range between 0 to 45 minutes. Depending on the composition and sample thickness the absorbed x-ray doses vary. An initial sample is examined without being exposed to x-rays and forms the reference. The aim is to analyze how the glass stability criteria of these samples depend on x-ray irradiation in increasing doses.

The procedure for irradiated samples consists of two parts. First, the samples are irradiated in the x-ray chamber for a certain amount of time. Then, these samples are loaded into the DSC cell for a heating scan. The duration between sample transfer from x-ray chamber to DSC and the start of measurement is roughly 1 to 2 minutes, a negligible time compared with typical structural recovery times observed on a-Se, which extend from hours to days. [5, 63] Thermal history of sample sets used in this experiment is presented in Table 3.3.

Table 3.3 Identification of a-Se alloy sample sets used for x-ray induced glass stability investigation.

Material	Age (days)	Temperature of Aging (K) $\mp$ 0.5	Duration of Measurements (days)
Pure a-Se	330	295	8
a-Se:0.5%As	179	295	10
a-Se6%As-140 ppm Cs	150	295	7

Characteristic temperatures and glass stability criteria obtained from the DSC measurements are plotted with respect to the absorbed x-ray dose. Plots for the temperatures, the fundamental and the advanced glass stability criteria are presented separately in Chapter 4.

3.6.3 Post Irradiation Resting at Different Annealing Temperatures

In the second part of the investigation on the glass stability of x-ray irradiated films, the plan was to inspect a probable effect of relaxation (resting) period on the characteristic temperatures and glass stability criteria after x-ray irradiation. It is presumed that absorbed x-rays

will become more effective in inducing nucleation and crystal growth. Previously, it has been observed that various resting periods of unirradiated a-Se samples have given different electronic and thermal properties. [5, 62, 63]

In this stage, an arbitrary post irradiation resting period of 5 hours is considered. Initially, a group of samples of pure a-Se, a-Se:0.5%As and a-Se:6%As-140 ppm Cs each composition is irradiated with different x-ray doses. After the irradiation process samples were relaxed (rested) for 5 hours at room temperature, 295 K (22 ºC) ∓ 0.5. Table 3.4 gives the thermal history of the sample sets used for glass stability investigation of 5-hour resting at room temperature after x-ray irradiation.

Table 3.4 Identification of a-Se alloy sample sets used for measurements of 5-hour post irradiation resting period at room temperature, 295 K.

Material	Age (days)	Ambient Temperature of Aging (K), ∓ 0.5	Duration of Measurements (days)
Pure a-Se	330	295	8
a-Se:0.5%As	179	295	10
a-Se6%As-140 ppm Cs	150	295	7

This investigation is expanded to study the effect of elevated annealing temperatures of 308 K (35 ^{0}C) and 328 K (55 ºC). In the study of Reznik et al [62], it has been discovered that a-Se based thin films stored at 308 K has shown improved photostructural properties with respect to the films stored at room temperature. Also, the a-Se based films stored at 328 K have been observed to exhibit reversible photodarkening phenomenon, whereas at room temperature the films have had both reversible and irreversible properties. Moreover, Tonchev et al [6] have examined the influence of specific annealing temperatures of 291 K, 308 K and 328 K on the glass stability of pure a-Se bulk samples. It has been reported that the highest crystallization temperature (T_x) was achieved during 24-hour annealing at 308 K. On the other hand, lowest T_x has been found for samples annealed at 291 K. As the resting period is extended over 10 days, the highest T_x has been again obtained on samples annealed at 308 K.

In this part of the experimental stage, one group of irradiated a-Se based alloy film samples are rested for 5 hours at 308 K. The annealing of samples is carried out in the isothermal chamber, as described in Section 3.1.4. After 5 hours of resting period, each film is scanned in a DSC experiment. This procedure is repeated at an annealing temperature of 328 K with a different group of samples from same production set of each composition, which the thermal history is given in Table 3.5.

Table 3.5 Identification of a-Se based alloy sample sets used for measurements of 5-hour post irradiation resting period at annealing temperatures of 308 K and 328 K.

Material	Age (days)	Ambient Temperature of Aging (K)	Duration of Measurements (days)
Pure a-Se	225	295.15 ∓ 0.5	12
a-Se:0.5%As	228	295.15 ∓ 0.5	14
a-Se6%As-140 ppm Cs	315	295.15 ∓ 0.5	11

3.6.4 Extended Post Irradiation Resting Periods at Elevated Annealing Temperatures

This last experimental stage focuses on the effect of extended resting (relaxation) periods on the characteristic temperatures and glass stability criteria of equally irradiated a-Se based films. Particularly, equal amount of x-ray dose is applied to each film sample for each composition. It is considered that the samples have been irradiated approximately by the same amount of absorbed dose. Thus, the objective is to examine the effect of various post irradiation resting periods at elevated annealing temperatures 308 K (35°C) and 328 K (55°C). The samples of each material are absorbed equal amount of x-ray dose. Then the samples are separately rested for various resting periods at annealing temperatures 308 K and 328 K. The resting periods span five different periods within one day. Information of samples sets analyzed in this stage is given in Table 3.6.

Table 3.6 Identification of a-Se based alloy sample sets used in the effect of extended post irradiation resting periods on glass stability at annealing temperatures of 308 K and 328 K.

Material	Age (days)	Absorbed Dose (kGy)	Duration of Measurements (days)
Pure a-Se	246	94.1	10
a-Se:0.5%As	254	133.1	7
a-Se:6%As-140 ppm Cs	329	111.7	7

3.7 Summary

In this chapter, the instrumentation and experimental stages have been presented. The instrumentation that were used for sample preparation, x-ray irradiation and DTA experiments are explained. Afterwards, the experimental stages are introduced. The preliminary stage of the experiments consists of reproducibility measurements of a-Se based alloy film samples. The intention is to test the spread of the characteristic temperatures and glass stability criteria values. In the first stage on the examination of x-ray induced effects, glass stability of samples irradiated with different x-ray doses was studied. In the next stage, the stability analysis was held for sample groups rested at different annealing temperatures, which were 295 K, 308 K and 328 K. In the final stage, the effect of x-ray irradiation on samples were examined by considering various extended annealing periods within a day. Results obtained from these experimental stages are presented in Chapter 4.

4. EXPERIMENTAL RESULTS

4.1 Introduction

In this chapter, experimental results obtained from the experimental stages which were introduced in the previous chapter are covered. Initially, the results for the reproducibility measurements of unirradiated a-Se based alloy films are presented. Then, results for pure a-Se, a-Se:0.5%As and a-Se:6%As-140 ppm Cs films that have been irradiated with high x-ray doses are introduced. Afterwards, the results of the samples that have been rested at annealing temperatures of 295 K, 308 K and 328 K are given. Finally, glass stability results obtained from extended post irradiation periods at elevated annealing temperatures of 308 K and 328 K are introduced. The experimental results are presented in tables. For the experiments that are associated with x-ray irradiation are presented in normalized plots. Thus, it is intended to find a correlation between the thermal parameters and x-ray irradiation.

4.2 Reproducibility of Characteristic Temperatures and Glass Stability Criteria

The reproducibility experiments are conducted with five samples from an a-Se based film alloy. Under defined DSC measurement procedure, the characteristic regions of pure a-Se, a-Se:0.5%As, a-Se:6%As-140 ppm Cs are shown in Figure 4.1. The glass transition, crystallization and melting peaks can be observed in pure a-Se and a-Se:0.5%As film samples. It can be observed that a-Se:6%As-140 ppm Cs does not exhibit crystallization exothermic peak. In fact, this composition displays a small endothermic peak relative to the melting peaks of pure a-Se and a-Se:0.5%As samples around 480 K. It is presumed that, this small melting-like (pseudo melt) endotherm is due to some small regions that become crystallized before they melt immediately. This situation disables to study the behaviour of glass stability criteria for a-Se:6%As-140 ppm Cs.

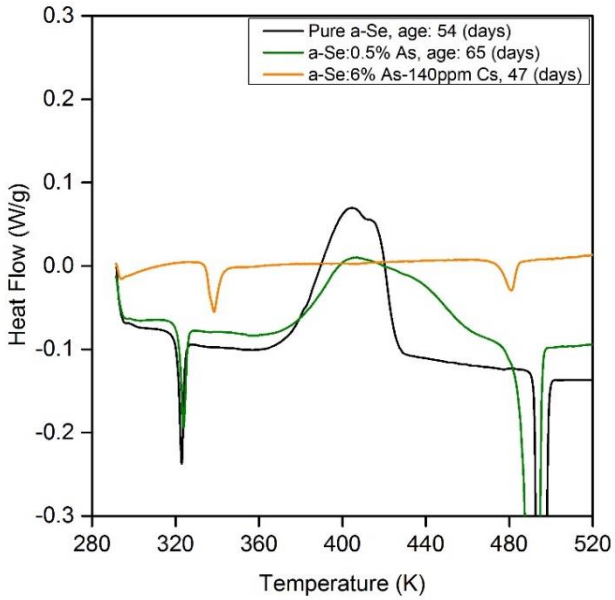

Figure 4.1 Characteristic phases of pure a-Se, a-Se:0.5%As and a-Se:6%As-140 ppm Cs film samples obtained from DSC first heating scan.

After DSC measurements, the characteristic temperatures are evaluated. Using these temperature values, the glass stability criteria are calculated. The average value ($\bar{M}$) and mean standard deviation ($\sigma_{C\pm}$) of the characteristic temperatures and the glass stability criteria obtained for the pure a-Se film samples, are given in Table 4.1 and Table 4.2. Results obtained for a-Se:0.5%As film samples are presented in Table 4.3 and Table 4.4. The mean value of T_g and pseudo melting onset temperature (T_{xm}) obtained for a-Se:6%As-140 ppm Cs film samples is presented in Table 4.5.

Table 4.1 Average characteristic temperatures and fundamental glass stability criteria of pure a-Se film samples.

	T_g (K)	T_x (K)	T_m (K)	ΔT_{mg} (K)	ΔT_{xg} (K)	α	K_T
$\bar{M}$	320.85	374.11	492.96	172.12	53.26	0.7589	0.6508
$\sigma_{C\pm}$	0.2693	1.5864	0.1963	0.3333	1.6091	0.0032	0.0006

Table 4.2 Average advanced glass stability criteria of pure a-Se film samples.

K_H	K_W	K_{LL}	ϕ	β	ω	ω_2	β'	ξ	γ_m

$\bar{M}$	0.3095	0.108	0.4597	0.5034	8.5027	0.0691	0.0999	1.8168	0.7932	0.8669
$\sigma_{C\pm}$	0.0194	0.0033	0.001	0.0084	0.0255	0.0037	0.0915	0.005	0.0037	0.0004

Table 4.3 Average characteristic temperatures and fundamental glass stability criteria of a-Se:0.5%As film samples.

	T_g (K)	T_x (K)	T_m (K)	ΔT_{mg} (K)	ΔT_{xg} (K)	α	K_T
$\bar{M}$	321.08	376.53	489.96	168.88	55.45	0.77	0.66
$\sigma_{C\pm}$	0.3917	1.5855	0.5519	0.6768	1.6332	0.0034	0.0011

Table 4.4 Advanced glass stability criteria of a-Se:0.5%As film samples.

	K_H	K_W	K_{LL}	ϕ	β	ω	ω_2	β'	ξ	γ_m
$\bar{M}$	0.33	0.11	0.46	0.51	9.41	0.06	0.09	1.83	0.8	0.88
$\sigma_{C\pm}$	0.0211	0.0033	0.0011	0.0086	0.0414	0.0037	0.0862	0.005	0.0037	0.001

Table 4.5 Average characteristic temperatures and fundamental glass stability criteria of a-Se:6%As-140 ppm Cs film samples.

	T_g (K)	T_{xm} (K)
$\bar{M}$	334.93	475.76
$\sigma_{C\pm}$	0.6209	0.8628

The comparison of the average characteristic temperatures of the examined alloys is shown in Figure 4.2. The average pseudo melting onset temperature (T_{xm}) of a-Se:6%As-140 ppm Cs is compared with the average melting temperature (T_m) of pure a-Se and a-Se:0.5%As films.

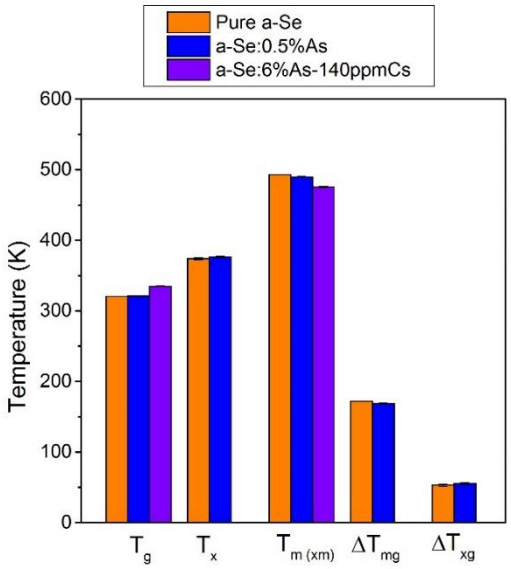

Figure 4.2 Average characteristic temperatures and interval regions of pure a-Se, a-Se:0.5%As and a-Se:6%As-140 ppm Cs film samples.

The average characteristic temperatures of liquid region interval (ΔT_{mg}) and supercooled region interval (ΔT_{xg}) are analyzed. Pure a-Se and a-Se:0.5%As have indistinguishably similar glass transition (T_g) temperatures, where for the case of a-Se:6%As-140 ppm Cs the T_g is higher. The crystallization (T_x) temperature of pure a-Se and a-Se:0.5%As are also very close. In contrast, the pseudo melting temperature (T_{xm}) of a-Se:6%As-140 ppm Cs is lower than the T_m of other two materials. As mentioned earlier, because of the absence of the crystallization exotherm, proper glass stability criterion analyses could not be used for this material. Thus, the stability criteria are only analyzed for pure a-Se and a-Se:0.5%As films. Figure 4.3 and Figure 4.4 show a semi-logarithmic plot of fundamental and advanced glass stability criteria of pure a-Se and a-Se:0.5%As film samples.

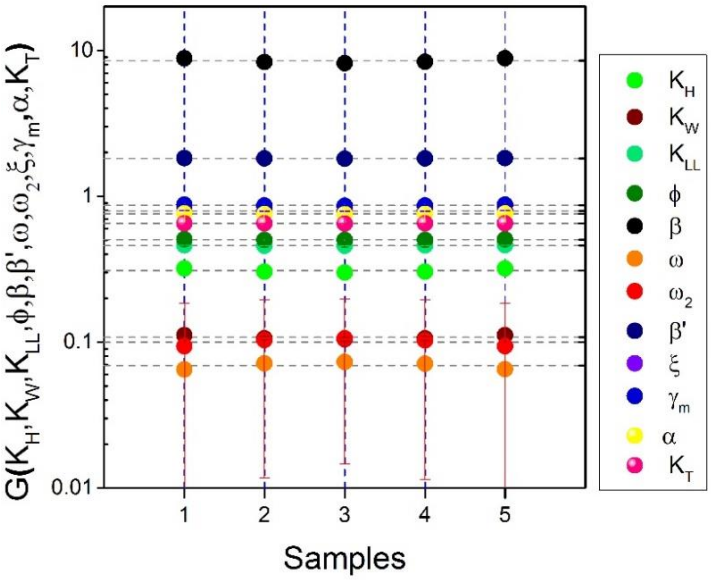

Figure 4.3 Semi-log plot of advanced glass stability criteria of pure a-Se samples.

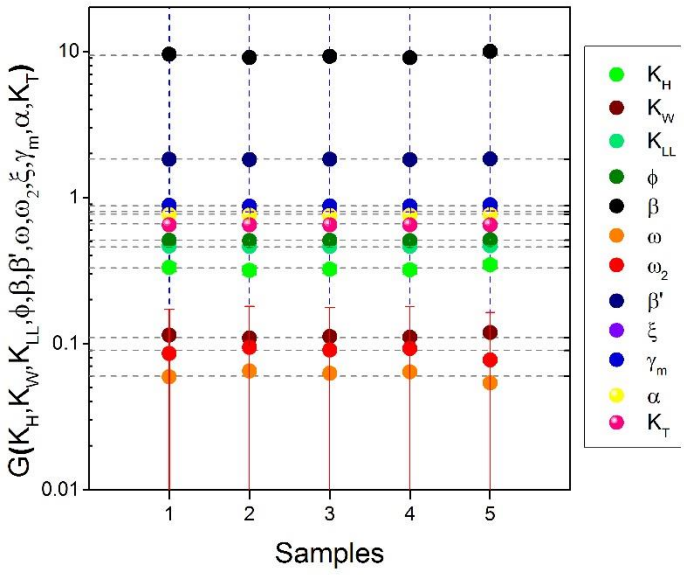

Figure 4.4 Semi-log plot of advanced glass stability criteria of a-Se:0.5%As samples.

For both pure a-Se and a-Se:0.5%As, the average advanced criteria ordering in magnitude can be given as $\beta > \beta' > \gamma_m > \xi > \alpha > K_T > \phi > K_{LL} > K_H > K_W > \omega_2 > \omega$. The criterion ordering is to be referred for comparison with the results of the upcoming sections. The comparisons are to be covered in Chapter 5.

In summary, statistical analysis was conducted to investigate the reproducibility of the onset characteristic temperatures. The glass stability of examined materials is therefore also analyzed in terms of statistical variations. The change in characteristic temperatures are compared with respect to As alloying and Cs doping. The variation and sensitivity of advanced glass stability criteria are investigated for each measured pure a-Se and a-Se:0.5%As samples. Amongst pure a-Se, a-Se:0.5%As and a-Se:6%As- 140 ppm Cs films, glass transition temperature (T_g) is the only characteristic temperature that can be compared. The data show that T_g increases by alloying with As. The crystallization temperature (T_x) shows a slight increase as a-Se is alloyed with As. This observation shows good correlation with bulk form a-Se based materials as shown in Figure 4.5.

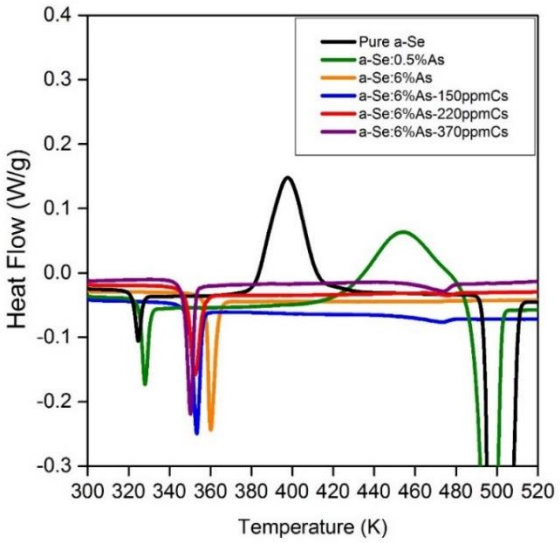

Figure 4.5 DSC thermograms of a-Se based bulk alloys.

4.3 X-ray Irradiated a-Se Based Alloy Thin Films

In the preliminary stage, the reproducibility experiment of characteristic temperatures and glass stability criteria of films with the same composition (either pure a-Se or a-Se:0.5%As) have been observed to be similar. The mean standard deviation, that defines the expected error in measurements, is observed to be small. The characteristic temperatures and glass stability criteria have been given to show similar amount of error for each composition. For this case, only one sample of each composition has been used in the study of x-ray irradiation effects.

A group of six unique samples from the same production set for each composition (as indicated in Chapter 3) are dosed with different amount of x-ray irradiation. DSC measurement is carried out for each sample right after x-ray irradiation, typically within 1 or 2 minutes.

Table 4.6 and Table 4.7 give the estimated absorbed dose, characteristic temperature and calculated glass stability criteria of pure a-Se samples.

Table 4.6 Absorbed x-ray dose, characteristic temperatures and fundamental glass stability criteria of x-ray irradiated pure a-Se samples.

N_S [3]	D (kGy)	T_g (K)	T_x (K)	T_m (K)	ΔT_{xg} (K)	ΔT_{mg} (K)	α	K_T
1	0	320.85	368.19	492.83	47.34	171.98	0.7471	0.651
2	5.6	320.70	371.53	492.81	50.83	172.11	0.7539	0.6508
3	10.8	320.26	371.16	493.03	50.9	172.77	0.7528	0.6496
4	26.9	320.21	371.45	493.26	51.24	173.05	0.7531	0.6492
5	37.7	320.13	372.17	492.73	52.04	172.6	0.7553	0.6497
6	53.8	320.06	375.06	492.91	55	172.85	0.7609	0.6493

Table 4.7 Advanced glass stability criteria of x-ray irradiated pure a-Se samples.

N_S	K_H	K_W	K_{LL}	ϕ	β	ω	ω_2	β'	ξ	γ_m
1	0.3798	0.0961	0.4525	0.4952	7.6043	0.0828	0.1211	1.7986	0.7796	0.8432
2	0.4191	0.1031	0.4567	0.5001	8.1005	0.0748	0.1085	1.8093	0.7876	0.857

[3] Number of the examined sample.

3	0.4177	0.1032	0.4564	0.4993	8.0033	0.0753	0.1092	1.8085	0.7867	0.8561
4	0.4207	0.1039	0.4566	0.4995	8.0162	0.0748	0.1084	1.8092	0.7871	0.8569
5	0.4317	0.1056	0.4579	0.5011	8.1971	0.0725	0.1049	1.8123	0.7895	0.8609
6	0.4667	0.1116	0.4613	0.5048	8.6432	0.066	0.0949	1.8212	0.796	0.8725

To investigate the possible changes (variations) in the characteristic temperatures and glass stability criteria with absorbed x-ray dose, the experimental values presented in the tables are normalized. Basically, normalization of a set of values is satisfied by dividing the values by the maximum value of the set. The normalization of the characteristic temperatures can be expressed as $T_n = T / T_{max}$, and $G_n = G / G_{max}$ for the glass stability criteria. This evaluation is referred in all the following figures in this chapter. The normalized characteristic temperatures and glass stability criteria of pure a-Se are shown in Figure 4.6, Figure 4.7 and Figure 4.8.

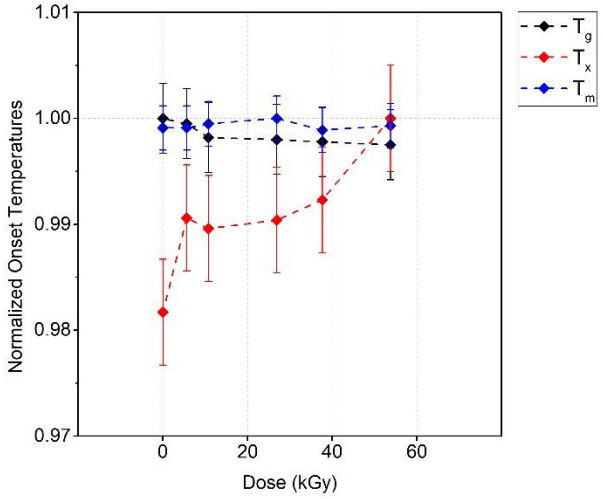

Figure 4.6 Normalized characteristic temperatures of pure a-Se samples.

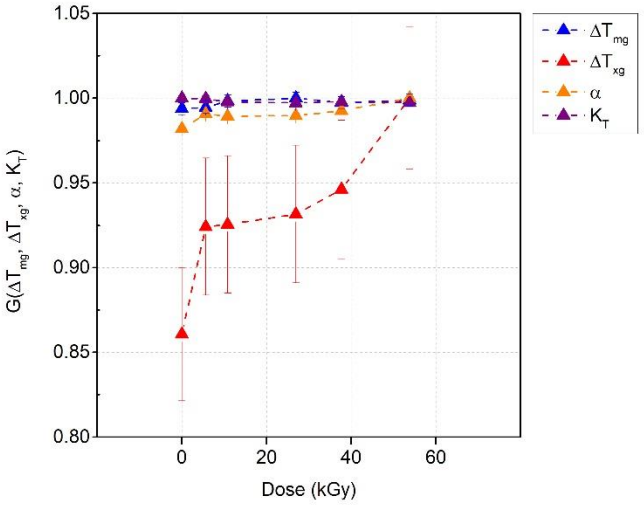

Figure 4.7 Normalized fundamental glass stability criteria of pure a-Se samples.

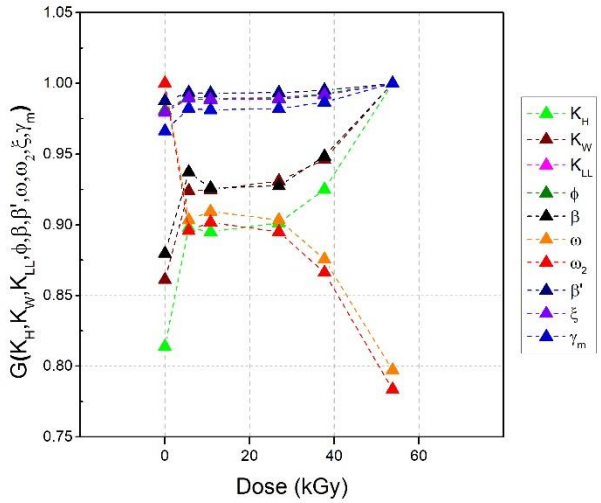

Figure 4.8 Normalized advanced stability criteria[4] of pure a-Se samples.

[4] For error analysis see Appendix C.

As observed in Figure 4.6, T_g and T_m have not been affected significantly by absorbed x-ray dose. On the other hand, T_x values increase with absorbed x-ray dose. In fact, the effect of irradiation on T_x can be seen for the sample with absorbed dose of 5.6 kGy. As it can be seen in Figure 4.7, the behaviour of ΔT_{xg} is directly driven by T_x, since the change in T_g are minimal. The variations in T_x with irradiation can also be detected in the α values shown Figure 4.7. The slight deviations in T_g and T_m produce nearly constant ΔT_{mg} and K_T. The rise of T_x values due to increasing absorbed x-ray dose causes a noticeable drop in ω and ω_2 criteria, seen in Figure 4.8. On the other hand, behaviour of K_H, K_W and β are directly related to this shift of T_x. Nonetheless, K_{LL}, β', ξ, ϕ and γ_m are observed to have a more stable behaviour.

Table 4.8 and Table 4.9 show the estimated absorbed dose, characteristic temperature and calculated glass stability criteria of a-Se:0.5%As samples.

Table 4.8 Absorbed x-ray dose, characteristic temperatures and fundamental glass stability criteria of x-ray irradiated a-Se:0.5%As samples.

N_S	D (kGy)	T_g (K)	T_x (K)	T_m (K)	ΔT_{xg} (K)	ΔT_{mg} (K)	α	K_T
1	0	324.06	385.52	492.58	61.46	168.52	0.7827	0.6579
2	11.0	322.3	374.91	490.53	52.61	168.23	0.7643	0.657
3	22.5	321.98	380.58	490.83	58.6	168.85	0.7754	0.656
4	56.2	321.99	379.22	490.28	57.23	168.29	0.7735	0.6567
5	83.1	322.14	382	489.37	59.86	167.23	0.7806	0.6583
6	122.6	321.92	379.79	489.08	57.87	167.16	0.7765	0.6582

Table 4.9 Advanced glass stability criteria of x-ray irradiated a-Se:0.5%As samples.

N_S	K_H	K_W	K_{LL}	ϕ	β	ω	ω_2	β'	ξ	γ_m
1	0.5741	0.1248	0.4721	0.5187	10.9	0.0469	0.0671	1.8475	0.8173	0.9074
2	0.455	0.1073	0.4612	0.507	9.039	0.0666	0.0968	1.8203	0.7974	0.8715
3	0.5315	0.1194	0.4682	0.5141	10.081	0.0538	0.0771	1.838	0.81	0.8948
4	0.5153	0.1167	0.4669	0.513	9.9	0.0563	0.081	1.8345	0.8077	0.8902
5	0.5575	0.1223	0.4707	0.5175	10.674	0.0494	0.0708	1.8441	0.815	0.9029
6	0.5295	0.1183	0.4683	0.515	10.24	0.0537	0.0773	1.838	0.8106	0.8949

Similar DSC measurements and evaluations of characteristic temperatures of x-ray irradiated a-Se:0.5%As samples have been carried out. Figure 4.9, Figure 4.10 and Figure 4.11 include the normalized characteristic temperatures and glass stability criteria of a-Se:0.5%As film samples.

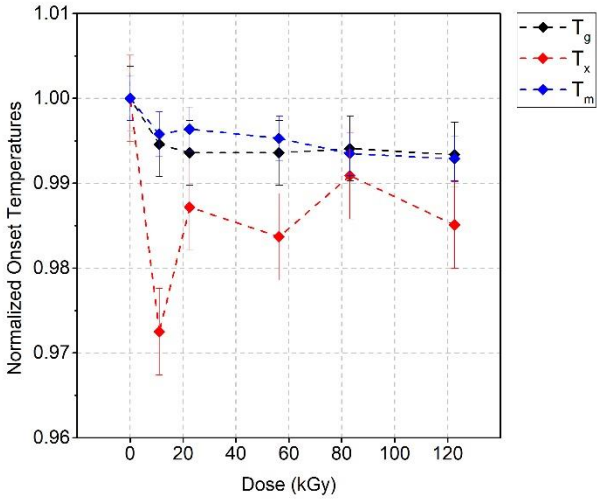

Figure 4.9 Normalized characteristic temperatures of a-Se:0.5%As samples.

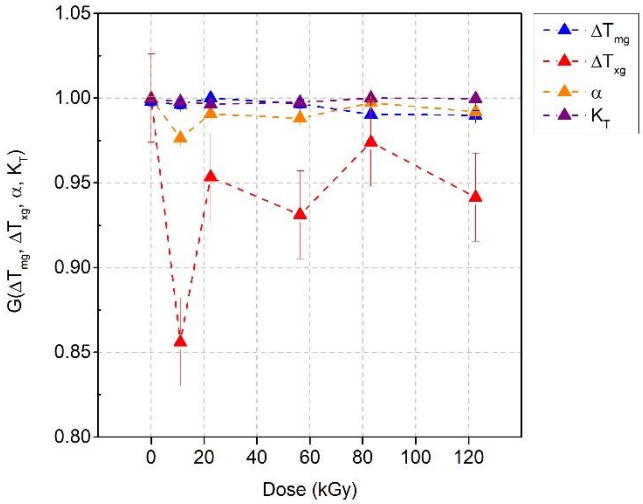

Figure 4.10 Normalized fundamental glass stability criteria of a-Se:0.5%As samples.

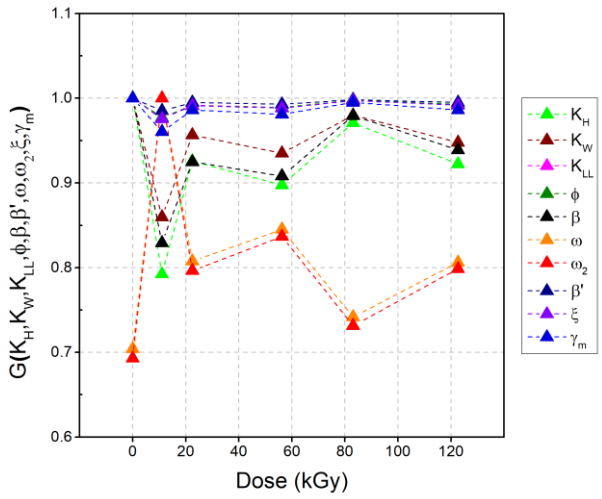

Figure 4.11 Normalized advanced glass stability criteria of a-Se:0.5%As samples.

The results for the a-Se:0.5%As samples show that higher absorbed x-ray doses lead to a slight decrease in all the characteristic temperatures. In fact, T_x is more affected by application of x-ray irradiation. However, the variation of T_x values are inconsistent, which disables to draw a correlation between this temperature and absorbed x-ray dose. On the other hand, T_g and T_m have a slight drop with absorbed x-ray dose, which is less than 1 percent (%). The more dominant variations in T_x affects ΔT_{xg} and α criteria, seen in Figure 4.10. Since T_g and T_m are more stable, ΔT_{xg} and K_T criteria look stable. In Figure 4.11, it has been observed that the behaviour of the K_H, K_W, and β criteria is similar to the behaviour of T_x. The ω and ω_2 criteria show significant variation, but in an inverse fashion with respect to T_x. The K_{LL}, β', ξ, ϕ and γ_m criteria are more stable.

The experimental procedure is repeated for a-Se:6%As-140 ppm Cs samples. The T_g and T_{xm} values of samples that had absorbed different x-ray doses are given in Table 4.10. The distributions of these characteristic temperatures are shown in Figure 4.12.

Table 4.10 Absorbed x-ray dose and characteristic temperatures of x-ray irradiated a-Se:6%As-140 ppm Cs samples.

N_S	D (kGy)	T_g (K)	T_{xm} (K)
1	0	333.41	473.63

2	12.2	342.82	476.43
3	24.9	343.9	476.7
4	59.2	346.69	473.83
5	89.3	343.43	471.11
6	131.5	345.53	470.12

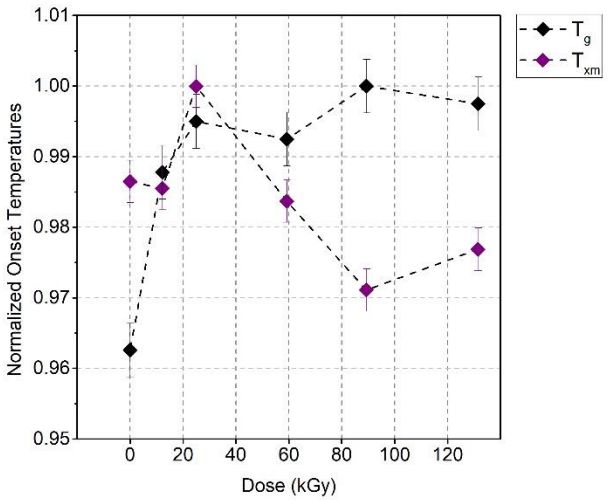

Figure 4.12 Normalized characteristic temperatures of a-Se:6%As-140 ppm Cs samples.

For a-Se:6%As-140 ppm Cs the T_g shifts towards higher temperatures with increasing x-ray dose. This shift can be considered as roughly 4%. There may be a correlation between the absorbed x-ray dose and T_g for this composition. Nevertheless, the T_{xm} shows an inconsistent variation, which seems that this temperature is independent of absorbed x-ray dose.

4.4 Relaxation of X-ray Irradiated a-Se Based Alloy Films at 295 K

As explained in the previous chapter, different x-ray doses are applied on 6 samples from each composition. After the x-ray irradiation, the samples are rested at room temperature, 295 K, for 5 hours. Subsequently, the samples are then scanned in the DSC.

Table 4.11 and Table 4.12 include the absorbed x-ray dose, measured characteristic onset temperatures and calculated glass stability criteria of pure a-Se samples.

Table 4.11 Absorbed x-ray dose, characteristic temperatures and fundamental glass stability criteria of x-ray irradiated pure a-Se samples.

N_S	D (kGy)	T_g (K)	T_x (K)	T_m (K)	ΔT_{xg} (K)	ΔT_{mg} (K)	α	K_T
1	0	320.81	368.22	492.74	47.41	171.93	0.7473	0.6511
2	5.6	320.64	372.65	492.84	52.01	172.2	0.7561	0.6506
3	10.8	320.5	374.11	492.92	53.61	172.42	0.759	0.6502
4	26.9	319.63	373.46	493.12	53.83	173.49	0.7573	0.6482
5	37.7	320.22	374.21	492.86	53.99	172.64	0.7593	0.6497
6	53.8	319.89	374.99	492.83	55.1	172.94	0.7609	0.6491

Table 4.12 Advanced glass stability criteria of x-ray irradiated pure a-Se samples.

N_S	K_H	K_W	K_{LL}	ϕ	β	ω	ω_2	β'	ξ	γ_m
1	0.3807	0.0962	0.4526	0.4953	7.6186	0.0826	0.1208	1.7989	0.7798	0.8435
2	0.4327	0.1055	0.4581	0.5016	8.2715	0.0721	0.1045	1.8128	0.7902	0.8617
3	0.4512	0.1088	0.4599	0.5035	8.4942	0.0687	0.0991	1.8175	0.7935	0.8677
4	0.4499	0.1092	0.4595	0.5024	8.3367	0.0693	0.0999	1.8166	0.7923	0.8665
5	0.455	0.1095	0.4602	0.5037	8.5119	0.0681	0.0981	1.8183	0.794	0.8688
6	0.4676	0.1118	0.4614	0.5047	8.6384	0.0659	0.0947	1.8213	0.796	0.8727

The normalized distribution of the characteristic temperatures and glass stability criteria can be observed in Figure 4.13, Figure 4.14 and Figure 4.15.

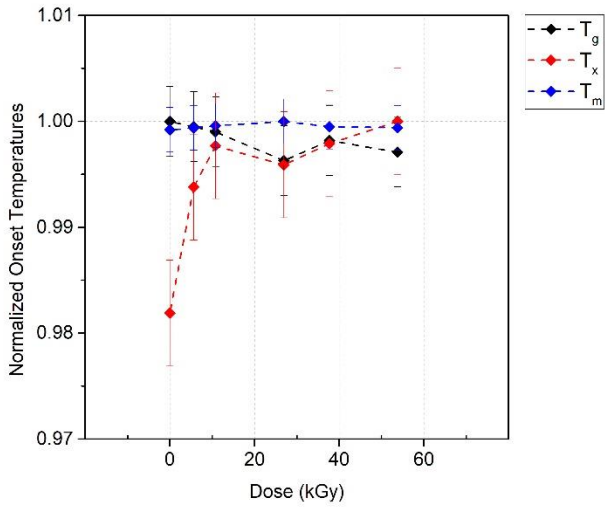

Figure 4.13 Normalized characteristic temperatures of pure a-Se samples.

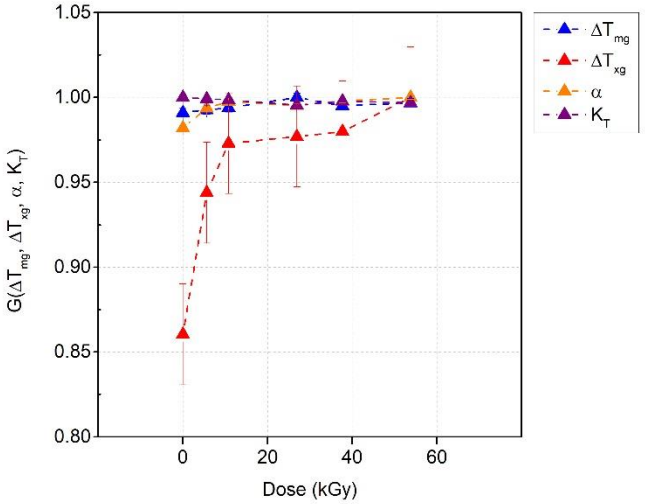

Figure 4.14 Normalized fundamental glass stability criteria of pure a-Se samples.

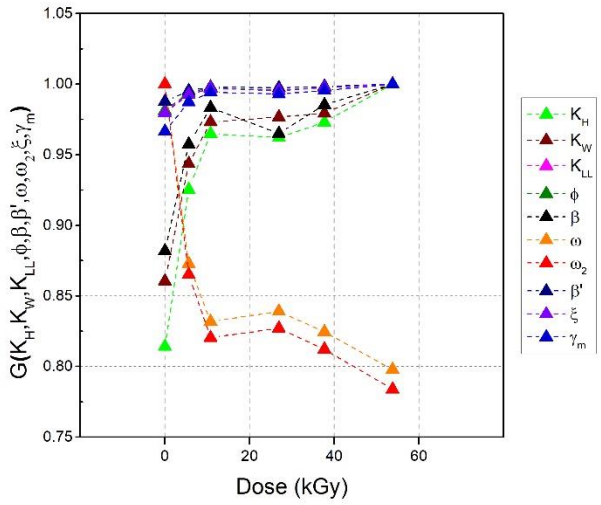

Figure 4.15 Normalized advanced glass stability criteria of pure a-Se samples.

5-hour at post irradiation resting at 295 K leads to a more significant change in the T_x values of pure a-Se samples. On the other hand, the T_g values tend to stay stable. The change in T_x with absorbed x-ray dose affects K_H, K_W, and β criteria. The drop in ω and ω_2 criteria is inversely related to the increase of the T_x. On the other hand, since T_g and T_m values are more stable, ΔT_{mg} and K_T values behave stable. Also, K_{LL}, β', ξ, ϕ and γ_m show stable behaviour.

The information of x-ray irradiation, characteristic temperatures and glass stability criteria of a-Se:0.5%As are given in Table 4.13 and Table 4.14.

Table 4.13 Absorbed x-ray dose, characteristic temperatures and fundamental glass stability criteria of x-ray irradiated a-Se:0.5%As samples.

N_S	D (kGy)	T_g (K)	T_x (K)	T_m (K)	ΔT_{xg} (K)	ΔT_{mg} (K)	α	K_T
1	0	322.42	380.09	490.62	57.67	168.2	0.7747	0.6572
2	11.1	322.49	380.56	490.54	58.07	168.05	0.7758	0.6574
3	22.0	322.3	378.92	490.93	56.62	168.63	0.7718	0.6565
4	57.2	322.22	380.37	490.63	58.15	168.41	0.7753	0.6567
5	84.1	322.46	382.78	489.33	60.32	166.87	0.7823	0.659
6	122.6	322.44	385.3	488.98	62.86	166.54	0.788	0.6594

Table 4.14 Advanced glass stability criteria of x-ray irradiated a-Se:0.5%As samples.

N_S	K_H	K_W	K_{LL}	ϕ	β	ω	ω_2	β'	ξ	γ_m
1	0.5218	0.1175	0.4675	0.5138	10.031	0.0552	0.0794	1.836	0.8089	0.8923
2	0.528	0.1184	0.4681	0.5145	10.147	0.0541	0.0778	1.8375	0.81	0.8942
3	0.5055	0.1153	0.4659	0.512	9.7341	0.0579	0.0835	1.8322	0.8059	0.8872
4	0.5274	0.1185	0.4679	0.5141	10.081	0.0543	0.078	1.8372	0.8096	0.8938
5	0.5661	0.1233	0.4715	0.5185	10.872	0.048	0.0688	1.846	0.8166	0.9055
6	0.6063	0.1286	0.4748	0.5219	11.557	0.0421	0.0601	1.8544	0.8226	0.9165

Distribution of normalized characteristic temperatures and glass stability criteria with respect to absorbed x-ray dose are given in Figure 4.16, Figure 4.17 and Figure 4.18.

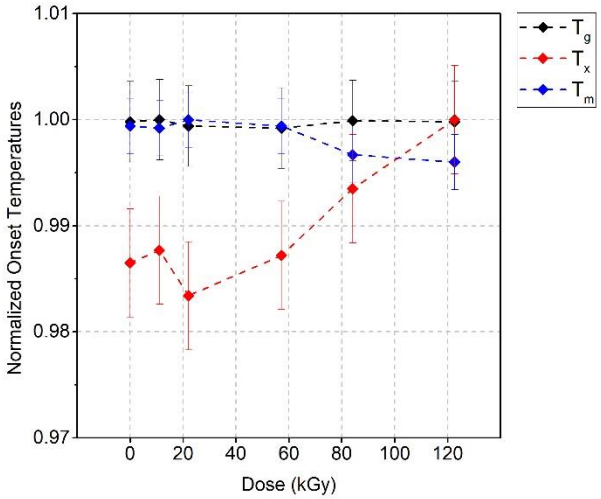

Figure 4.16 Normalized characteristic temperatures a-Se:0.5%As samples.

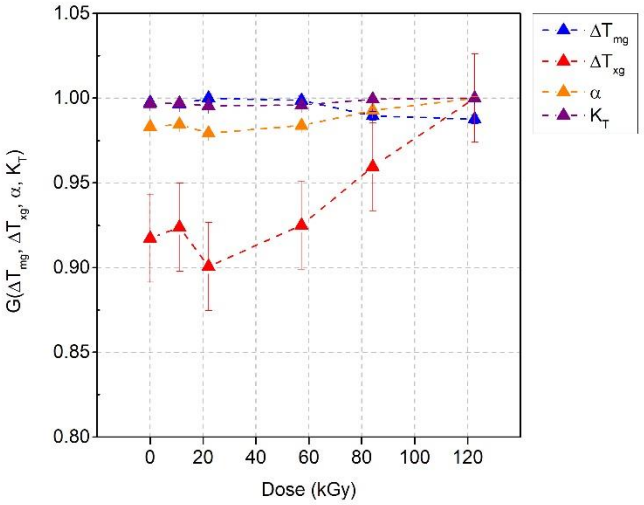

Figure 4.17 Normalized fundamental glass stability criteria a-Se:0.5%As samples.

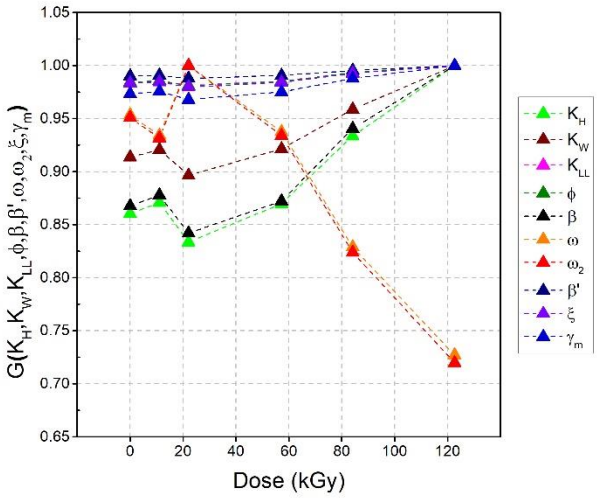

Figure 4.18 Normalized advanced glass stability criteria a-Se:0.5%As samples.

It is observed that 5-hour post irradiation resting leads to an increase in T_x of a-Se:0.5%As samples, specifically after absorbing 57.2 kGy. The T_g values seem to be unaffected, and exhibit a stable trend. There is an observable minor drop in the melting temperature for samples that have absorbed

more than 84.1 kGy. However, since the variation in T_m is 2%, this drop is essentially negligible. As observed in Figure 4.17 and Figure 4.18, the stable glass criteria are ΔT_{mg}, K_T K_{LL}, β', ξ, ϕ and γ_m, which follow trends that are similar to the ones of T_g and T_m values. Also observed in the previous results, it is the variation in T_x (rather than T_g) that controls the behaviour of the ΔT_{xg} for both a-Se:0.5%As samples. Similar correlation between ΔT_{xg} and K_H, K_W, ϕ and β are observed in Figure 4.17 and Figure 4.18. Also, β', ξ, γ_m, ϕ show direct correlation but minimal variation, where ω and ω_2 behave in an inverse fashion to the change in T_x.

The absorbed dose and measure characteristic temperatures of a-Se:6%As-140 ppm Cs samples are shown in Table 4.15.

Table 4.15 Absorbed x-ray dose and characteristic temperatures of x-ray irradiated a-Se:6%As-140 ppm Cs samples.

N_S	D (kGy)	T_g (K)	T_{xm} (K)
1	0	333.41	473.63
2	11.7	342.82	476.43
3	23.4	343.9	476.7
4	62.1	346.69	473.83
5	88.9	343.43	471.11
6	127.5	345.53	470.12

The distribution of characteristic temperatures of a-Se:6%As-140 ppm Cs samples with respect to absorbed x-ray dose is shown in Figure 4.19.

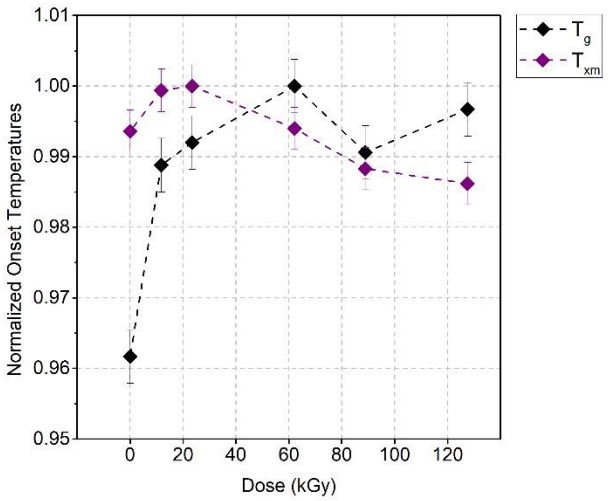

Figure 4.19 Normalized characteristic temperatures of a-Se:6%As-140 ppm Cs samples.

For a-Se:6%As-140 ppm Cs samples, the effect of the 5-hour resting period at 295 K results in an increase in the T_g. On the other hand, T_{xm} decreases with absorbed doses over 23.2 kGy.

4.5 Relaxation of X-ray Irradiated a-Se Based Alloy Films at 308 K

Experimental x-ray irradiation procedure is repeated for different sample sets of pure a-Se, a-Se:0.5%As and a-Se:6%As-140 ppm Cs. As described in Section 3.2.3, the 5-hour resting period is applied to the irradiated samples at an annealing temperature of 308 K. Table 4.16 and Table 4.17 show the results obtained from the measurements of pure a-Se samples.

Table 4.16 Characteristic temperatures and fundamental glass stability criteria of pure a-Se films relaxed at 308 K for 5 hours after x-ray irradiation.

N_S	D (kGy)	T_g (K)	T_x (K)	T_m (K)	ΔT_{xg} (K)	ΔT_{mg} (K)	α	K_T
1	0	310.68	367.81	492.95	57.13	182.27	0.7461	0.6302
2	7.3	311.22	368.39	493.03	57.17	181.81	0.7472	0.6312
3	14.4	311.42	368.66	492.94	57.24	181.52	0.7479	0.6318
4	36.1	311.68	368.81	492.87	57.13	181.19	0.7483	0.6324

5	50.6	312.2	368.96	493	56.76	180.8	0.7484	0.6333
6	72.1	312.42	369.07	493.01	56.65	180.59	0.7486	0.6337

Table 4.17 Advanced glass stability criteria of pure a-Se samples rested at 308 K for 5 hours x-ray after irradiation.

N_S	K_H	K_W	K_{LL}	ϕ	β	ω	ω_2	β'	ξ	γ_m
1	0.4565	0.1159	0.4577	0.4947	7.297	0.0715	0.1009	1.8141	0.7856	0.862
2	0.4587	0.116	0.4581	0.4954	7.3801	0.0709	0.1001	1.8149	0.7864	0.8632
3	0.4606	0.1161	0.4583	0.4959	7.4331	0.0704	0.0994	1.8156	0.787	0.864
4	0.4605	0.1159	0.4584	0.4961	7.4688	0.0703	0.0994	1.8157	0.7873	0.8642
5	0.4576	0.1151	0.4582	0.4963	7.4867	0.0707	0.1001	1.8151	0.7871	0.8635
6	0.4571	0.1149	0.4582	0.4964	7.5063	0.0707	0.1002	1.815	0.7872	0.8635

Figure 4.20, Figure 4.21 and Figure 4.22 show the results obtained for pure a-Se samples.

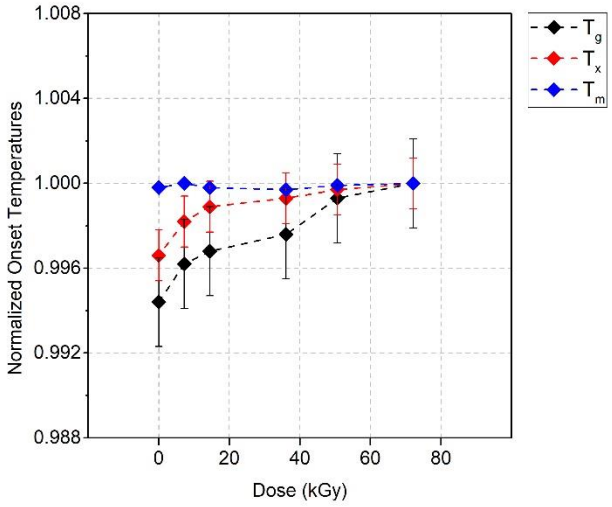

Figure 4.20 Normalized characteristic temperatures pure a-Se samples rested at 308 K for 5 hours after x-ray irradiation.

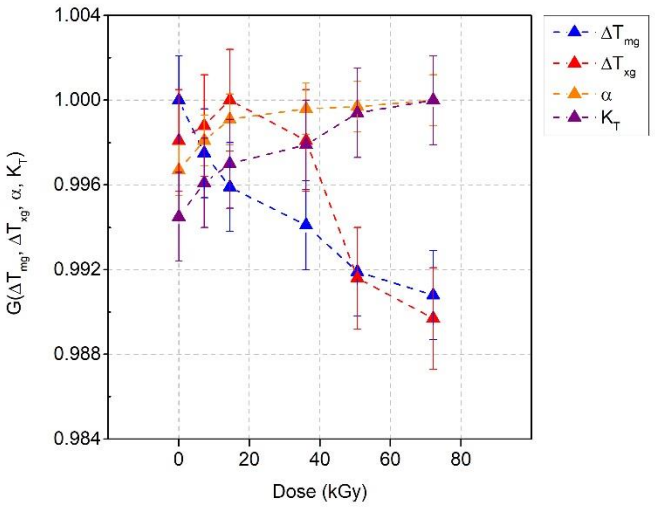

Figure 4.21 Normalized fundamental glass stability criteria pure a-Se samples rested at 308 K for 5 hours after x-ray irradiation.

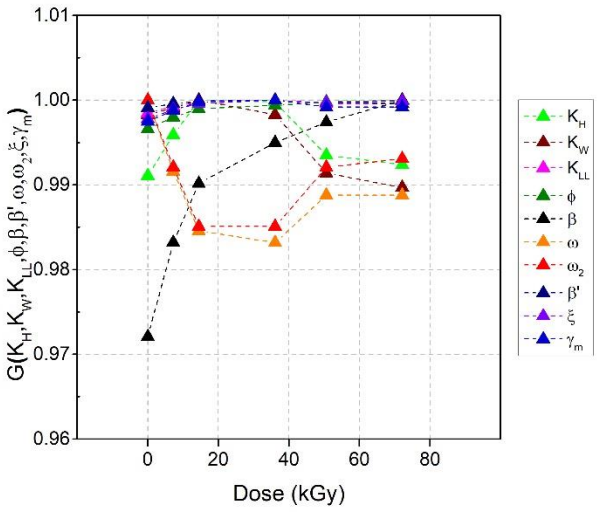

Figure 4.22 Normalized advanced glass stability criteria pure a-Se samples rested at 308 K for 5 hours after x-ray irradiation.

In the most reasonable case, it can be said that the elevation of annealing temperature to 308K shows a noteworthy effect in pure a-Se samples. It is observed in Figure 4.20 that the T_g and T_x increase with the absorbed x-ray dose. The increase in the T_g is larger than in the T_x by 0.2%. T_m, as would be expected, appears to be constant. Thus, seen in Figure 4.21, the drop in ΔT_{mg} can be directly related to the increase in T_g with respect to increasing absorbed x-ray dose. K_T and α criteria show minimal increase due to the increase in T_g and T_x. Samples receiving up to an absorbed dose of 14.4 kGy show an increase in their ΔT_{xg}. However, this interval drops for samples receiving higher doses. In Figure 4.22, the advanced glass stability criteria show interesting results. The ω and ω_2 criteria do not follow a similar trend for doses above 14.4 kGy. However, this inconsistency appears within the normalized range between 0.98 and 1. Apparently, all the variations that appear for some advanced glass stability criteria are within a very small normalized range, which in other words represent a negligible uncertainty range (<5%). Thus, it can be said that the criteria are quite stable. Specifically, the most stable criteria again appear to be β', ξ, (γ_m), ϕ and K_{LL}. The order of variation in the stability criteria can be given as $\omega > \omega_2 > K_W > K_H$. As a noteworthy fact, the only criterion that shows a significant increase with absorbed x-ray dose is the β criterion.

The results obtained from the measurements of a-Se:0.5%As samples are shown in Table 4.18 and Table 4.19.

Table 4.18 Characteristic temperatures and fundamental glass stability criteria of a-Se:0.5%As rested at 308 K for 5 hours after x-ray irradiation.

N_S	D (kGy)	T_g (K)	T_x (K)	T_m (K)	ΔT_{xg} (K)	ΔT_{mg} (K)	α	K_T
1	0	313.96	380.74	489.95	66.78	175.99	0.7771	0.6408
2	10.2	312.81	378.06	490.33	65.25	177.52	0.771	0.638
3	20.6	313.26	376.97	490.42	63.71	177.16	0.7687	0.6388
4	50.7	312.5	379.35	489.84	66.85	177.34	0.7744	0.638
5	72.8	313.14	378.79	489.44	65.65	176.3	0.7739	0.6398
6	104.0	313.05	377.43	490.33	64.38	177.28	0.7697	0.6384

Table 4.19 Advanced glass stability criteria of a-Se:0.5%As rested at 308 K for 5 hours after x-ray irradiation.

N_S	K_H	K_W	K_{LL}	ϕ	β	ω	ω_2	β'	ξ	γ_m

1	0.6115	0.1363	0.4736	0.5136	10.023	0.0435	0.0608	1.8535	0.8162	0.9134
2	0.5812	0.1331	0.4707	0.5099	9.3824	0.0484	0.0677	1.8466	0.8105	0.9041
3	0.5616	0.1299	0.4691	0.5087	9.1749	0.0514	0.0721	1.8421	0.8078	0.8986
4	0.605	0.1365	0.4728	0.5117	9.7106	0.0448	0.0624	1.8519	0.8142	0.9109
5	0.5933	0.1341	0.472	0.5117	9.688	0.0464	0.0648	1.8494	0.8131	0.9081
6	0.5702	0.1313	0.4698	0.5092	9.2696	0.0501	0.0701	1.8441	0.809	0.901

Figure 4.23, Figure 4.24 and Figure 4.25 show the normalized plots obtained for a-Se:0.5%As samples.

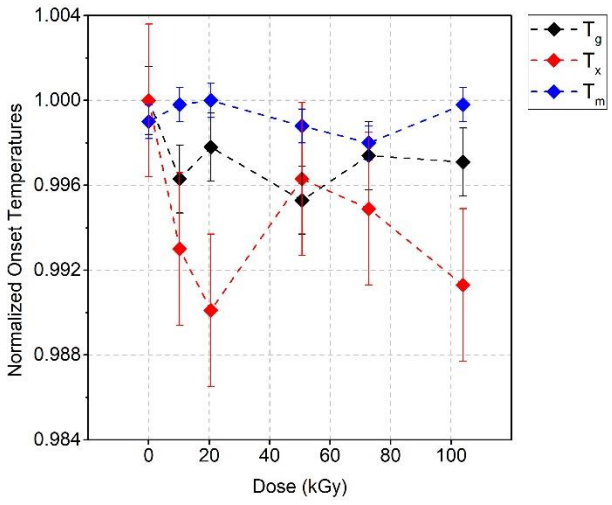

Figure 4.23 Normalized characteristic temperatures a-Se:0.5%As samples rested at 308 K for 5 hours after x-ray irradiation.

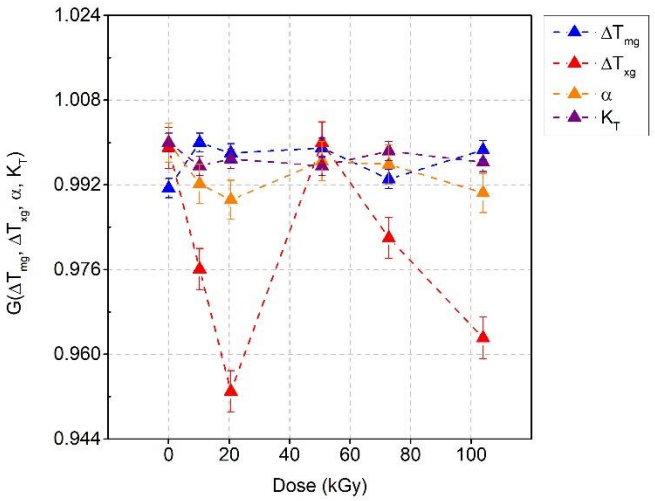

Figure 4.24 Normalized fundamental glass stability criteria of a-Se:0.5%As samples rested at 308 K for 5 hours after x-ray irradiation.

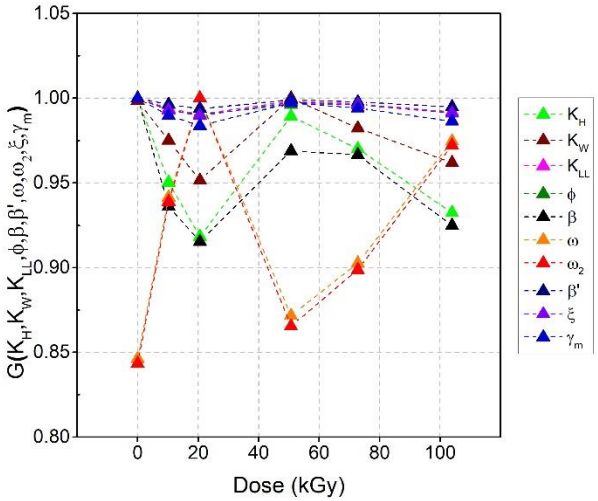

Figure 4.25 Normalized advanced glass stability criteria of a-Se:0.5%As samples rested at 308 K for 5 hours after x-ray irradiation.

Unlike in pure a-Se, the annealing temperature of 308 K has a very small influence on the a-Se:0.5%As samples. Observed in Figure 4.23, the variations of T_g and T_x fall in the normalized range between 0.988 and 1. Thus, as seen in Figure 4.24, ΔT_{mg}, α and K_T are not affected from the change of the characteristic temperatures. This provides an argument that the phases that exist during DSC heating do not have a significant shift upon irradiation. The only significant variation appears in ΔT_{xg} due to variation of T_x. In Figure 4.25, the advanced criteria, β', ξ, γ_m, ϕ and K_{LL} show minimal variation due to the variation in T_x. Moreover, K_H and K_W follow the trend of ΔT_{xg}, where β follows α. In addition, ω and ω_2 show an inverse trend with respect to the trend of T_x, as it has been observed in the previous sections.

The absorbed x-ray doses and evaluated characteristic temperatures of a-Se:6%As-140 ppm Cs samples for this experimental stage are given in Table 4.20.

Table 4.20 Characteristic temperatures of a-Se:6%As-140 ppm Cs samples rested at 308 K for 5 hours after x-ray irradiation.

N_S	D (kGy)	T_g (K)	T_{xm} (K)
1	10.6	333.41	477.19
2	20.9	333.7	476.46
3	52.4	333.87	477.32
4	77.0	334.21	477.95
5	102.1	333.96	478.89

The distribution of characteristic temperatures of a-Se:6%As-140 ppm Cs samples with respect to absorbed x-ray dose is shown in Figure 4.26.

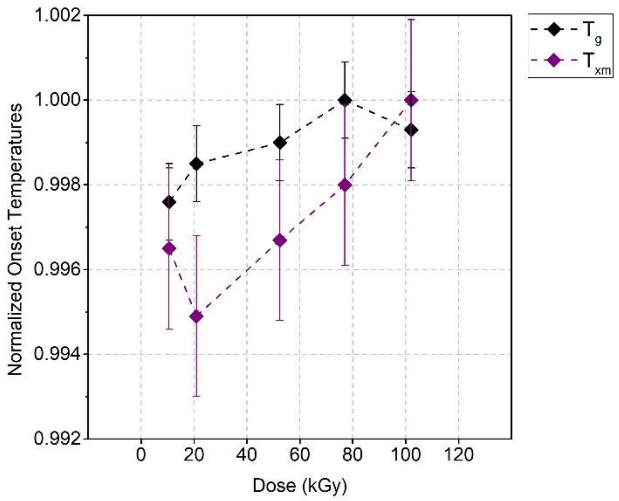

Figure 4.26 Normalized characteristic temperatures a-Se:6%As-140 ppm Cs samples rested at 308 K for 5 hours after x-ray irradiation.

The T_g values obtained for a-Se:6%As-140 ppm Cs samples are quite stable. The T_{xm} is also stable but more sensitive to the absorbed x-ray dose. However, the variations of both T_g and T_{xm} do not show a proportional change with respect to the absorbed dose or annealing temperature.

4.6 Relaxation of X-ray Irradiated a-Se Based Alloy Films at 328 K

The 5-hour post irradiation resting was applied for samples at 328 K for the studied compositions. Tables 4.21 and 4.22 show the results obtained from the measurements of pure a-Se samples.

Table 4.21 Characteristic temperatures and fundamental glass stability criteria of pure a-Se samples rested at 328 K for 5 hours after x-ray irradiation.

N_S	D (kGy)	T_g (K)	T_x (K)	T_m (K)	ΔT_{xg} (K)	ΔT_{mg} (K)	α	K_T
1	0	308.92	361.29	492.9	52.37	183.98	0.733	0.6267
2	7.3	309.17	362.07	493.14	52.9	183.97	0.7342	0.6269

3	14.7	310.05	362.41	493.1	52.36	183.05	0.735	0.6288
4	36.9	310.19	363.23	492.96	53.04	182.77	0.7368	0.6292
5	50.9	310.48	363.87	492.99	53.39	182.51	0.7381	0.6298
6	73.6	310.77	363.97	492.92	53.2	182.15	0.7384	0.6305

Table 4.22 Advanced glass stability criteria of pure a-Se samples rested at 328 K for 5 hours after x-ray irradiation.

N_S	K_H	K_W	K_{LL}	ϕ	β	ω	ω_2	β'	ξ	γ_m
1	0.3979	0.1062	0.4506	0.4863	6.4435	0.0845	0.1201	1.7963	0.7717	0.8392
2	0.4036	0.1073	0.4513	0.4871	6.516	0.0832	0.1181	1.798	0.773	0.8415
3	0.4006	0.1062	0.4512	0.4876	6.5788	0.0834	0.1187	1.7977	0.7733	0.8411
4	0.4088	0.1076	0.4523	0.4888	6.6947	0.0815	0.1159	1.8002	0.7753	0.8444
5	0.4135	0.1083	0.4529	0.4896	6.7763	0.0804	0.1143	1.8017	0.7765	0.8464
6	0.4126	0.1079	0.4529	0.4898	6.8024	0.0805	0.1145	1.8017	0.7766	0.8463

Figure 4.27, Figure 4.28 and Figure 4.29 show the results obtained for pure a-Se samples rested at 328 K for 5 hours after x-ray irradiation.

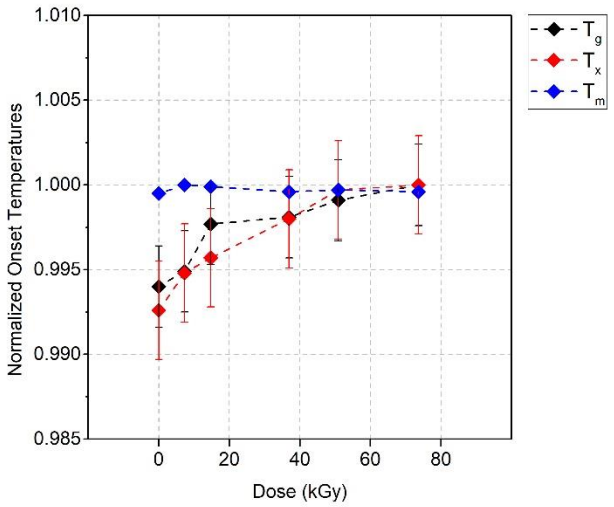

Figure 4.27 Normalized characteristic temperatures pure a-Se samples rested at 328 K for 5 hours after x-ray irradiation.

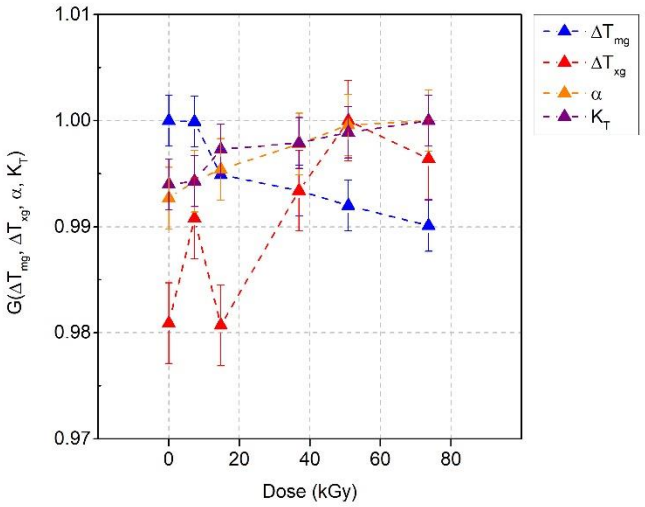

Figure 4.28 Normalized fundamental glass stability criteria of pure a-Se samples rested at 328 K for 5 hours after x-ray irradiation.

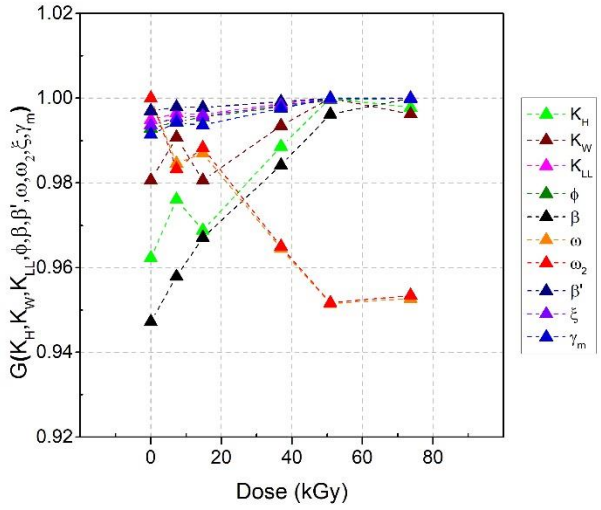

Figure 4.29 Normalized advanced glass stability criteria of pure a-Se samples rested at 328 K for 5 hours after x-ray irradiation.

In Figure 4.27, T_g and T_x show minimal increase with deposited dose. However, T_x shows a tendency to increase with deposited dose. The relatively higher amount of increase in T_g can be detected in the drop of ΔT_{mg}, which can be seen in Figure 4.28. The behaviour of T_x with respect to deposited dose is clearly observed in the behavior of ΔT_{xg}. and in K_H and K_W criteria, which can be seen in Figure 4.29. In contrast, ω and ω_2 show similar inverse correlation with T_x, has also been observed in the previous stages. The β criterion shows a proportional increase with absorbed x-ray dose. This resembles the behaviour of the β criterion obtained for annealing at 308 K. K_T and α show less variation than the above mentioned fundamental criteria. β', ξ, γ_m, ϕ and K_{LL}, again show minimal change.

The results obtained from the measurements of a-Se:0.5%As samples are shown in Table 4.23 and Table 4.24.

Table 4.23 Characteristic temperatures and fundamental glass stability criteria of a-Se:0.5%As samples rested at 328 K for 5 hours after x-ray irradiation.

N_S	D (kGy)	T_g (K)	T_x (K)	T_m (K)	ΔT_{xg} (K)	ΔT_{mg} (K)	α	K_T
1	0	311.63	381.08	489.68	69.45	178.05	0.7782	0.6364

2	10.9	311.54	366.49	489.16	54.95	177.62	0.7492	0.6369
3	22.9	311.53	381.01	489.37	69.48	177.84	0.7786	0.6366
4	55.6	311.42	376.85	490.14	65.43	178.72	0.7689	0.6354
5	81.3	312.18	382.68	489.69	70.5	177.51	0.7815	0.6375
6	113.1	312.73	374.39	488.58	61.66	175.85	0.7663	0.6401

Table 4.24 Advanced glass stability criteria of a-Se:0.5%As samples rested at 328 K for 5 hours after x-ray irradiation.

N_S	K_H	K_W	K_{LL}	ϕ	β	ω	ω_2	β'	ξ	γ_m
1	0.6395	0.1418	0.4756	0.5134	10.069	0.04	0.0553	1.8593	0.8186	0.92
2	0.4479	0.1123	0.4577	0.4969	7.5875	0.0719	0.1023	1.8133	0.7868	0.8616
3	0.6412	0.142	0.4757	0.5137	10.109	0.0397	0.0549	1.8596	0.819	0.9206
4	0.5775	0.1335	0.4701	0.5083	9.1439	0.0493	0.0688	1.8455	0.809	0.9024
5	0.6588	0.144	0.4772	0.5153	10.433	0.0371	0.0514	1.8633	0.8217	0.9254
6	0.54	0.1262	0.4672	0.5075	8.9792	0.0548	0.0771	1.8372	0.8048	0.8925

Figure 4.30, Figure 4.31 and Figure 4.32 show the results obtained for a-Se:0.5%As samples rested at 328 K for 5 hours after x-ray irradiation.

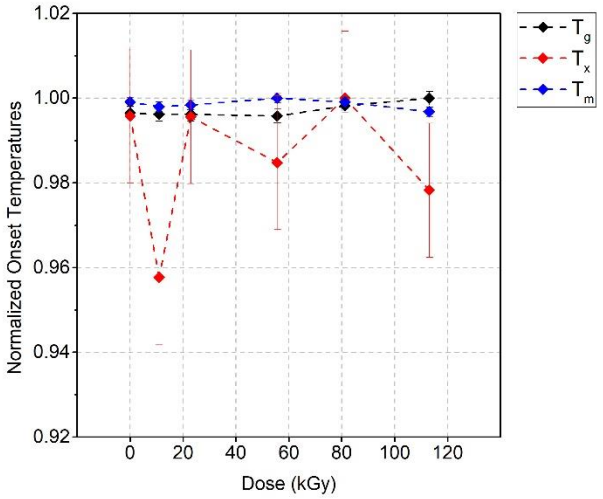

Figure 4.30 Normalized characteristic temperatures a-Se:0.5%As samples rested at 328 K for 5 hours after x-ray irradiation.

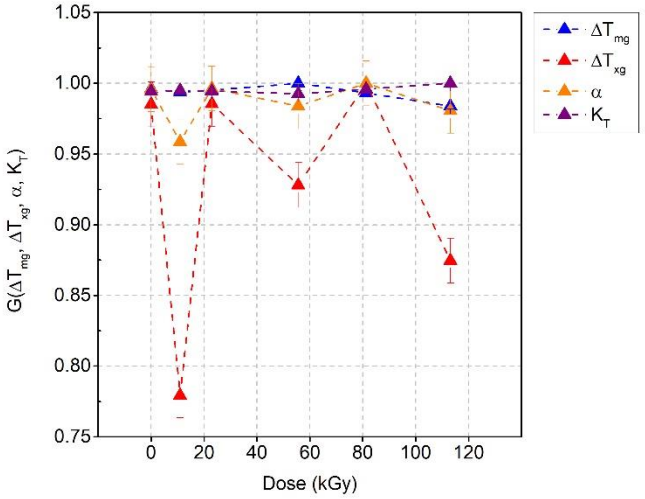

Figure 4.31 Normalized fundamental glass stability criteria a-Se:0.5%As samples rested at 328 K for 5 hours after x-ray irradiation.

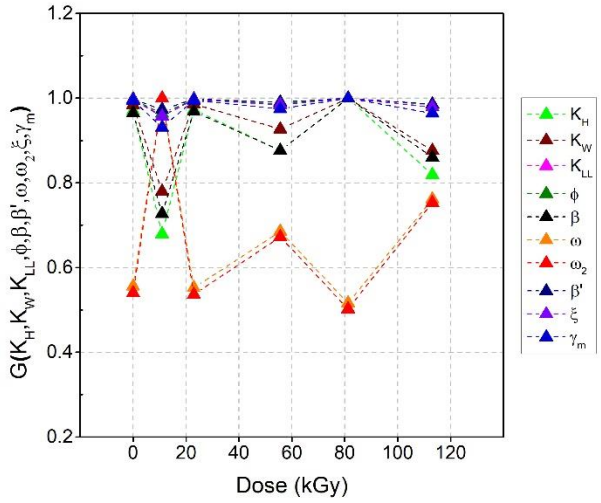

Figure 4.32 Normalized advanced glass stability criteria a-Se:0.5%As samples rested at 328 K for 5 hours after x-ray irradiation.

For a-Se:0.5%As samples, T_g appears to be quite stable. This condition is also noticed for ΔT_{mg} and K_T in Figure 4.31. In contrast, T_x appears to be very unstable, which is also observed in the behaviour of ΔT_{xg} and α, and in K_H, K_w and β, which can be observed in Figure 4.32. The ω and ω_2 criteria show an inverse relation to the behaviour to T_x as in pure a-Se. The β', ξ, γ_m, ϕ and K_{LL} criteria show minimal change.

Table 4.25 gives the results obtained from a-Se:6%As-140 ppm Cs samples rested at 328 K for 5 hours after x-ray irradiation.

Table 4.25 Characteristic temperatures criteria of a-Se:6%As-140 ppm Cs samples rested at 328 K for 5 hours after x-ray irradiation.

N_S	D (kGy)	T_g (K)	T_{xm} (K)
1	10.6	332.2	478.75
2	20.9	331.03	478.81
3	52.4	331.97	478.73
4	77.0	319.18	478.63
5	102.1	320.09	478.78

The absorbed x-ray dose and evaluated characteristic temperatures of a-Se:6%As-140 ppm Cs samples rested at 328 K after x-ray irradiation are given in Figure 4.33.

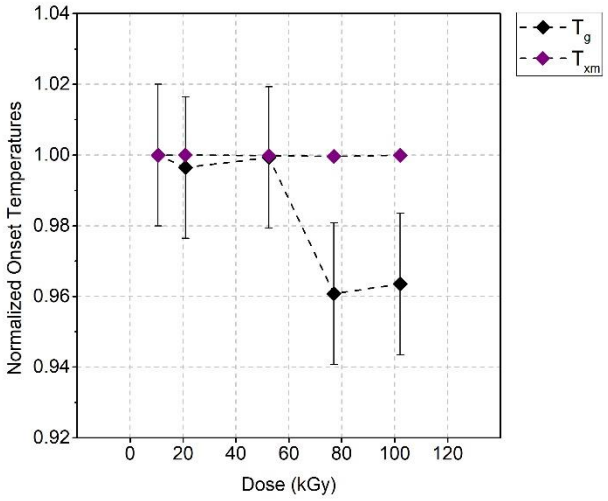

Figure 4.33 Normalized characteristic temperatures a-Se:6%As-140ppmCs samples rested at 328 K for 5 hours after x-ray irradiation.

The a-Se:6%As-140 ppm Cs samples rested at 328 K show very stable T_{xm}. The T_g values are stable up to nearly an absorbed dose of 52.4 kGy, beyond which it falls by 6% with further irradiation.

4.7 Extended Post Irradiation Resting Periods at 308 K

The results of the experiments of extended post irradiation periods of equally irradiated samples at 308 K-annealing temperature are presented in this section. Table 4.26 and Table 4.27 show the results obtained for pure a-Se samples.

Table 4.26 Characteristic temperatures and fundamental glass stability criteria of pure a-Se samples rested at 308 K with extending post irradiation resting periods.

N_S	t_r (hr)	T_g (K)	T_x (K)	T_m (K)	ΔT_{xg} (K)	ΔT_{mg} (K)	α	K_T
1	1	317.37	370.81	493.3	53.44	175.93	0.7517	0.6434
2	2	313.64	364.81	493.1	51.17	179.46	0.7398	0.6361

3	5	312.55	362.58	493	50.03	180.45	0.7355	0.634
4	10	311.55	359.41	493.05	47.86	181.5	0.729	0.6319
5	24	311.37	356.9	493.1	45.53	181.73	0.7238	0.6315

Table 4.27 Advanced glass stability criteria of pure a-Se samples rested at 308 K with extending post irradiation resting periods.

N_S	K_H	K_W	K_{LL}	ϕ	β	ω	ω_2	β'	ξ	γ_m
1	0.4363	0.1083	0.4574	0.4987	7.8436	0.0729	0.1047	1.8117	0.7875	0.86
2	0.3989	0.1038	0.4522	0.4908	6.952	0.0822	0.1179	1.7992	0.7763	0.8436
3	0.3836	0.1015	0.4501	0.4879	6.6625	0.086	0.1235	1.794	0.772	0.8369
4	0.3581	0.0971	0.4467	0.4834	6.2697	0.0924	0.1331	1.7855	0.765	0.826
5	0.3343	0.0923	0.4436	0.4797	5.9906	0.0983	0.1423	1.7777	0.759	0.8161

Figure 4.34, Figure 4.35 and Figure 4.36 present the normalized plot of characteristic temperatures and glass stability criteria of pure a-Se used in the measurements.

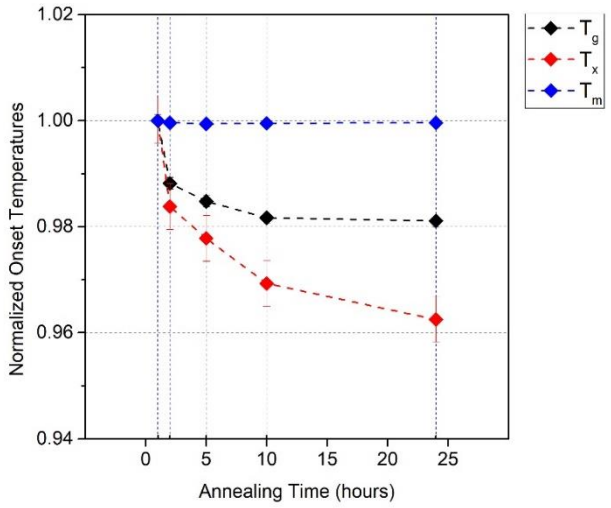

Figure 4.34 Normalized characteristic temperatures pure a-Se samples rested at 308 K with extending post irradiation resting periods.

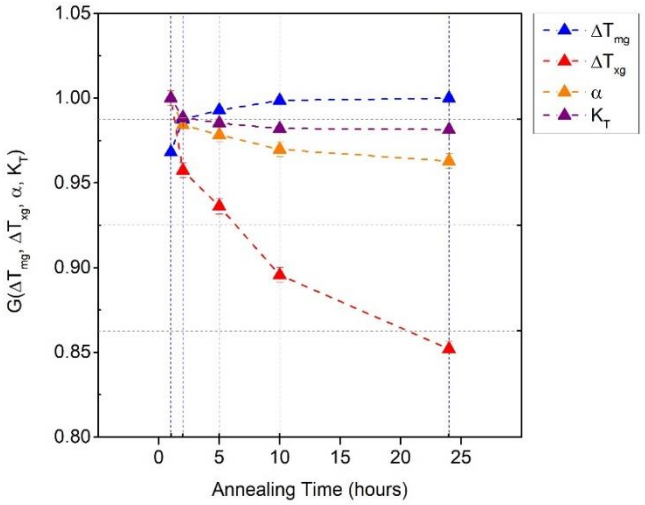

Figure 4.35 Normalized fundamental glass stability criteria of pure a-Se samples rested at 308 K with extending post irradiation resting periods.

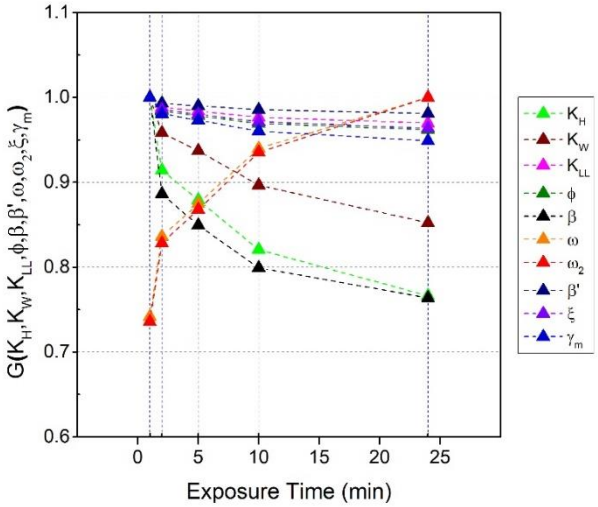

Figure 4.36 Normalized advanced glass stability criteria of pure a-Se samples rested at 308 K with extending post irradiation resting periods.

It can be observed in Figure 4.34 that T_g and T_x decrease with increasing annealing time (period). In fact, the decreasing trend of the drop is exponential-like for both T_g and T_x. Apparently, the T_x is more sensitive to the increasing annealing period than the T_g, based on the percentage drop that can be obtained from the graph. As observed in Figure 4.35, the drop in α is greater than the drop in K_T. Also, the trend of ΔT_{xg} signifies that the amount of drop in T_x is larger than that in the T_g. As observed in Figure 4.36, ω and ω_2 criteria increase with the annealing period. Surprisingly, the rest of the criteria decrease in an exponential-like trend. This trend is more significant in K_H, K_w and β, where for β', ξ, γ_m, ϕ and K_{LL} this behaviour is minimal.

Table 4.28 and Table 4.29 show the results obtained for a-Se:0.5%As samples rested at 308 K.

Table 4.28 Characteristic temperatures and fundamental glass stability criteria of a-Se:0.5%As samples rested at 308 K with extending post irradiation resting periods.

N_S	t_r (hr)	T_g (K)	T_x (K)	T_m (K)	ΔT_{xg} (K)	ΔT_{mg} (K)	α	K_T
1	1	319.5	372.55	489.88	53.05	170.38	0.7605	0.6522
2	2	317.6	364.78	490.09	47.18	172.49	0.7443	0.648
3	5	312.14	362.81	489.7	50.67	177.56	0.7409	0.6374
4	10	312.48	365.81	489.85	53.33	177.37	0.7468	0.6379
5	24	312.73	371.11	489.77	58.38	177.04	0.7577	0.6385

Table 4.29 Advanced glass stability criteria of a-Se:0.5%As samples rested at 308 K with extending post irradiation resting periods.

N_S	K_H	K_W	K_{LL}	ϕ	β	ω	ω_2	β'	ξ	γ_m
1	0.4521	0.1083	0.4603	0.5045	8.6464	0.0681	0.0985	1.8182	0.7946	0.8688
2	0.3765	0.0963	0.4516	0.4934	7.378	0.0842	0.1229	1.7966	0.7774	0.8406
3	0.3993	0.1035	0.4525	0.4915	7.0335	0.0818	0.1175	1.7997	0.7771	0.8444
4	0.4299	0.1089	0.4559	0.4954	7.4294	0.0753	0.1076	1.8086	0.7837	0.8556
5	0.492	0.1192	0.4624	0.5023	8.2426	0.0633	0.0896	1.8252	0.7958	0.8769

Figure 4.37, Figure 4.38 and Figure 4.39 present the normalized plot of characteristic temperatures and glass stability criteria of a-Se:0.5%As used in the measurements.

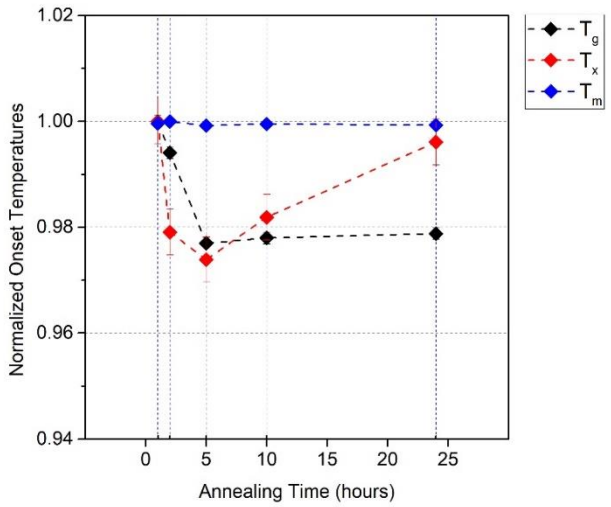

Figure 4.37 Normalized characteristic temperatures a-Se:0.5%As samples rested at 308 K with extending post irradiation resting periods.

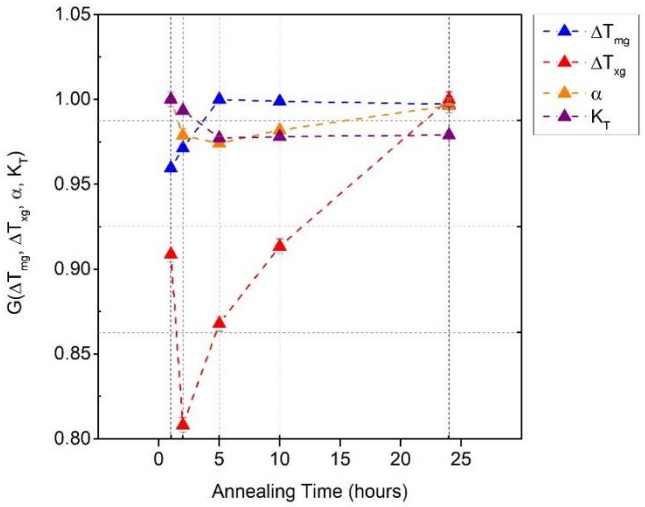

Figure 4.38 Normalized fundamental glass stability criteria of a-Se:0.5%As samples rested at 308 K with extending post irradiation resting periods.

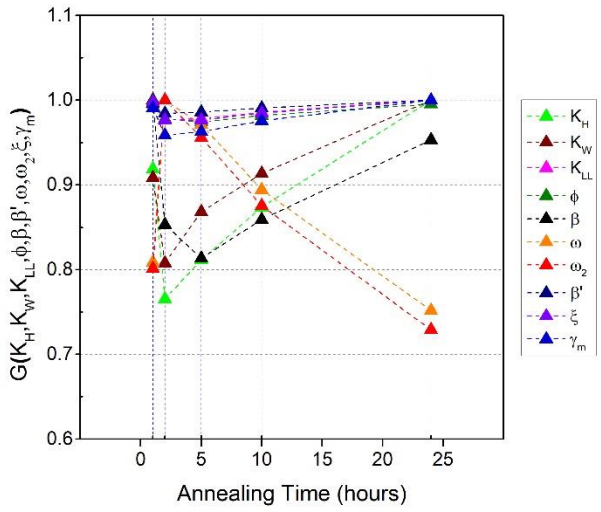

Figure 4.39 Normalized advanced glass stability criteria of a-Se:0.5%As samples rested at 308 K with extending post irradiation resting periods.

As can be seen from Figure 4.37, the annealing times have a different influence on the characteristic temperatures. T_g drops by nearly 2% when annealing time is increased to 5 hours. Consequently, it tends to stay approximately at constant value. On the other hand, the T_x drops for the samples rested for 1 hour, 2 hours and 5 hours. However, the recovery of this temperature is seen as for the samples annealed over 5 hours. In Figure 4.38, the recovery of T_x has a dominant effect on the ΔT_{xg}. In fact, this effect can be traced in α, K_H, K_w and β criteria, which can be seen in Figure 4.39. As observed in the previous results, the β', ξ, γ_m, ϕ and K_{LL} criteria show very small changes, but these variations are due to the changes in T_x. The ω and ω_2 criteria show a reciprocal behaviour with respect to other advanced criteria.

Table 4.30 shows the results for a-Se:6%As-140 ppm Cs.

Table 4.30 Characteristic temperatures of a-Se:6%As-140 ppm Cs samples rested at 308 K with extending post irradiation resting periods.

N_S	t_r (hr)	T_g (K)	T_{xm} (K)
1	1	335.31	478.48
2	2	335.42	478.29

3	5	340.43	478.31
4	10	341.48	477.78
5	24	340.03	478.07

Figure 4.40 shows the results obtained for a-Se:6%As-140 ppm Cs samples rested at 308 K.

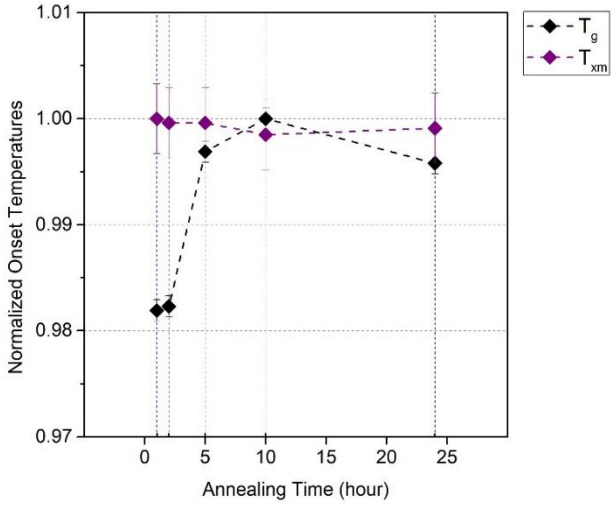

Figure 4.40 Normalized characteristic temperatures a-Se:6%As-140 ppm Cs samples rested at 308 K annealing temperature with extending post irradiation resting periods.

a-Se:6%As-140 ppm Cs samples show stable T_{xm} values. Uniquely, the T_g increases for samples annealed over 2 hours, which then stays nearly stable.

4.8 Extended Post Irradiation Resting Periods at 328 K

The extended post irradiation resting periods are applied for pure a-Se, a-Se:0.5%As and a-Se:6%As-140 ppm Cs samples. The samples are rested at 328 K, as described in Section 3.2.4. Table 4.31 and Table 4.32 show the results obtained for pure a-Se samples.

Table 4.31 Characteristic temperatures and fundamental glass stability criteria of pure a-Se samples rested at 328 K with extending post irradiation resting periods.

N_S	$t_{an.}$ (hr)	T_g (K)	T_x (K)	T_m (K)	ΔT_{xg} (K)	ΔT_{mg} (K)	α	K_T
1	1	312.82	374.5	493.01	61.68	180.19	0.7596	0.6345
2	2	312.08	366.76	493.05	54.68	180.97	0.7439	0.633
3	5	310.92	359.59	493.12	48.67	182.2	0.7292	0.6305
4	10	310.58	358.89	493.05	48.31	182.47	0.7279	0.6299
5	24	310.49	356.39	493.04	45.9	182.55	0.7228	0.6297

Table 4.32 Advanced glass stability criteria of pure a-Se samples rested at 328 K with extending post irradiation resting periods.

N_S	K_H	K_W	K_{LL}	ϕ	β	ω	ω_2	β'	ξ	γ_m
1	0.5205	0.1251	0.4647	0.503	8.3413	0.0589	0.0827	1.8317	0.7992	0.8847
2	0.433	0.1109	0.4555	0.4934	7.1765	0.0757	0.1076	1.8082	0.782	0.8548
3	0.3645	0.0987	0.4472	0.4836	6.2704	0.0913	0.1311	1.7871	0.7659	0.8279
4	0.3601	0.098	0.4466	0.4827	6.1928	0.0924	0.1328	1.7855	0.7645	0.8259
5	0.3359	0.0931	0.4435	0.4791	5.9259	0.0984	0.1421	1.7776	0.7585	0.8159

Figure 4.41, Figure 4.42 and Figure 4.43 give the normalized plot of characteristic temperatures and glass stability criteria of pure a-Se used in the measurements.

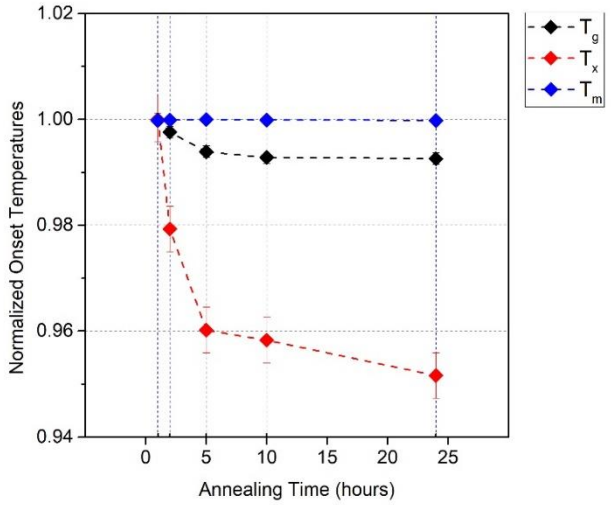

Figure 4.41 Normalized characteristic temperatures pure a-Se samples rested at 328 K with extending post irradiation resting periods.

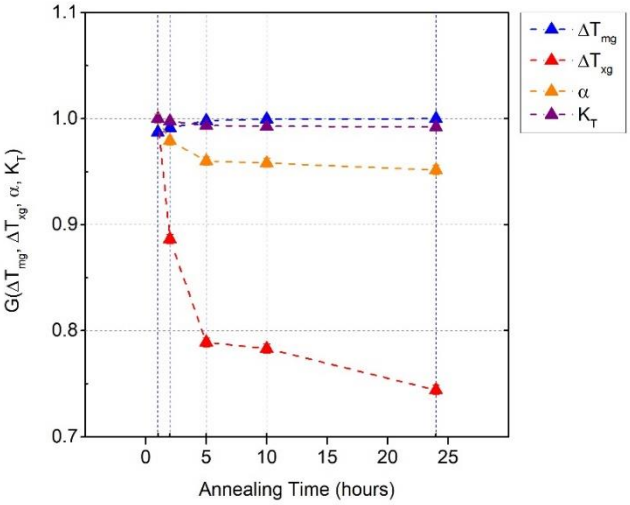

Figure 4.42 Normalized fundamental glass stability criteria of pure a-Se samples rested at 328 K with extending post irradiation resting periods.

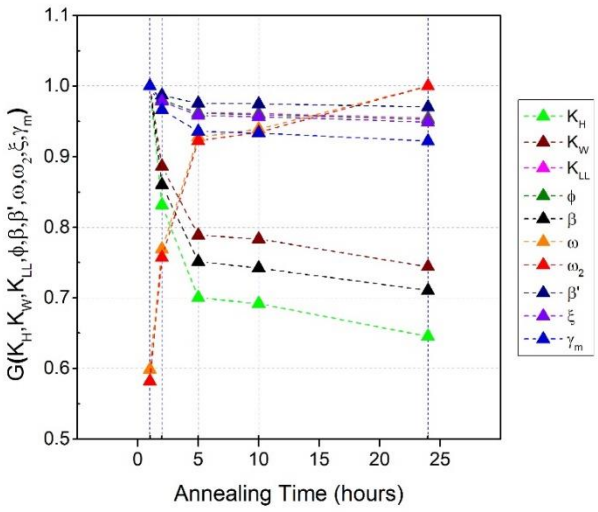

Figure 4.43 Normalized advanced glass stability criteria of pure a-Se samples rested at 328 K with extending post irradiation resting periods.

In Figure 4.41, the T_g slightly drops, where T_x values are more affected by the annealing time, dropping significantly within 1 to 5 hours of annealing period. Correspondingly, as observed in Figure 4.42, α and ΔT_{xg} criteria also drop. This shows that the drop of the T_x is more dominant than the drop of the T_g. Considering Figure 4.43, due to the small drift of T_g, the K_T and ΔT_{mg} criteria are nearly unaffected. The advanced criteria have similar outcomes as for those of the same composition that are annealed at 308 K.

Table 4.33 and Table 4.34 give the results obtained for a-Se:0.5%As samples rested at the annealing temperature of 328 K.

Table 4.33 Characteristic temperatures and fundamental glass stability criteria of a-Se:0.5%As samples rested at 328 K with extending post irradiation resting periods.

N_S	$t_{an.}$ (hr)	T_g (K)	T_x (K)	T_m (K)	ΔT_{xg} (K)	ΔT_{mg} (K)	α	K_T
1	1	311.13	374.76	490.28	63.63	179.15	0.7644	0.6346
2	2	311.7	373.02	490.37	61.32	178.67	0.7607	0.6356
3	5	312.21	372.73	490.2	60.52	177.99	0.7604	0.6369
4	10	312.33	380.53	490.34	68.2	178.01	0.7761	0.637

5	24	312.43	363.36	489.82	50.93	177.39	0.7418	0.6378

Table 4.34 Advanced glass stability criteria of a-Se:0.5%As samples rested at 328 K with extending post irradiation resting periods.

N_S	K_H	K_W	K_{LL}	ϕ	β	ω	ω_2	β'	ξ	γ_m
1	0.5508	0.1298	0.4676	0.5057	8.7374	0.0538	0.0751	1.8391	0.8044	0.8942
2	0.5225	0.125	0.4651	0.5038	8.4431	0.0584	0.082	1.8324	0.8	0.8857
3	0.5152	0.1235	0.4645	0.5037	8.4331	0.0594	0.0837	1.8307	0.7993	0.8838
4	0.6211	0.1391	0.4741	0.5124	9.8564	0.0425	0.0591	1.8553	0.8162	0.9151
5	0.4027	0.104	0.4529	0.4921	7.0988	0.081	0.1163	1.8009	0.778	0.8458

Figure 4.44, Figure 4.45 and Figure 4.46 show the normalized characteristic temperatures and glass stability criteria for the a-Se:0.5%As samples.

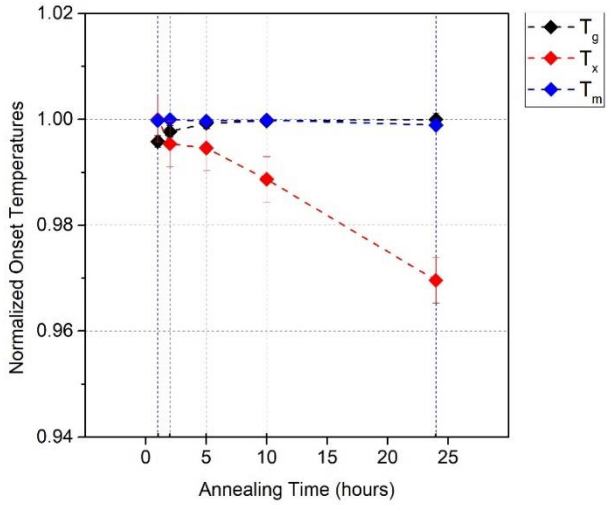

Figure 4.44 Normalized characteristic temperatures of a-Se:0.5%As samples rested at 328 K with extending post irradiation resting periods.

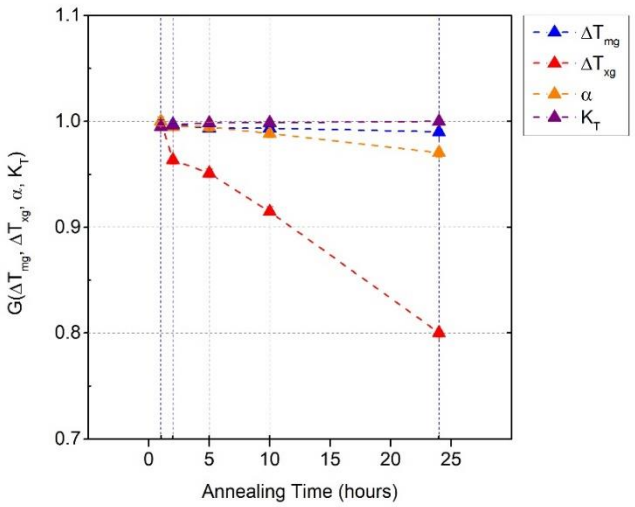

Figure 4.45 Normalized fundamental glass stability criteria of a-Se:0.5%As samples rested at 328 K with extending post irradiation resting periods.

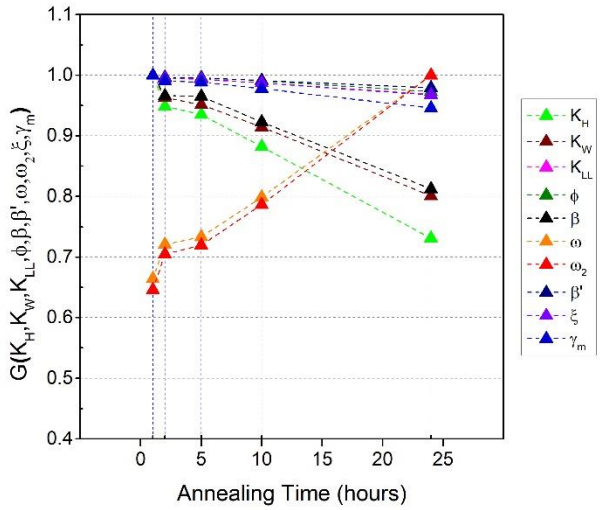

Figure 4.46 Normalized advanced glass stability criteria of a-Se:0.5%As samples rested at 328 K with extending post irradiation resting periods.

a-Se:0.5%As samples show stable T_g values. Moreover, as the annealing time of the samples increase, the T_x drops in a linear trend. This drop in T_x also influences α and ΔT_{xg}, where T_g-dependent criteria are more stable. In addition, all the advanced criteria show a linear trend. This is quite reasonable since T_x is the only temperature that exhibits a strong variation.

Table 4.35 shows the results obtained for a-Se:6%As-140 ppm Cs samples.

Table 4.35 Characteristic temperatures and fundamental glass stability criteria of a-Se:6%As-140 ppm Cs samples relaxed at 328 K with extending post irradiation resting periods.

N_S	t_r (hr)	T_g (K)	T_{xm} (K)
1	1	336.45	477.54
2	2	323.41	476.79
3	5	322.97	475.34
4	10	323.84	476.18
5	24	324.17	476.06

Figure 4.47 shows the normalized characteristic temperatures for a-Se:6%As-140 ppm Cs.

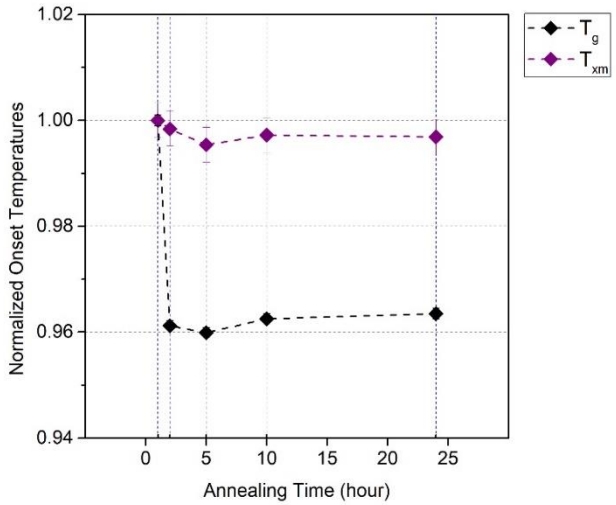

Figure 4.47 Normalized characteristic temperatures of a-Se:6%As-140 ppm Cs samples rested at 328 K with extending post irradiation resting periods.

As observed at 308 K annealing temperature, the merged crystallization and melting regions appear to be quite stable. The T_g has a more significant drop up to 2-hour annealing time. However, the percentage difference of this drop is quite small, so that this change can be neglected on a broad scale.

4.9 Summary

In this chapter, the results of the four stages introduced in the Chapter 3 were covered. Initially, reproducibility analysis was held for unirradiated film samples of pure a-Se, a-Se:0.5%As and a-Se:6%As-140 ppm Cs. It was found that the shift in T_g is correlated with the percentage of the As alloy and Cs doping, which had been already observed for bulk samples. Pure a-Se and a-Se:0.5%As films have given the same criterion ordering in the reproducibility test. Clearly, as observed in Figure 4.3 and Figure 4.4, Zhang (ω_2) criterion was observed to have the highest spread (standard deviation), which gives a low confidence of the usefulness of this criterion for glass stability investigations of a-Se based alloys.

In the first stage, glass stability investigation of x-ray irradiated films was covered. In pure a-Se samples, T_x showed a slight increase with absorbed x-ray dose, where for a-Se:0.5%As samples T_x showed an inconsistent variation. Also, a-Se:6%As-140 ppm Cs samples displayed variant T_x with absorbed x-ray dose. In the second stage, a group of x-ray irradiated samples from each composition were rested at room temperature, 295 K, for an arbitrary period of 5 hours after the irradiation process. For pure a-Se, the overall increase in T_x with respect to maximum applied dose was found to be the same, roughly 2%, which was also observed in the previous section. However, with 5-hour resting at 295 K, relatively larger increase of T_x was seen in the sample with absorbed 5.6 kGy x-ray dose. But, the T_x values then stayed nearly constant even when the absorbed x-ray dose was increased. The a-Se:0.5%As samples also showed an increase in T_x by 2% with absorbed x-ray dose over 22 kGy. This, increase in T_x with respect to x-ray dose appeared to be linear. The T_g values observed in both irradiated pure a-Se and a-Se:0.5%As sample groups didn't show significant changes. In contrast, the T_g of x-ray dosed a-Se:6%As-140 ppm Cs samples showed noticeable increase after 5-hour post irradiation resting at 295 K. Nevertheless, the T_{xm} appeared to be unaffected.

The post irradiation resting of 5 hours at 308 K have given more stable T_g and T_x values were observed for pure a-Se and a-Se:0.5%As samples. But, the variation of T_g and T_x appeared to be more significant in a-Se:0.5%As samples. Nevertheless, the variations were simply within 1.4%, without showing any consistency with increasing x-ray dose. Moreover, T_g and T_{xm} of a-Se:6%As-140 ppm Cs was found to be very stable. The samples annealed at 328 K for 5 hours after x-ray irradiation showed similar behaviour with the results obtained for resting at 308 K. However, the variations of the T_x values for a-Se:0.5%As samples observed to be larger after resting at 328 K.

DSC measurements of equally dosed samples that are rested extensively throughout 24 hours have given interesting results. At 308 K, the T_g and T_x values of pure a-Se samples that are equally irradiated have shown an exponential-like decrease as the resting period extended from 1 hour to 24 hours. For a-Se:0.5%As samples, T_g also showed an exponential-like decrease. On the other hand, T_x valued first displayed a drop between 1 and 5 hour-rest, but then recovered when the resting period as extended up to 24 hours. For a-Se:6%As-140 ppm Cs samples, when 1-hour and 24-hour rested samples are compared, the T_g shows an increase within 2%. The T_{xm} values are very stable. At 328 K, for both pure a-Se and a-Se:0.5%As samples, T_x showed the largest change. However, the T_gs obtained for both compositions were not affected by extended resting period at 328 K. For a-Se:6%As-140 ppm Cs the T_g showed a 4% drop by 2-hour rest. Then, it stayed stable. Additionally, T_{xm}s were observed very stable at when rested at various periods at 328 K.

The behaviour glass stability criteria were studied in each experimental stage. In general, high sensitivity was detected for ΔT_{xg}, K_H, K_W, β, ω and ω_2 criteria with respect to the variations in T_x. ΔT_{mg}, α, K_T, β', ζ, γ_m, ϕ and K_{LL} have shown minimal changes. To determine the usefulness of a criterion, the results obtained from the experimental stages should be compared. Comprehensive comparison of the results and related discussions are covered in the following chapter.

5. COMPARISONS AND DISCUSSIONS

5.1 Introduction

In the previous chapter, the experimental stages are introduced. For each stage, experimental results of characteristic temperatures and calculated glass stability criteria have been examined for all a-Se based films in this work. In this chapter, discussions are made for all three alloy materials under the investigated conditions. For this purpose, graphs including results of characteristic temperatures and glass stability criteria are introduced for comparison. The discussions are separated into four parts:

1. The characteristic temperatures obtained from the experiments for each material are compared.
2. Supercooled region interval (ΔT_{xg}), liquid region interval (ΔT_{mg}) and reduced temperature criteria, Wakasugi (α) and Turnbull (K_T), of pure a-Se and a-Se:0.5%As films are covered.
3. Advanced glass stability criteria of pure a-Se and a-Se:0.5%As for the x-ray irradiation and post irradiation resting period experiments are compared. Results from x-ray irradiated samples without post irradiation resting period are included for comparison. Criteria that exhibit similar behaviour with respect to the behaviour of characteristic temperatures are discussed in pairs.
4. Overall discussion on the effect of various post irradiation resting periods obtained at elevated temperatures, 308 K and 328 K, on all materials is given.
5. Advanced glass stability criteria order of each a-Se based alloy obtained from each experimental stage is presented and compared. The α and K_T criteria, the reduced temperature representations of T_g and T_x with respect to T_m, are included as reference to the arrangement. Criteria displaying distinctive behaviour are pointed out.

5.2 Comparison of Characteristic Temperatures

5.2.1 Comparison of Characteristic Temperatures of X-ray Irradiated pure a-Se and a-Se:0.5%As Films

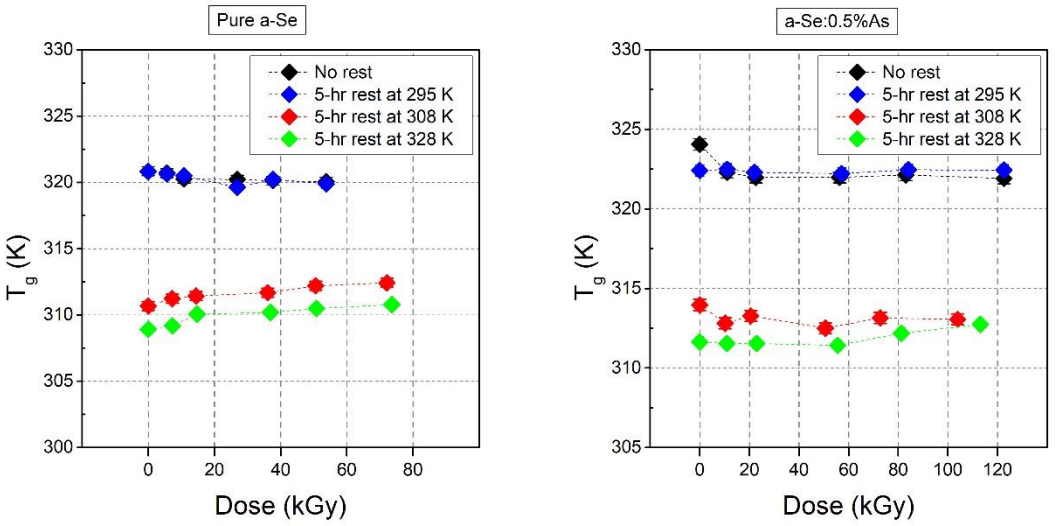

Figure 5.1 Comparison of T_g of pure a-Se and a-Se:0.5%As films obtained from various sample resting conditions after x-ray irradiation.

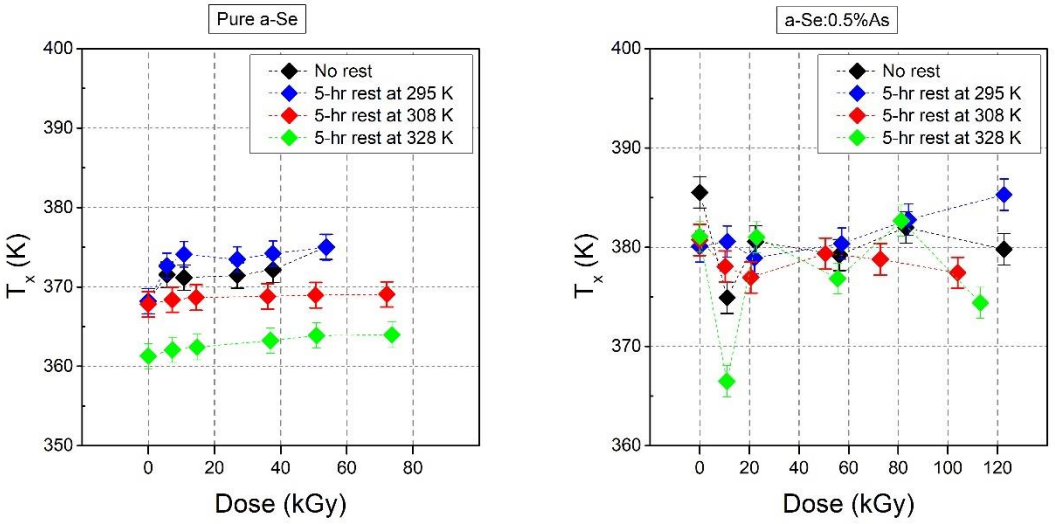

Figure 5.2 Comparison of T_x of pure a-Se and a-Se:0.5%As films obtained from various sample resting conditions after x-ray irradiation.

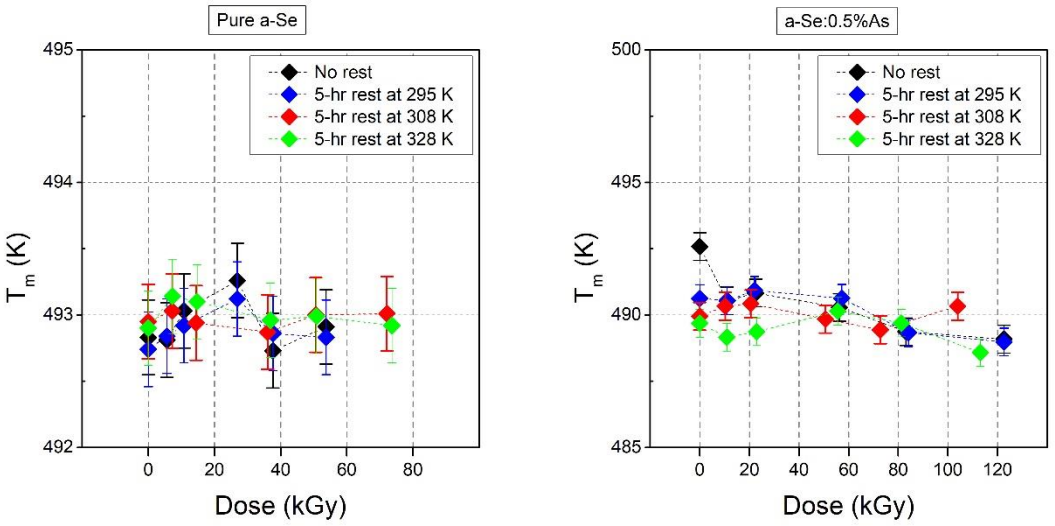

Figure 5.3 Comparison of T_m of pure a-Se and a-Se:0.5%As films obtained from various sample resting conditions after x-ray irradiation.

Considering Figure 5.1, both pure a-Se and a-Se:0.5%As show T_g that is unaffected by the resting period at 295 K. It is seen that as the annealing temperature increases, the T_g drops. Observed in Figure 5.2, T_x of pure a-Se has a behaviour similar to the T_g with respect to increasing annealing time. For a-Se:0.5%As, it is difficult to observe any proportional change of T_xs in all experimental stages. As observed, T_xs obtained for irradiated samples that are not rested after irradiation show variations, but are disproportional. Also, T_x values of samples rested at rested at 295 K, 308 K and 328 K annealing temperatures exhibit significant variations. In this case, it is hard to say that there is a significant effect of x-ray irradiation on the T_x under given experiments. Thus, since the T_x has already been observed to exhibit variation, a-Se:0.5%As has unaffected T_xs. In addition, T_m values observed in Figure 5.3 show very little variation and are within the confidence interval throughout the experimental stages. This temperature is not affected by the annealing temperature or the absorbed x-ray dose.

5.2.2 Comparison of Characteristic Temperatures of X-ray Irradiated a-Se:6%As-140 ppm Cs Films

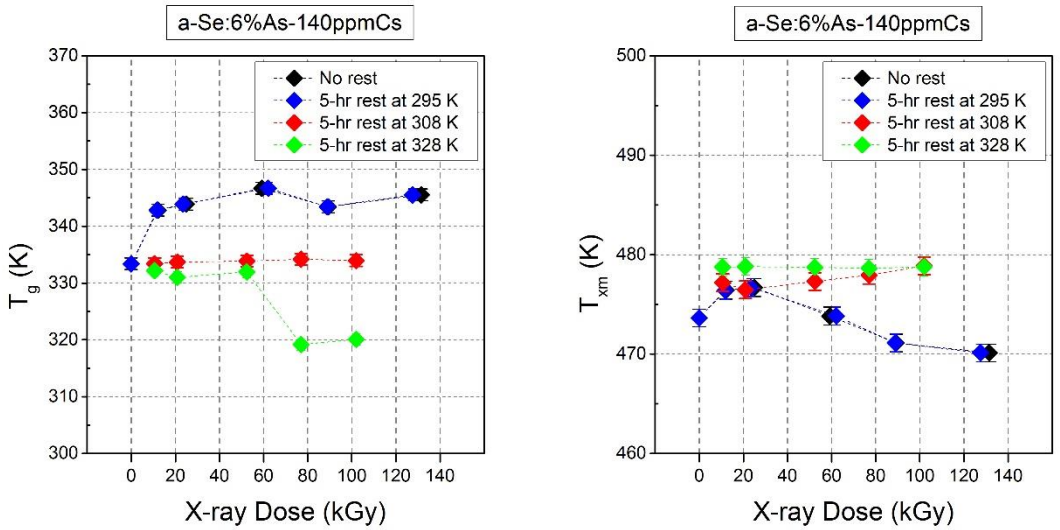

Figure 5.4 Comparison of characteristic temperatures of a-Se:6%As-140 ppm Cs films obtained from various sample resting conditions after x-ray irradiation.

The glass transition temperatures (T_g) of a-Se:6%As:140 ppm Cs as a function of absorbed x-ray dose and at different annealing temperatures are shown in Figure 5.4. Samples rested at 308 K and 328 K also show equal trend to a certain extent. However, after absorbing x-ray doses over 70 kGy, the $T_{g(328K)}$ drops to values below $T_{g(308K)}$. More interesting behavior is observed on the pseudo melt temperatures (T_{xm}). These values are inversely affected by the x-ray dose and the annealing temperature. In this case, $T_{xm\ (328K)}$ is quite stable and greater than other T_{xm}s. $T_{xm\ (308K)}$ values are slightly lower than $T_{xm\ (328K)}$ but seems to catch up after absorbed doses of 100 kGy or more. $T_{xm\ (no\ rest)}$ and $T_{xm(295K)}$ drop equally with the absorbed x-ray dose.

5.3 Comparison of Fundamental Glass Stability Criteria of pure a-Se and a-Se:0.5%As Films Examined in Various X-ray Irradiation Conditions

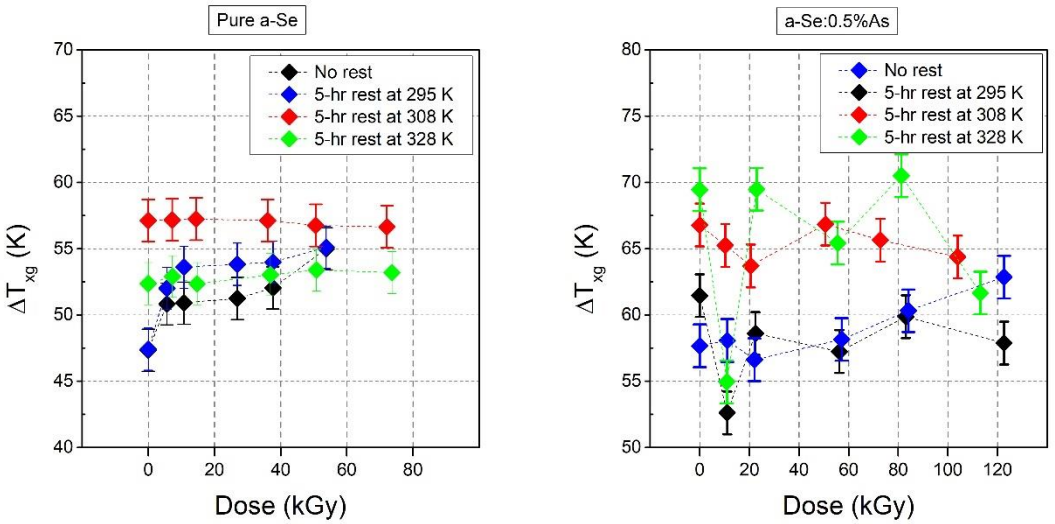

Figure 5.5 Comparison of ΔT_{xg} of pure a-Se and a-Se:0.5%As samples obtained from various sample resting conditions after x-ray irradiation.

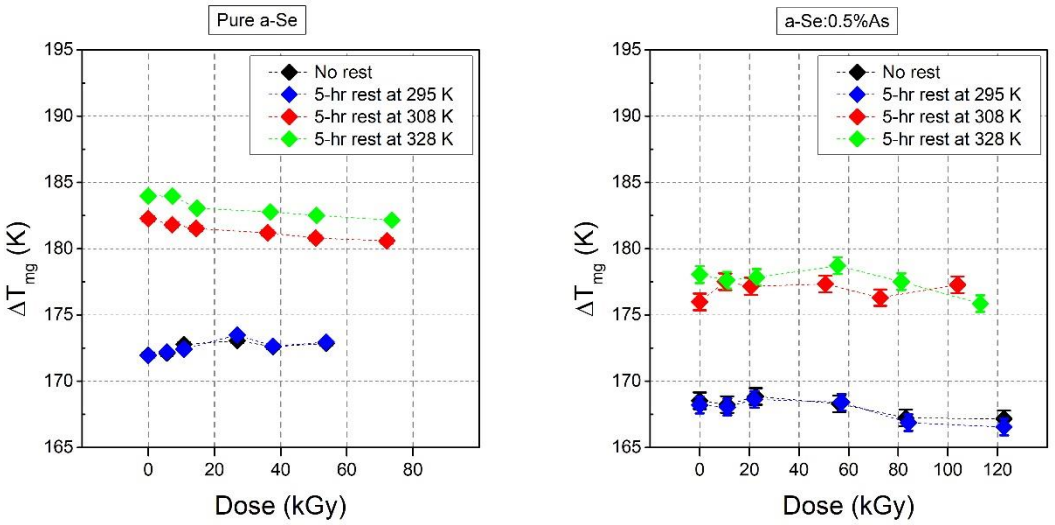

Figure 5.6 Comparison of ΔT_{mg} of pure a-Se and a-Se:0.5%As samples obtained from various sample resting conditions after x-ray irradiation.

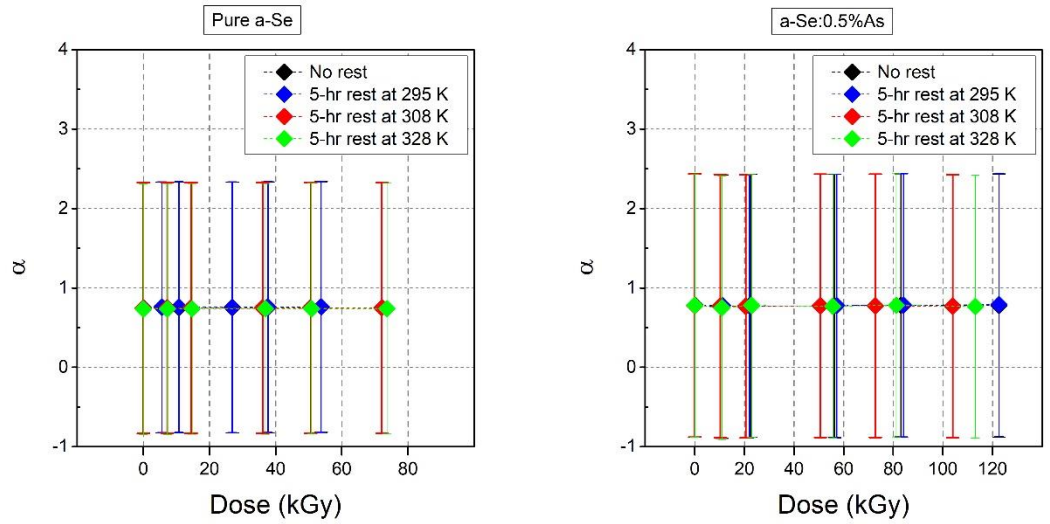

Figure 5.7 Comparison of α-criterion of pure a-Se and a-Se:0.5%As samples obtained from various sample resting conditions after x-ray irradiation.

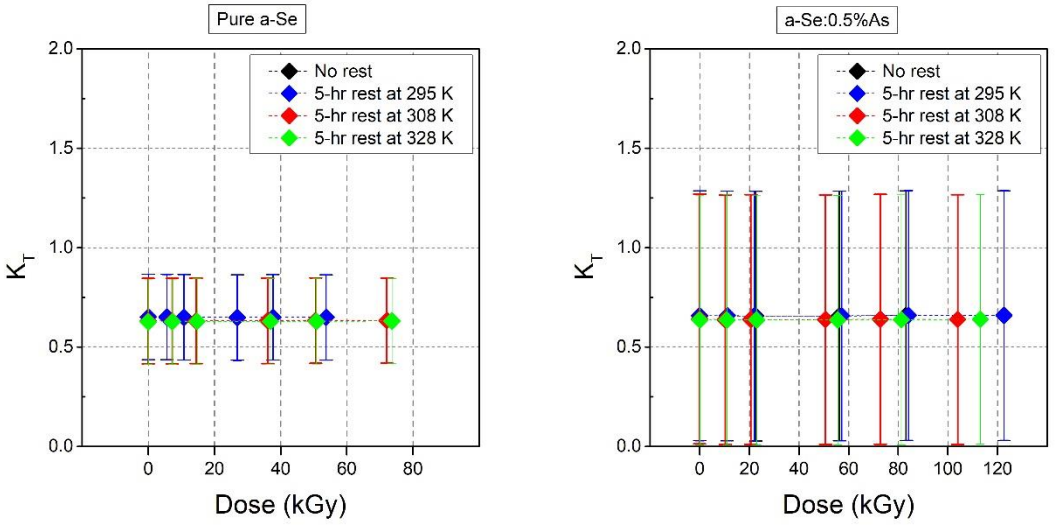

Figure 5.8 Comparison of K_T-criterion of pure a-Se and a-Se:0.5%As samples obtained from various sample resting conditions after x-ray irradiation.

Considering Figure 5.5, for pure a-Se, the highest ΔT_{xg} is observed at 308 K. This interval is higher for samples rested at 295 K, than samples rested at 328 K. Samples with no rest after x-ray irradiation, have slightly lower ΔT_{xg} than samples rested at 328 K. For a-Se:0.5%As, ΔT_{xg} does not change with respect to increasing annealing temperature. This is perhaps due to the experimental variations of T_x. Considering Figure 5.6, the order of ΔT_{mg} observed for pure a-Se samples is inversely related to the T_g order, since T_m is nearly constant in all experimental stages. It is difficult to formulate an exact relation between the results obtained from elevated annealing temperatures for the a-Se:0.5%As samples. However, obviously these elevated temperatures show higher ΔT_{mg} than the ones that are rested at 295 K and not rested. In conclusion, annealing temperatures affect the T_gs and T_xs of pure a-Se. For a-Se:0.5%As, the T_gs follow same behaviour as T_gs of pure a-Se. However, the T_xs don't show specific order, somehow not being affected from the annealing temperature and high x-ray doses. The stability of T_g, T_x and T_m can be examined in ΔT_{xg} and ΔT_{mg}. As can be seen in Figure 5.7 and Figure 5.8, the Wakasugi (α) and Turnbull (K_T) criteria are not reliable when a comparison with errors of measurements is considered.

5.4 Comparison of Advanced Glass Stability Criteria of pure a-Se and a-Se:0.5%As Films Examined in Various X-ray Irradiation Conditions

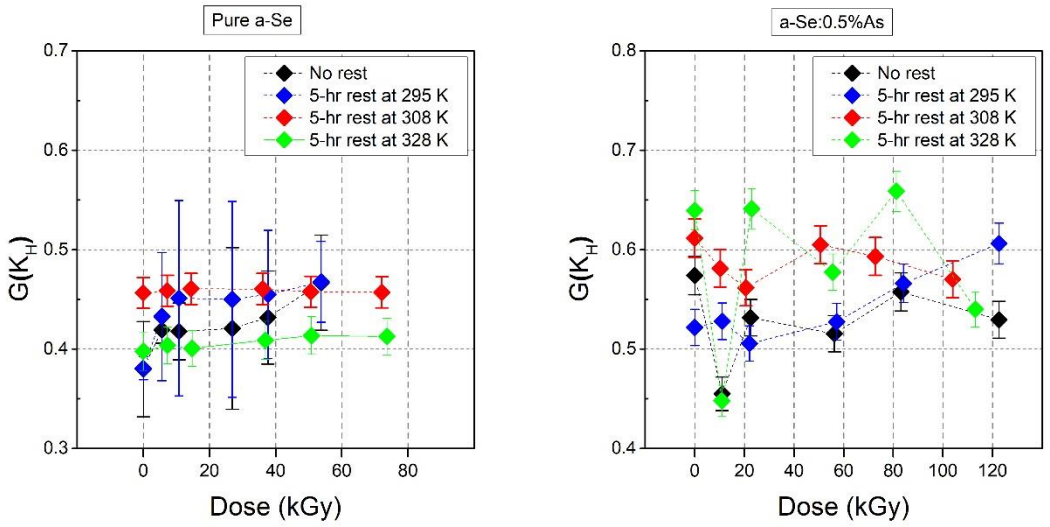

Figure 5.9 Comparison of K_H-criteria of pure a-Se and a-Se:0.5%As samples obtained from various sample resting conditions after x-ray irradiation.

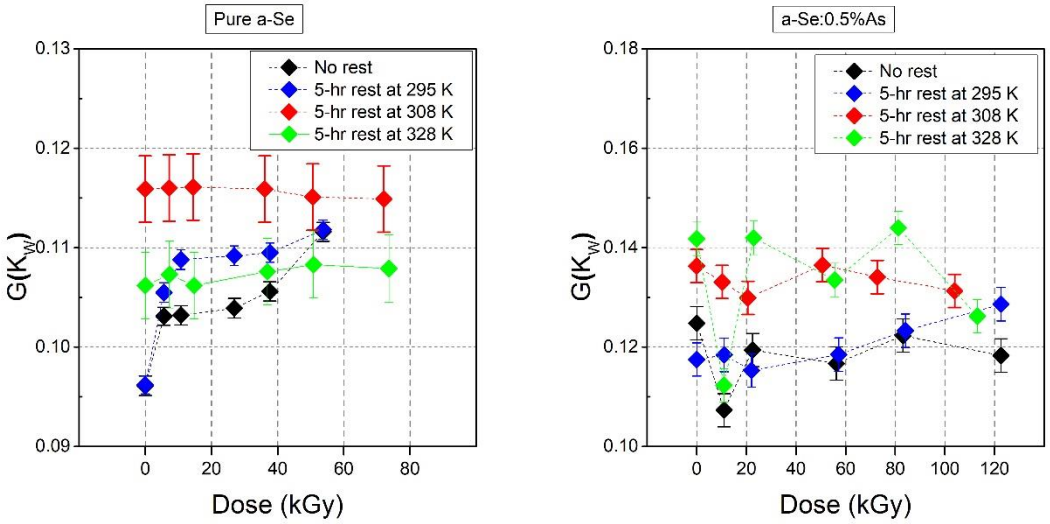

Figure 5.10 Comparison of K_W-criteria of pure a-Se and a-Se:0.5%As samples obtained from various sample resting conditions after x-ray irradiation.

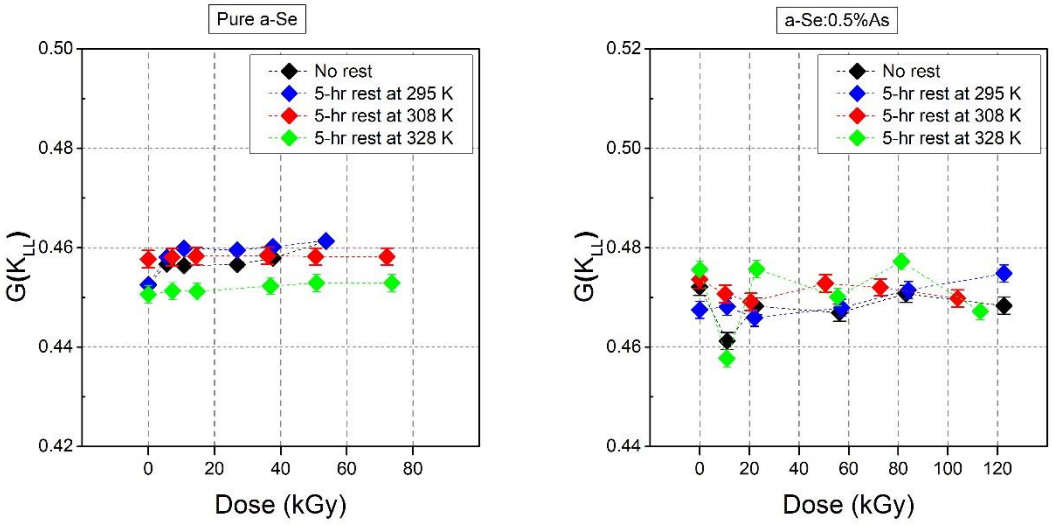

Figure 5.11 Comparison of K_{LL}-criteria of pure a-Se and a-Se:0.5%As samples obtained from various sample resting conditions after x-ray irradiation.

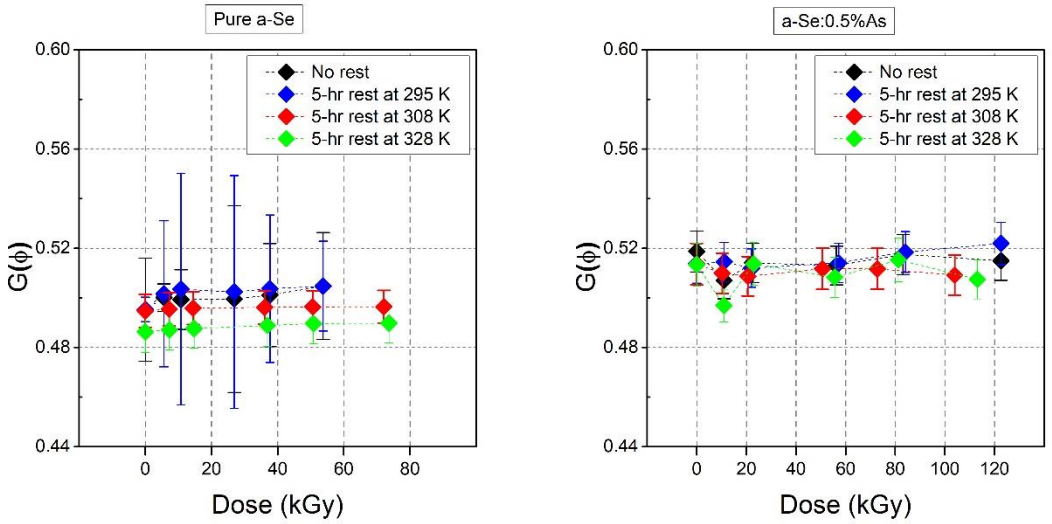

Figure 5.12 Comparison of ϕ-criteria of pure a-Se and a-Se:0.5%As samples obtained from various sample resting conditions after x-ray irradiation.

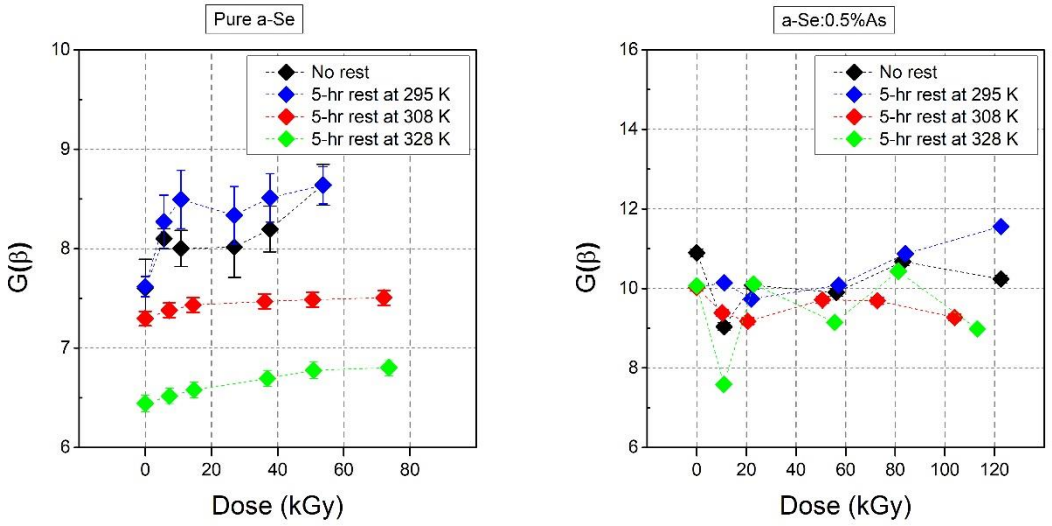

Figure 5.13 Comparison of β-criteria of pure a-Se and a-Se:0.5%As samples obtained from various sample resting conditions after x-radiation.

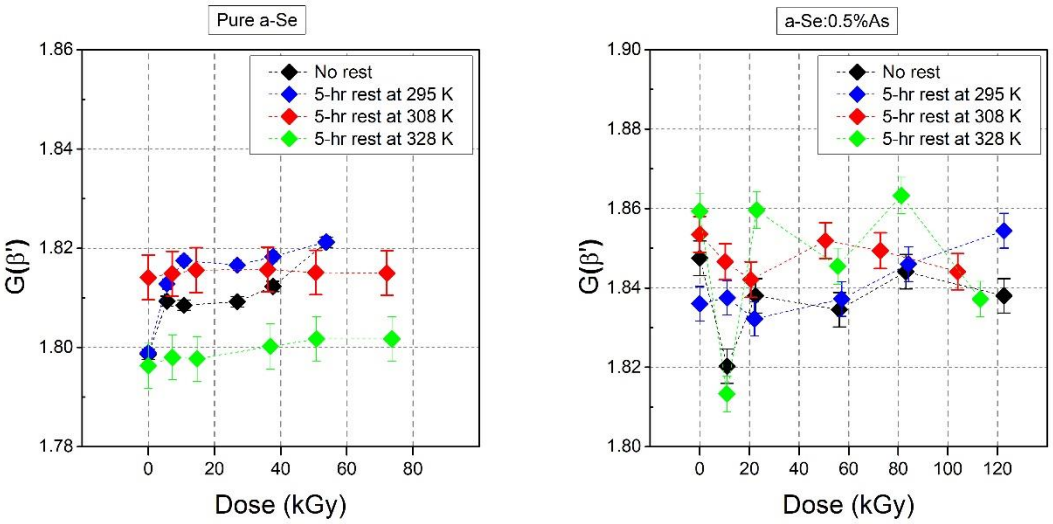

Figure 5.14 Comparison of β'-criteria of pure a-Se and a-Se:0.5%As samples obtained from various sample resting conditions after x-ray irradiation.

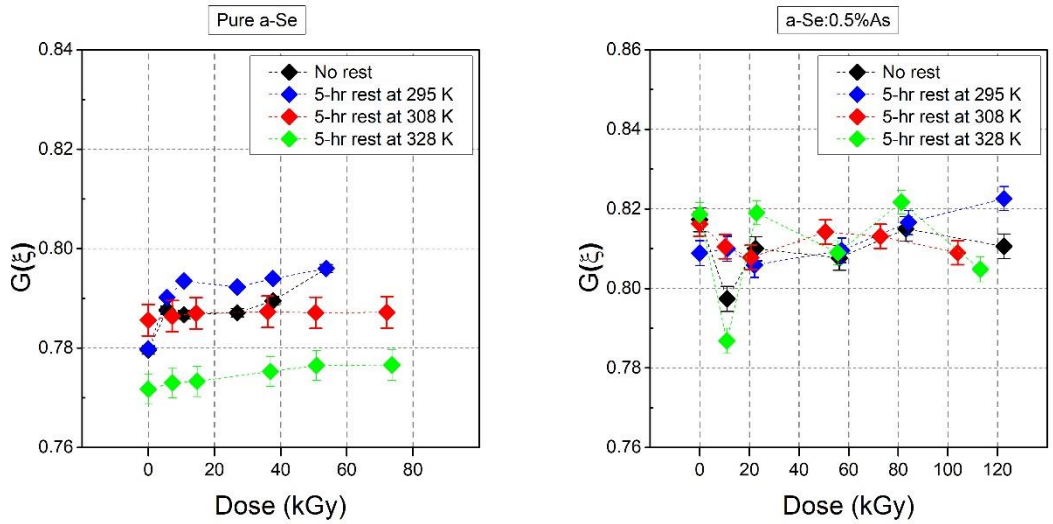

Figure 5.15 Comparison of ξ-criteria of pure a-Se and a-Se:0.5%As samples obtained from various sample resting conditions after x-ray irradiation.

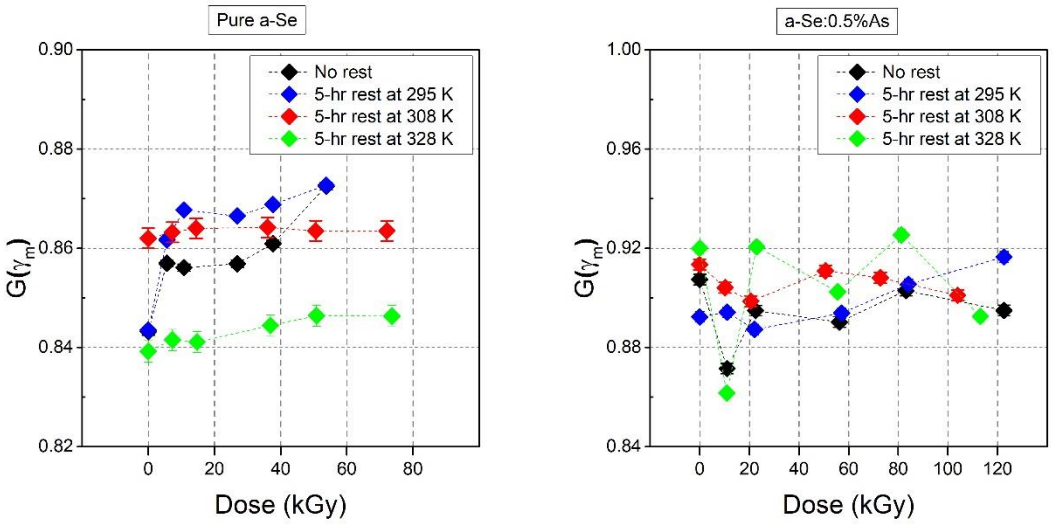

Figure 5.16 Comparison of γ_m-criteria of pure a-Se and a-Se:0.5%As samples obtained from various sample resting conditions after x-ray irradiation.

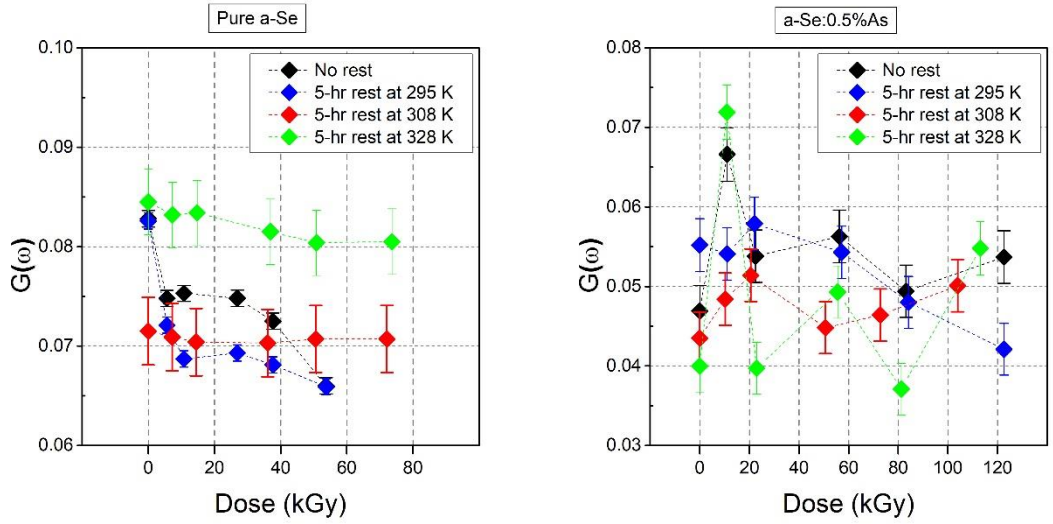

Figure 5.17 Comparison of ω-criteria of pure a-Se and a-Se:0.5%As samples obtained from various sample resting conditions after x-ray irradiation.

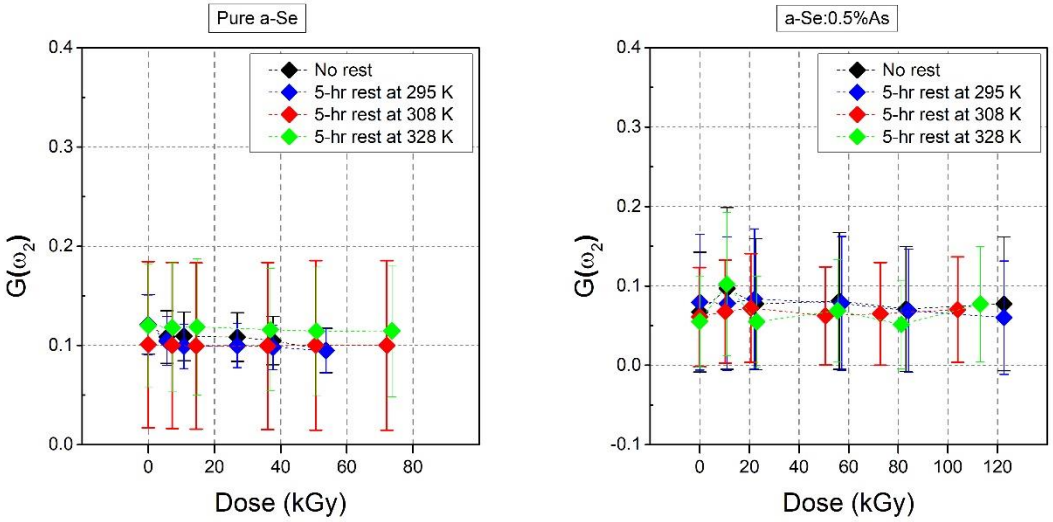

Figure 5.18 Comparison of ω_2-criteria of pure a-Se and a-Se:0.5%As samples obtained from various sample resting conditions after x-ray irradiation.

From the figures presented above, Figure 5.9 can be considered for discussion on the behaviour of K_H criterion. For pure a-Se, results obtained from 5-hour rested samples show minimal difference from the samples that are not rested after exposure. For unirradiated samples, the values are approximately equal. As the applied x-ray dose increases, samples that are rested at 295 K show higher K_H-values. Nevertheless, at maximum absorbed dose, $K_{H\,(no\ rest)}$ and $K_{H\,(295K)}$ are equal. Thus, annealing at 295 K for 5 hours does not prove to be a reliable annealing temperature. Samples annealed at 308 K give the most stable values. In fact, at 328 K resting condition, the glass stability criteria are slightly less stable, but apparently more stable than $K_{H\,(no\ rest)}$ and $K_{H\,(295K)}$. For a-Se:0.5%As: Maximum invariance is obtained for samples annealed at 328 K. This means that the supercooled region interval becomes more unstable at 328 K. The results obtained for $K_{H\,(no\ rest)}$ and $K_{H\,(295K)}$ show less variation than in pure a-Se. However, they differ in value in increasing x-ray dose. In Figure 5.10, the comparison of Weinberg (K_W) criterion of pure a-Se values obtained from samples annealed at 295 K, $K_{W\,(295K)}$, show higher increase than the values obtained without resting period, $K_{W\,(no\ rest)}$. The $K_{W\,(308K)}$ and $K_{W\,(328K)}$ values are observed to be more stable. For a-Se:0.5%As, the results show behaviour similar with the K_H criterion. However, this time the quantity of K_W of pure a-Se is higher than of a-Se:0.5%As samples. The reason is that the

supercooled region interval (ΔT_{xg}) is supressed only by T_m, where the ΔT_{xg} is supressed by the ΔT_{mg} in K_H.

Lu-Liu (K_{LL}) and Fan (ϕ) criteria act in identical style to the changes in characteristic temperatures. These criteria can be observed in Figure 5.11 and Figure 5.12. It is challenging to declare which annealing temperature particularly has the most influence on these criterion values. For both samples, these criteria show an increase in applied 20 kGy absorbed x-ray dose, suppressing the values obtained for 308 K and 328 K annealing times. The variations of the temperatures have minimal effect on the K_{LL} criterion, but ϕ criterion is significantly affected. Thus, K_{LL} has a higher confidence level with respect to ϕ.

Another pair of glass stability criteria that show similar style are Yuan (β) and Mondal (β') criteria, which are shown in Figure 5.13 and Figure 5.14. Considering β-values in pure a-Se, a drop corresponding to T_g with respect to annealing temperature is detected. Samples annealed at 295 K mostly have higher β values than the samples that are not rested after x-ray irradiation. Values of these two stages are higher than β values obtained from samples annealed at 308 K and 328 K. The order can be given as: $\beta_{(295K)} \geq \beta_{(no\ rest)} > \beta_{(308K)} > \beta_{(328K)}$. For the Mondal ($\beta'$) criterion of pure a-Se, $\frac{T_x}{T_g}$ has more influence on the criterion, since $\frac{T_g}{T_m}$ is relatively small. In this case, the ordering is similar to which of T_xs. The β' criterion of samples annealed at 295 K, $\beta'_{(295K)}$, show the highest values over 10 kGy of absorbed x-ray dose. The $\beta'_{(295K)}$ and $\beta'_{(no\ rest)}$ values drop by a factor due to $\frac{T_g}{T_m}$. Clearly, in the absorbed x-ray dose range between 10 kGy and 40 kGy the ordering is $\beta'_{(295K)} > \beta'_{(308K)} > \beta'_{(no\ rest)} > \beta'_{(325K)}$. For a-Se:0.5%As samples, the unstable behaviour of the T_x dominates both criteria. However, these criteria do not show any distinguishable relation with the annealing temperature and absorbed x-ray dose. Thus, no proper effect can be attributed to the criteria with respect to these factors.

In the analysis of Du (ξ) and 2nd Du (γ_m) criteria of pure a-Se samples, values give comparable arrangement with the β'-criterion values. For comparison Figure 5.14, 5.15 and 5.16 can be examined. Under an applied x-ray irradiation, values obtained from unirradiated samples $\xi_{(no\ rest)}$, and 5-hour resting at 295 K, $\xi_{(295K)}$, are higher than the values obtained at 308 K and 328 K annealing temperatures. It can be noticed that that 308 K gives higher criterion values than those at 328 K: $\xi_{(308K)} > \xi_{(328K)}$. The 2nd Du ($\gamma_m$) criterion presents a similar behaviour, but the $\gamma_{m(no\ rest)}$ is

more separated from $\gamma_{m(295K)}$ falling below $\gamma_{m(308K)}$, which is always higher than $\gamma_{m(328K)}$. Over 10 kGy of absorbed dose, the γ_m values can be ordered as: $\gamma_{m(295K)} > \gamma_{m(308K)} > \gamma_{m(328K)}$. For values obtained from a-Se:0.5%As samples, no certain ordering can be given. However, the values obtained at 308 K annealing temperature for both criteria are more stable. This can be related to the more stable behaviour of T_x at this annealing temperature.

Lastly, Long (ω) and Zhang (ω_2) criteria can be discussed by considering Figure 5.17 and Figure 5.18. The ω criterion displays an inverse behaviour to the γ_m criterion. Above 10 kGy of absorbed x-ray dose: $\omega_{(328K)} > \omega_{(no\ rest)} > \omega_{(308K)} > \omega_{(295K)}$. Zhang ($\omega_2$) values are too condensed on each other for both pure a-Se and a-Se:0.5%As glasses. Also, The Zhang (ω_2) criterion has as high errors as the Wakasugi (α) criterion. In fact, due to the high instance of measurement error, this criterion is not trustworthy for stability analysis of present materials.

5.5 Discussion on the Extended Post Irradiation Relaxation Periods at Elevated Temperatures

As introduced in the sections 4.7 and 4.8, the effect of extended post irradiation resting period was investigated at 308 K and 328 K annealing temperatures. General discussion on characteristic temperatures and glass stability criteria are considered in this section. Pure a-Se and a-Se:0.5%As samples show a decrease in T_g and T_x, in which T_x has a sharper drop over the extended resting period. Correspondingly, ΔT_{xg}, α and K_T criteria show a similar trend of drop with respect to these temperatures. Moreover, K_H, K_W, K_{LL}, β, β', ϕ and γ_m obey the trend of decrease in T_g and T_x, more specifically in ΔT_{xg}**.** In contrast, ω and ω_2 have an inverse relation to the change in T_g and T_x. In a-Se:6%As-140 ppm Cs samples, T_g shows an increase by 2% in after 5-hour resting at 308 K. For 328 K annealing, T_g drops by 4% when the irradiated sample resting period is 2 hours, which then stays stable between 2 hours to 24 hours of resting periods.

5.6 Comparison of Glass Stability Criterion Ordering

In this section, the glass stability criterion ordering is covered. The criterion ordering for pure a-Se and a-Se:0.5%As samples for each dose, post irradiation resting period and annealing

temperature application is compared with the criterion ordering of the unirradiated sample. Further, the variation of criteria ordering with respect to aging (relaxation) period is also presented. The criterion orderings obtained for pure a-Se are shown in Tables 5.1, 5.3, 5.5, 5.7, 5.9 and 5.11. For a-Se:0.5%As, the criterion orderings are given in Tables 5.2, 5.4, 5.6, 5.8, 5.10 and 5.12.

Table 5.1 Criterion order of pure a-Se samples irradiated with increasing x-ray doses.

N_S	D (kGy)	Criterion Order
1	0	$\beta>\beta'>\gamma_m>\xi>\alpha>K_T>\phi>K_{LL}>K_H>\omega_2>K_W>\omega$
2	5.6	$\beta>\beta'>\gamma_m>\xi>\alpha>K_T>\phi>K_{LL}>K_H>\omega_2>K_W>\omega$
3	10.8	$\beta>\beta'>\gamma_m>\xi>\alpha>K_T>\phi>K_{LL}>K_H>\omega_2>K_W>\omega$
4	26.9	$\beta>\beta'>\gamma_m>\xi>\alpha>K_T>\phi>K_{LL}>K_H>\omega_2>K_W>\omega$
5	37.7	$\beta>\beta'>\gamma_m>\xi>\alpha>K_T>\phi>K_{LL}>K_H>\omega_2>K_W>\omega$
6	53.8	$\beta>\beta'>\gamma_m>\xi>\alpha>K_T>\phi>K_H>K_{LL}>K_W>\omega_2>\omega$

Table 5.2 Criterion order of a-Se:0.5%As samples irradiated with increasing x-ray doses.

N_S	D (kGy)	Criterion Order
1	0	$\beta>\beta'>\gamma_m>\xi>\alpha>K_T>K_H>\phi>K_{LL}>K_W>\omega_2>\omega$
2	11.0	$\beta>\beta'>\gamma_m>\xi>\alpha>K_T>\phi>K_{LL}>K_H>K_W>\omega_2>\omega$
3	22.5	$\beta>\beta'>\gamma_m>\xi>\alpha>K_T>K_H>\phi>K_{LL}>K_W>\omega_2>\omega$
4	56.2	$\beta>\beta'>\gamma_m>\xi>\alpha>K_T>K_H>\phi>K_{LL}>K_W>\omega_2>\omega$
5	83.1	$\beta>\beta'>\gamma_m>\xi>\alpha>K_T>K_H>\phi>K_{LL}>K_W>\omega_2>\omega$
6	122.6	$\beta>\beta'>\gamma_m>\xi>\alpha>K_T>K_H>\phi>K_{LL}>K_W>\omega_2>\omega$

Table 5.3 Criterion order of pure a-Se samples irradiated with increasing x-ray doses with 5-hour post irradiation time at 295 K.

N_S	D (kGy)	Criterion Order
1	0	$\beta>\beta'>\gamma_m>\xi>\alpha>K_T>\phi>K_{LL}>K_H>\omega_2>K_W>\omega$
2	5.6	$\beta>\beta'>\gamma_m>\xi>\alpha>K_T>\phi>K_{LL}>K_H>K_W>\omega_2>\omega$
3	10.8	$\beta>\beta'>\gamma_m>\xi>\alpha>K_T>\phi>K_{LL}>K_H>K_W>\omega_2>\omega$
4	26.9	$\beta>\beta'>\gamma_m>\xi>\alpha>K_T>\phi>K_{LL}>K_H>K_W>\omega_2>\omega$
5	37.7	$\beta>\beta'>\gamma_m>\xi>\alpha>K_T>\phi>K_{LL}>K_H>K_W>\omega_2>\omega$
6	53.8	$\beta>\beta'>\gamma_m>\xi>\alpha>K_T>K_H>\phi>K_{LL}>K_W>\omega_2>\omega$

Table 5.4 Criterion order of a-Se:0.5%As samples irradiated with increasing x-ray doses with 5-hour post irradiation time at 295 K.

N_S	D (kGy)	Criterion Order
1	0	$\beta>\beta'>\gamma_m>\xi>\alpha>K_T>K_H>\phi>K_{LL}>K_W>\omega_2>\omega$
2	11.1	$\beta>\beta'>\gamma_m>\xi>\alpha>K_T>K_H>\phi>K_{LL}>K_W>\omega_2>\omega$
3	22.0	$\beta>\beta'>\gamma_m>\xi>\alpha>K_T>\phi>K_H>K_{LL}>K_W>\omega_2>\omega$
4	57.2	$\beta>\beta'>\gamma_m>\xi>\alpha>K_T>K_H>\phi>K_{LL}>K_W>\omega_2>\omega$
5	84.1	$\beta>\beta'>\gamma_m>\xi>\alpha>K_T>K_H>\phi>K_{LL}>K_W>\omega_2>\omega$
6	122.6	$\beta>\beta'>\gamma_m>\xi>\alpha>K_T>K_H>\phi>K_{LL}>K_W>\omega_2>\omega$

Table 5.5 Criterion order of pure a-Se samples irradiated with increasing x-ray doses with 5-hour post irradiation time at 308 K.

N_S	D (kGy)	Criterion Order
1	0	$\beta>\beta'>\gamma_m>\xi>\alpha>K_T>\phi>K_{LL}>K_H>\omega_2>K_W>\omega$
2	7.3	$\beta>\beta'>\gamma_m>\xi>\alpha>K_T>\phi>K_H>K_{LL}>\omega_2>K_W>\omega$
3	14.4	$\beta>\beta'>\gamma_m>\xi>\alpha>K_T>\phi>K_H>K_{LL}>\omega_2>K_W>\omega$
4	36.1	$\beta>\beta'>\gamma_m>\xi>\alpha>K_T>\phi>K_H>K_{LL}>\omega_2>K_W>\omega$
5	50.6	$\beta>\beta'>\gamma_m>\xi>\alpha>K_T>\phi>K_{LL}>K_H>\omega_2>K_W>\omega$
6	72.1	$\beta>\beta'>\gamma_m>\xi>\alpha>K_T>\phi>K_{LL}>K_H>\omega_2>K_W>\omega$

Table 5.6 Criterion order of a-Se:0.5%As samples irradiated with increasing x-ray doses with 5-hour post irradiation time at 308 K.

N_S	D (kGy)	Criterion Order
1	0	$\beta>\beta'>\gamma_m>\xi>\alpha>K_T>K_H>\phi>K_{LL}>\omega_2>K_W>\omega$
2	10.2	$\beta>\beta'>\gamma_m>\xi>\alpha>K_T>K_H>\phi>K_{LL}>\omega_2>K_W>\omega$
3	20.6	$\beta>\beta'>\gamma_m>\xi>\alpha>K_T>K_H>\phi>K_{LL}>\omega_2>K_W>\omega$
4	50.7	$\beta>\beta'>\gamma_m>\xi>\alpha>K_T>K_H>\phi>K_{LL}>\omega_2>K_W>\omega$
5	72.8	$\beta>\beta'>\gamma_m>\xi>\alpha>K_T>K_H>\phi>K_{LL}>\omega_2>K_W>\omega$
6	104.0	$\beta>\beta'>\gamma_m>\xi>\alpha>K_T>K_H>\phi>K_{LL}>\omega_2>K_W>\omega$

Table 5.7 Criterion order of pure a-Se samples irradiated with increasing x-ray doses with 5-hour post irradiation time at 328 K.

N_S	D (kGy)	Criterion Order
1	0	$\beta>\beta'>\gamma_m>\xi>\alpha>K_T>\phi>K_{LL}>K_H>K_W>\omega_2>\omega$
2	7.3	$\beta>\beta'>\gamma_m>\xi>\alpha>K_T>\phi>K_{LL}>K_H>K_W>\omega_2>\omega$
3	14.7	$\beta>\beta'>\gamma_m>\xi>\alpha>K_T>\phi>K_{LL}>K_H>K_W>\omega_2>\omega$
4	36.9	$\beta>\beta'>\gamma_m>\xi>\alpha>K_T>\phi>K_{LL}>K_H>K_W>\omega_2>\omega$
5	50.9	$\beta>\beta'>\gamma_m>\xi>\alpha>K_T>\phi>K_{LL}>K_H>K_W>\omega_2>\omega$
6	73.6	$\beta>\beta'>\gamma_m>\xi>\alpha>K_T>\phi>K_{LL}>K_H>K_W>\omega_2>\omega$

Table 5.8 Criterion order of a-Se:0.5%As samples irradiated with increasing x-ray doses with 5-hour post irradiation time at 328 K.

N_S	D (kGy)	Criterion Order
1	0	$\beta>\beta'>\gamma_m>\xi>\alpha>K_H>K_T>\phi>K_{LL}>K_W>\omega_2>\omega$
2	10.9	$\beta>\beta'>\gamma_m>\xi>\alpha>K_T>\phi>K_{LL}>K_H>K_W>\omega_2>\omega$
3	22.9	$\beta>\beta'>\gamma_m>\xi>\alpha>K_H>K_T>\phi>K_{LL}>K_W>\omega_2>\omega$
4	55.6	$\beta>\beta'>\gamma_m>\xi>\alpha>K_T>K_H>\phi>K_{LL}>K_W>\omega_2>\omega$
5	81.3	$\beta>\beta'>\gamma_m>\xi>\alpha>K_H>K_T>\phi>K_{LL}>K_W>\omega_2>\omega$
6	113.1	$\beta>\beta'>\gamma_m>\xi>\alpha>K_T>K_H>\phi>K_{LL}>K_W>\omega_2>\omega$

Table 5.9 Criterion order of equally x-ray irradiated pure a-Se samples with increasing post irradiation resting periods at 308 K. Absorbed x-ray dose: 94.1 kGy.

N_S	Annealing Time (hr)	Criterion Order
1	1	$\beta>\beta'>\gamma_m>\xi>\alpha>K_T>\phi>K_{LL}>K_H>K_W>\omega_2>\omega$
2	2	$\beta>\beta'>\gamma_m>\xi>\alpha>K_T>\phi>K_{LL}>K_H>\omega_2>K_W>\omega$
3	5	$\beta>\beta'>\gamma_m>\xi>\alpha>K_T>\phi>K_{LL}>K_H>\omega_2>K_W>\omega$
4	10	$\beta>\beta'>\gamma_m>\xi>\alpha>K_T>\phi>K_{LL}>K_H>\omega_2>K_W>\omega$
5	24	$\beta>\beta'>\gamma_m>\xi>\alpha>K_T>\phi>K_{LL}>K_H>\omega_2>\omega>K_W$

Table 5.10 Criterion order of equally x-ray irradiated a-Se:0.5%As samples with increasing post irradiation resting periods at 308 K. Absorbed x-ray dose: 133.1 kGy.

N_S	Annealing Time (hr)	Criterion Order
1	1	$\beta>\beta'>\gamma_m>\xi>\alpha> K_T> \phi> K_{LL}> K_H >K_W> \omega_2 > \omega$
2	2	$\beta>\beta'>\gamma_m>\xi>\alpha> K_T> \phi> K_{LL}> K_H > \omega_2 > K_W>\omega$
3	5	$\beta>\beta'>\gamma_m>\xi>\alpha> K_T> \phi> K_{LL}> K_H > \omega_2 > K_W> \omega$
4	10	$\beta>\beta'>\gamma_m>\xi>\alpha> K_T> \phi> K_{LL}> K_H > K_W>\omega_2 > \omega$
5	24	$\beta>\beta'>\gamma_m>\xi>\alpha> K_T> \phi> K_H >K_{LL}> K_W>\omega_2 > \omega$

Table 5.11 Criterion order of equally x-ray irradiated pure a-Se samples with increasing post irradiation resting periods at 328 K. Absorbed x-ray dose: 94.1 kGy.

N_S	Annealing Time (hr)	Criterion Order
1	1	$\beta>\beta'>\gamma_m>\xi>\alpha> K_T> K_H > \phi> K_{LL}> K_W> \omega_2 > \omega$
2	2	$\beta>\beta'>\gamma_m>\xi>\alpha> K_T> \phi> K_{LL}> K_H > K_W> \omega_2 > \omega$
3	5	$\beta>\beta'>\gamma_m>\xi>\alpha> K_T> \phi> K_{LL}> K_H > \omega_2 > K_W>\omega$
4	10	$\beta>\beta'>\gamma_m>\xi>\alpha> K_T> \phi> K_{LL}> K_H > \omega_2 > K_W>\omega$
5	24	$\beta>\beta'>\gamma_m>\xi>\alpha> K_T> \phi> K_{LL}> K_H > \omega_2 > \omega> K_W$

Table 5.12 Criterion order of equally x-ray irradiated pure a-Se samples with increasing post irradiation resting periods at 328 K. Absorbed x-ray dose: 133.1 kGy.

N_S	Annealing Time (hr)	Criterion Order
1	1	$\beta>\beta'>\gamma_m>\xi>\alpha> K_T> K_H > \phi> K_{LL}> K_W> \omega_2 > \omega$
2	2	$\beta>\beta'>\gamma_m>\xi>\alpha> K_T> K_H > \phi> K_{LL}> K_W> \omega_2 > \omega$
3	5	$\beta>\beta'>\gamma_m>\xi>\alpha> K_T> K_H > \phi> K_{LL}> K_W> \omega_2 > \omega$
4	10	$\beta>\beta'>\gamma_m>\xi>\alpha> K_T> K_H > \phi> K_{LL}> K_W> \omega_2 > \omega$
5	24	$\beta>\beta'>\gamma_m>\xi>\alpha> K_T> \phi> K_{LL}> K_H > \omega_2 > K_W>\omega$

The comparison of the glass stability criteria ordering in the tables above, show that the Hruby (K_H) and Weinberg (K_W) criteria vary under the various experimental conditions studied. If Table 5.1 is considered, K_W shows lower order than ω_2. At an absorbed dose of 53.8 kGy, both

K_H and K_W increase by one criterion order. If Table 5.1 is considered, the criteria ordering of a-Se:0.5%As samples are generally stable. In

Table 5.3, K_W increases above ω_2 in the x-ray irradiated pure a-Se samples. At 53.8 kGy of absorbed dose, K_H dominates over ϕ and K_{LL}. In Table 5.4, the criterion order of a-Se:0.5%As is broadly stable, only showing a shift in K_H at 22 kGy absorbed dose, which then recovers its dominance over ϕ. Nevertheless, the ordering recovers as the absorbed x-ray dose increases. In Table 5.5, pure a-Se samples with absorbed doses from 7.3 kGy to 36.1 kGy display higher K_H than K_{LL}. However, the values of these criteria drop for higher absorbed x-ray doses and the ordering of unirradiated sample is recovered. Surprisingly, the criterion ordering for a-Se:0.5%As samples given in Table 5.6 is permanent throughout all applied x-ray doses. In Table 5.7, pure a-Se samples relaxed at 328 K have stable criteria arrangement. However, in Table 5.8, a-Se:0.5%As samples show variations in K_H with increasing x-ray dose. Referring to Table 5.9, the x-ray irradiated pure a-Se samples tested in the extended resting period measurements at 308 K show a drop in K_W. This criterion falls below ω_2 between 2 and 10 hours of resting period. Eventually, it reaches the minimum under ω. In Table 5.10, a-Se:0.5%As samples also show variation in K_W, where it drops below ω_2 for two and 5-hour resting periods. Afterwards, the ordering between K_W, ω_2 and ω recovers at longer resting periods. Nevertheless, the K_H becomes larger than K_{LL}. In Table 5.11, K_W of pure a-Se drops with increasing resting period at 328 K, similar to the behaviour found for annealing at 308 K. K_H decreases below K_{LL} over a one-hour resting period. In contrast, a-Se:0.5%As samples have stable criterion ordering up to 24-hour of resting period, which can be seen in Table 5.12. After a day of post irradiation relaxation, the K_H decrease by two orders and K_W decrease by one order.

Additionally, criterion ordering of unirradiated pure a-Se and a-Se:0.5%As samples with respect to the aging period at 295 K can be presented. According to Table 5.13, it can be observed that only K_W drops by an order in additional 276 days for pure a-Se, where K_H increases by two orders over ϕ and K_{LL} in 114 days.

Table 5.13 Criterion order of pure a-Se and a-Se:0.5%As films with respect to aging period.

Pure a-Se	
Resting Period (days)	Criterion Order
54	$\beta>\beta'>\gamma_m>\xi>\alpha>K_T>\phi>K_{LL}>K_H>K_W>\omega_2>\omega$

330	$\beta>\beta'>\gamma_m>\xi>\alpha>K_T>\phi>K_{LL}>K_H>\omega_2>K_W>\omega$
a-Se:0.5%As	
Resting Period (days)	Criterion Order
65	$\beta>\beta'>\gamma_m>\xi>\alpha>K_T>\phi>K_{LL}>K_H>K_W>\omega_2>\omega$
179	$\beta>\beta'>\gamma_m>\xi>\alpha>K_T>K_H>\phi>K_{LL}>K_W>\omega_2>\omega$

5.7 Summary

In this chapter, the characteristic temperatures obtained from the experimental stages that involved various x-ray irradiation conditions for each material was compared. For pure a-Se, the $T_{g(\text{no rest})}$ and $T_{g(295\ K)}$ were observed to be quite stable, where $T_{g(308\ K)}$ and $T_{g(328\ K)}$ values show a minimal increase with absorbed x-ray dose. For a-Se:0.5%As samples, the T_gs were stable, but $T_{g(308\ K)}$ and $T_{g(328\ K)}$ showed slight variation with absorbed x-ray dose. For a-Se:6%As-140 ppm Cs samples, $T_{g(\text{no rest})}$ and $T_{g(295\ K)}$ has shown an increase with absorbed dose. $T_{g(328\ K)}$ dropped with absorbed x-ray dose 77 kGy but then stayed stable. T_x values of pure a-Se were observed to be stable, especially for the samples were annealed at 308 K after x-ray irradiation. On the other hand, a-Se:0.5%As samples were observed to exhibit variations. It is assumed that, since the T_x is normally variant due to the nature of crystallization peak, the T_xs of a-Se:0.5%As samples were unaffected. The $T_{xm(\text{no rest})}$ and $T_{xm(295\ K)}$ of examined a-Se:6%As-140 ppm Cs samples showed similar trend. $T_{xm(308\ K)}$ and $T_{xm(328\ K)}$ were more stable, increasing very slightly with absorbed x-ray dose.

The glass stability criteria of pure a-Se and a-Se:0.5%As films were also compared. Considering the fundamental criteria, the $\Delta T_{xg(308\ K)}$ values of pure a-Se samples was observed to be the largest and the most stable. For a-Se:0.5%As, ΔT_{xg} values obtained from the experimental stages appeared to fall in the same range. The effect x-ray dose and annealing temperatures could not be distinguished. The α and K_T criteria obtained for both materials have shown large errors. No distinction in the results obtained from the stages was detected. K_H and K_W appeared to show similar correlation to the behaviour of T_x and ΔT_{xg}. Results obtained for K_{LL} and ϕ were not very distinguishable. The β criterion showed distinguishable results and similar behaviour to T_x and ΔT_{xg}. Results of β', ξ and γ_m criteria compared similarly. The ω and ω_2 criterion showed a reciprocal

trend to the compared results of β', ξ and γ_m. These criteria didn't show similar behaviour with the T_x values. Also, ω_2 found to be unreliable due to the high errors.

In addition, the effect of the behaviour of T_g and T_x on the glass stability criteria of the studied samples obtained from extending resting hours was discussed. Subsequently, the criterion orders were compared for pure a-Se and a-Se:0.5%As. It was found that K_H and K_W values appeared to be variant, changing the order in different experimental conditions.

6. CONCLUSIONS AND FUTURE WORK

6.1 Introduction

This research concentrated on investigating the glass stability of x-ray irradiated pure a-Se, a-Se:0.5%As and a-Se:6%As-140 ppm Cs thin films by use of differential scanning calorimetry (DSC). The stability analysis was conducted by considering characteristic onset temperatures and fourteen different glass stability criteria that are frequently encountered in the literature for various classes of glasses. The experimental stages included the stability analyses of x-ray irradiated films with different absorbed doses, the effect of post irradiation relaxation times at annealing temperatures of 295 K, 308 K and 328 K, and the effect of extending post irradiation periods at 308 K and 328 K on the stability of equally dosed a-Se films. In this chapter, conclusions on the characteristic onset temperatures obtained from the experimental stages are given. Afterwards, the useful glass stability criteria are clarified. In addition, few ideas for future studies are suggested.

6.2 X-ray Induced Changes in Characteristic Temperatures

Characteristic temperatures of interest were the onset glass transition temperature (T_g), onset crystallization temperature (T_x) and onset melting temperature (T_m). These temperatures were obtained from heating scan experiments in DSC with heating rate of 5 K/min in the temperature range between 293 K and 523 K. This range was chosen to ensure that glass transition, crystallization and melting which could be observed in the DSC experiments.

In the first stage, the glass transition temperatures (T_g) obtained from the x-ray irradiated pure a-Se films were observed to be unaffected by deposited x-ray dose up to 53.8 kGy. Similar result was observed for samples that were rested at room temperature 295 K after x-ray irradiation. The T_gs obtained for a-Se:0.5%As films from the same experimental procedures were observed to

be unaffected up to 122.8 kGy absorbed x-ray dose. In the measurements that involved five-hour post irradiation resting period at 308 K and 328 K annealing temperatures, the T_gs appeared to be stable. For a-Se:6%As-140 ppm Cs samples the T_gs showed increase with absorbed x-ray dose. Similar behaviour was observed for samples rested for five hours after irradiation at 295 K. The most stable T_gs were obtained for the samples rested for five hours at 308 K. At 328 K annealing temperature, the T_gs showed a drop over 52.4 kGy absorbed x-ray dose.

The crystallization temperatures (T_x) of pure a-Se samples have shown different behaviour than the behaviour of T_g. In the first stage of x-ray irradiation procedure, the T_x values increased with absorbed x-ray dose. Similar outcome was observed for samples that were rested for 5 hours after x-ray irradiation at 295 K. The samples rested for five hours after irradiation at 308 K have given the most stable T_x values. For samples rested at 328 K, the T_xs showed minimal increase with absorbed x-ray dose. However, T_x values of a-Se:0.5%As films were observed to be unstable. The least stable T_xs was observed in x-ray irradiated films annealed at 328 K. Considering the effect of extended post irradiation resting periods on equally irradiated pure a-Se films, the T_xs of the samples rested at 328 K showed greater drop than the T_xs of the samples rested at 308 K. For equally irradiated a-Se:0.5%As films that were rested at 308 K, the T_x slightly dropped, but then improved (increased) for samples rested over five hours. Yet, at 328 K annealing temperature, T_x fell distinctly with increasing resting periods.

As expected, the T_m values of both pure a-Se and a-Se:0.5%As were unaffected from applied x-ray doses and various annealing conditions. For a-Se:6%As-140 ppm Cs samples, the T_{xm} values from x-ray irradiation dropped at doses over 25 kGy. Similar outcome was observed for samples that were rested for five hours at 295 K after irradiation. More stable T_{xm}s were found when samples were rested at 308 K and 328 K after irradiation. All in all, high absorbed x-ray doses have not shown any significant effect on the T_g and T_x temperatures, hence on the glass stability of a-Se based alloy films.

6.3 X-ray Induced Changes in Glass Stability Criteria

The variations of characteristic temperatures were observed in the normalized plots. Results of each experimental stage have shown that the supercooled region interval (ΔT_{xg}) is directly

related to the variations in T_g and T_x. This fundamental criterion can be referred for basic evaluation of glass stability. Amongst the investigated advanced glass stability criteria, Hruby (K_H) and Weinberg (K_W) were found to be sensitive indicators of change in T_g and T_x and ΔT_{xg}. Especially, the sensitivity of K_H and K_W can be detected in the criterion orderings obtained from the experiments. On the other hand, Yuan (β) criterion also showed similar type of behaviour with K_H and K_W in normalized scale. However, due to the large nominal value of this criterion, it is almost impossible to determine the minimal variations related to T_g and T_x. Therefore, considering characteristic onset temperatures, ΔT_{xg}, K_H and K_W are found to be the most useful criteria in analyzing the glass stability for the present pure a-Se and a-Se:0.5%As films.

6.4 Future Works

In this project, no significant effect of x-ray irradiation on the characteristic onset temperatures was obtained. Analysis of the enthalpy of the characteristic regions was neglected. As a progress, further analysis can be conducted on the overall enthalpy of the x-ray irradiated samples examined in this work. Specifically, the changes in the crystallization enthalpy with deposited x-ray dose (radiation energy) would be a useful study since energy is deposited into the structure. Additionally, analysis of crystallization peak temperature will be useful to signify the shifts in the crystallization peak obtained in DSC heating scan.

The stability of pure a-Se, a-Se:0.5%As and a-Se:6%As-140 ppm Cs thin films were investigated at three different annealing temperatures, 295 K, 308 K and 328 K. The convenience of 308 K on achieving stability in characteristic temperatures was verified for the x-ray irradiated films of pure a-Se and a-Se:6%As-140 ppm Cs. However, due to the variation of T_x obtained from a-Se:0.5%As films, the convenience of this temperature cannot be stated clearly. Experiments can be repeated for a-Se:0.5%As films to determine 308 K is an ideal storage temperature for glass stability.

The samples that were used in this research were specifically aged long enough to achieve sufficient relaxation to become more stable and avoid experimental artifacts arising from different thermal histories. In contrast to this method, the effect of x-ray irradiation can be studied for film samples with shorter aging period (within one month of age) to observe whether x-ray irradiation

may induce crystallization in films that aren't sufficiently relaxed. Thus, a more comprehensive understanding can be established on the stability of x-ray irradiated a-Se based thin films related to pre-irradiation relaxation period.

REFERENCES

[1] Kasap, S. O. and Rowlands, J. A., "Direct-conversion flat-panel X-ray image sensors for digital radiography", Proceedings of the IEEE, **90**(4), 2002, pp. 591-604.

[2] Kasap, S. O., Haugen, C., Nesdoly, M. and Rowlands, J. A., "Properties of a-Se for use in flat panel X-ray image detectors", Journal of Non-Crystalline Solids, **266**, 2000, pp. 1163-1167.

[3] Kasap S.O., Frey J.B., Belev G., Tousignant O., Mani H., Greenspan J., Laperriere Luc., Bubon O., Reznik A., DeCrescenzo G., Karim K.S. and Rowlands J.A. "Amorphous and Polycrystalline Photoconductors for Direct Conversion Flat Panel X-Ray Image Sensors" Sensors 2011, **11**(5), pp. 5112-5157.

[4] Yang, J., *X-ray Induced Changes in Electronic Properties of Stabilized Amorphous Selenium Based Photoconductors*, M. Sc. Thesis, University of Saskatchewan, Saskatoon, Canada, 2016.

[5] Tonchev, D. and Kasap, S. O., "Effect of aging on glass transformation measurements by temperature modulated DSC", Materials Science and Engineering: A, **328**(1), 2002, pp. 62-66.

[6] Tonchev, D., Mani, H., Belev, G., Kostova, I. and Kasap, S. "X-Ray Sensing Materials Stability: Influence of Ambient Storage Temperature on Essential Thermal Properties of Undoped Vitreous Selenium", In Journal of Physics: Conference Series, **558**(1), p. 012007, 2014.

[7] Kasap, S. O., "Photoreceptors: The Chalcogenides", In *Handbook of Imaging Materials*. 2nd ed. (Revised and Expanded), Diamond, A. S. and Weiss, D. S., Eds. New York: Marcel Dekker Inc., 2002, pp.333-368.

[8] Lucovsky, G. “Selenium, the amorphous and liquid states”, In *The Physics of Selenium and Tellurium*. Springer Series in Solid-State Sciences, vol. 13. Gerlach, E. and Grosse, P, Eds. 1979, pp. 178-192.

[9] Lucovsky, G. and Galeener, F. L., “Intermediate range order in amorphous solids”, Journal of Non-Crystalline Solids, vol. 35, pp. 1209-1214, 1980.

[10] Adler, D., “Amorphous-semiconductor devices”, Scientific American, **236**(5), pp. 36-49, 1977.

[11] Fritzsche, H., “The Nature of Localized States and the Effect of Doping in Amorphous Semiconductors”, Chinese Journal of Physics, **15**(2), pp. 73-91, 1977.

[12] Kastner, M., Adler, D. and Fritzsche, H., “Valence-alternation model for localized gap states in lone-pair semiconductors”, Physical Review Letters, **37**(22), p. 1504, 1976.

[13] Venables, J. A., Spiller, G. D. T. and Hanbucken, M., “Nucleation and Growth in Thin Films”, Rep. Prog. Phys., vol. 47, pp. 399-459, 1984.

[14] Fulcher, G. S., “Analysis of recent measurements of the viscosity of glasses”, Journal of the American Ceramic Society, **8**(6), pp. 339-355, 1925.

[15] Wong, J., and Angell, C. A., “Glass: structure by spectroscopy”. New York: M. Dekker., p.864, 1976.

[16] V.M. Golschmidt, Skrifter Norske Videnskaps Akad. (Oslo) I. Math.-naturwis. K1, p.7, 1926.

[17] W.H. Zachariasen. “The Atomic Arrangement in Glass”. Journal of American Chemical Society, vol. 54, p.3841, 1932.

[18] Rawson, H., “Inorganic glass-forming systems”, vol. 2. Academic press, 1967.

[19] Gutzow, I., Avramov, I. and Kästner, K., “Glass formation and crystallization”, Journal of Non-Crystalline Solids, **123**(1-3), pp. 97-113, 1990.

[20] Gutzow. I., Kashchiev, D., In *Advances in Nucleation and Crystallization in Glasses*. L.L. Hench and S.W.Freiman, Eds. Columbus, OH: Am. Ceram. Soc., 1971, p. 116.

[21] Minaev, V.S., "Criterion of glass-formation in cha1cogenide systems", Proceedings of International Conference on Amorphous Semiconductors-78. Pardubice, Prague: AS ChSSR Publishers, 1978, pp. 71- 74.

[22] Kaplow, R., Rowe, T. A. and Averbach, B. L., "Atomic arrangement in vitreous selenium", Physical Review, **168**(3), p. 1068, 1968.

[23] Wunderlich, B., "The Nature of the Glass Transition and Its Determination by Thermal Analysis," in Assignment of the Glass Transition. ASTM STP 1249, R. J. Seyler, Ed. Philadelphia: American Society for Testing and Materials, 1994, pp. 17-31.

[24] Seyler, R. J. (1994). *Assignment of the Glass Transition*. ASTM STP 1249, Seyler, R.J. Ed. Philadelphia: American Society for Testing and Materials, 1994, p.14.

[25] Svoboda, R. and Málek, J., "Thermal behavior of Se-rich Ge 2 Sb 2 Se (5− y) Tey chalcogenide system", Journal of Alloys and Compounds, **627**, pp. 287-298, 2015.

[26] Svoboda, R., Kincl, M. and Málek, J., "Thermal characterization of Se–Te thin films", Journal of Alloys and Compounds, **644**, pp. 40-46, 2015.

[27] Elliott, S. R. *Physics of Amorphous Materials*. Longman, Harlow, 1983, pp. 23-52.

[28] Prigogine, I., Defay, R., and Everett, D. H. *Chemical thermodynamics*. vol. 543, London: Longmans, Green, 1954.

[29] Kauzmann, W., "The Nature of the Glassy State and the Behavior of Liquids at Low Temperatures", Chemical Reviews, **43**(2), pp. 219-256, 1948.

[30] Stillinger, F. H., "Supercooled liquids, glass transitions, and the Kauzmann paradox", The Journal of Chemical Physics, **88**(12), pp. 7818-7825, 1988.

[31] Cohen, M. H. and Turnbull, D., "Molecular transport in liquids and glasses", The Journal of Chemical Physics, **31**(5), pp. 1164-1169, 1959.

[32] Fox Jr, T. G. and Flory, P. J., "Second-order transition temperatures and related properties of polystyrene. I. Influence of molecular weight", Journal of Applied Physics, **21**(6), pp. 581-591, 1950.

[33] Doolittle, A. K. "Studies in Newtonian flow. II. The dependence of the viscosity of liquids on free-space", Journal of Applied Physics, **22**(12), pp. 1471-1475, 1951.

[34] Borisova, Z. U. (1981). *Glassy Semiconductors*. New York: Plenum Press, vol. 76.

[35] Mullin, J. W. *Crystallization*. Butterworth-Heinemann. 2001, pp.182-203.

[36] A. Kolmogoroff, Zur Statistik der Kristallisationsvorgänge in Metallen, Izv. Akad. Nauk SSSR Ser. Mat., 1937, Volume 1, Issue 3, pp. 355–359.

[37] Kasap, S. O. and Juhasz, C., "Theory of thermal analysis of non-isothermal crystallization kinetics of amorphous solids", Journal of the Chemical Society, Faraday Transactions 2: Molecular and Chemical Physics, **81**(6), pp. 811-831, 1985.

[38] Dresner, J. and Stringfellow, G. B., "Electronic processes in the photo-crystallization of vitreous selenium", Journal of Physics and Chemistry of Solids, **29**(2), pp. 303IN1305-304IN2311, 1968.

[39] Kim, K. S. and Turnbull, D., "Crystallization of Amorphous Selenium Films. I. Morphology and Kinetics", Journal of Applied Physics, **44**(12), pp. 5237-5244, 1973.

[40] Kim, K. S. and Turnbull, D., "Crystallization of Amorphous Selenium Films. II. Photo and Impurity Effects", Journal of Applied Physics, **45**(8), pp. 3447-3452, 1974.

[41] Turnbull, D., "Under what conditions can a glass be formed?", Contemporary Physics, **10**(5), pp. 473-488, 1969.

[42] Wakasugi, T., Ota, R. and Fukunaga, J., "Glass-Forming Ability and Crystallization Tendency Evaluated by the DTA Method in the Na2O–B2O3–Al2O3 System", Journal of the American Ceramic Society, **75**(11), pp. 3129-3132, 1992.

[43] Hrubý, A., "Evaluation of glass-forming tendency by means of DTA", Czechoslovak Journal of Physics, **22**(11), pp. 1187-1193, 1972.

[44] Nascimento, M. L., Souza, L. A., Ferreira, E. B. and Zanotto, E. D., "Can glass stability parameters infer glass forming ability?", Journal of Non-Crystalline Solids, **351**(40), pp. 3296-3308, 2005.

[45] Kozmidis-Petrovic, A. and Šesták, J., "Forty years of the Hrubý glass-forming coefficient via DTA when comparing other criteria in relation to the glass stability and vitrification ability", Journal of thermal analysis and calorimetry, **110**(2), pp. 997-1004, 2012.

[46] Weinberg, M. C., "An Assessment of Glass Stability Criteria", Physics and Chemistry of Glasses, **35**(3), pp. 119-123, 1994.

[47] Lu, Z. P. and Liu, C. T., "A New Glass-forming Ability Criterion for Bulk Metallic Glasses", Acta materialia, **50**(13), pp. 3501-3512, 2002.

[48] Guo, S., Lu, Z. P. and Liu, C. T., "Identify the Best Glass Forming Ability Criterion", Intermetallics, **18**(5), pp. 883-888, 2010.

[49] Long, Z., Xie, G., Wei, H., Su, X., Peng, J., Zhang, P. and Inoue, A., "On the New Criterion to Assess the Glass-forming Ability of Metallic Alloys", Materials Science and Engineering: A, **509**(1), pp. 23-30, 2009.

[50] Lu, Z. P., Bei, H. and Liu, C. T., "Recent Progress in Quantifying Glass-forming Ability of Bulk Metallic Glasses", Intermetallics, **15**(5), pp. 618-624, 2007.

[51] Mondal, K. and Murty, B. S., "On the Parameters to Assess the Glass Forming Ability of Liquids", Journal of non-crystalline solids, **351**(16), pp. 1366-1371, 2005.

[52] Fan, G. J., Choo, H. and Liaw, P. K., "A New Criterion for the Glass-forming Ability of Liquids", Journal of Non-crystalline Solids, **353**(1), pp. 102-107, 2007.

[53] Zhang, P., Wei, H., Wei, X., Long, Z., and Su, X., "Evaluation of Glass-forming Ability for Bulk Metallic Glasses Based on Characteristic Temperatures" Journal of Non-Crystalline Solids, **355**(43), pp. 2183-2189, 2009.

[54] Yuan, Z. Z., Bao, S. L., Lu, Y., Zhang, D. P. and Yao, L., "A New Criterion for Evaluating the Glass-forming Ability of Bulk Glass Forming Alloys", Journal of Alloys and Compounds, **459**(1), pp. 251-260, 2008.

[55] Du, X. H. and Huang, J. C., "New Criterion in Predicting Glass Forming Ability of Various Glass-forming Systems", Chinese Physics B, **17**(1), p. 249, 2008.

[56] Du, X. H., Huang, J. C., Liu, C. T. and Lu, Z. P., "New Criterion of Glass Forming Ability for Bulk Metallic Glasses", 2007.

[57] Lu, Z. P. and Liu, C. T., "Glass Formation Criterion for Various Glass-forming Systems", Physical Review Letters, **91**(11), p. 115505, 2003.

[58] G.W.H. Höhne, W.F. Hemminger, H.-J.Flammersheim. *Differential Scanning Calorimetry*. (2nd revised and enlarged ed.) Springer, 2003, pp. 1-9.

[59] Kasap, S., Malek J., Svoboda R. "Thermal Properties and Thermal Analysis: Fundamentals, Experimental Techniques and Applications", In *Springer Handbook of Electronic and Photonic Materials*. Kasap S., Capper P., Eds. New York: Springer Science+Business Media, Inc., 2006, pp. 385-408.

[60] Fogal, B. J. "Electronic Transport Properties of Stabilized Amorphous Selenium X-ray Photoconductors", M. Sc. Thesis, University of Saskatchewan, Saskatoon, Canada, 2005.

[61] Siemens.com. Simulation of x-ray spectra: online tool for the simulation of x-ray spectra, 2017. Available: https://www.oem-xray-components.siemens.com/x-ray-spectra-simulation. (Accessed on August 15, 2017).

[62] Reznik, A., Lui, B. J. M., Rowlands, J. A., Baranovskii, S. D., Rubel, O., Lyubin, V., ... and Miyakawa, K., "Kinetics of the photostructural changes in a-Se films", Journal of Applied Physics, **100**(11), p. 113506, 2006.

[63] Walornyj, M. and Kasap, S. O., "X-ray irradiation induced changes in electron transport in stabilized a-Se photoconductors", Journal of Applied Physics, **114**(21), p. 214505, 2013.

[64] Nist.gov. Xcom: National Institute of Standards and Technology, Physical Measurement Laboratory. 2017. Available: https://physics.nist.gov/PhysRefData/Xcom/html/xcom1.html. (Accessed on November 3, 2017).

[65] Barlow, R. J. Statistics: A Guide to the Use of Statistical Methods in the Physical Sciences. vol. 29. West Sussex: John Wiley and Sons Ltd., 1989, pp. 55-58.

APPENDIX A

The absorbed dose calculation for pure a-Se, a-Se:0.5%As and a-Se:6%As-140 ppm Cs films of various thicknesses is calculated, using the mass attenuation and energy absorption coefficients obtained from the NIST website [64] for photon energies generated from a 70 kVp x-ray tube. The mass attenuation coefficients are presented in Figure A.1. Followingly, energy absorption coefficients are presented in Figure A.2. In addition, the exposure rate (R/min) at sample-to-source distance of 9.7 cm is estimated with respect to the extrapolation of measured exposure rates at applicable sample-to-source distances. This estimation can be observed in Figure A.3.

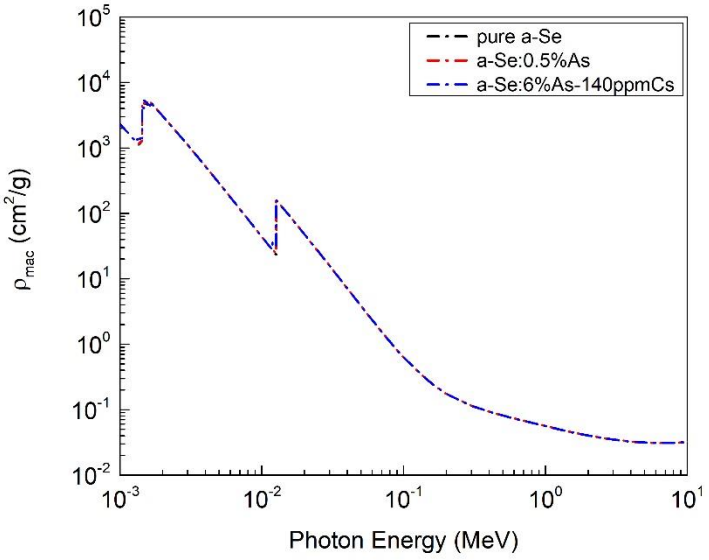

Figure A.1 Mass attenuation coefficients of pure a-Se, a-Se:0.5%As, a-Se:6%As-140 ppm Cs.

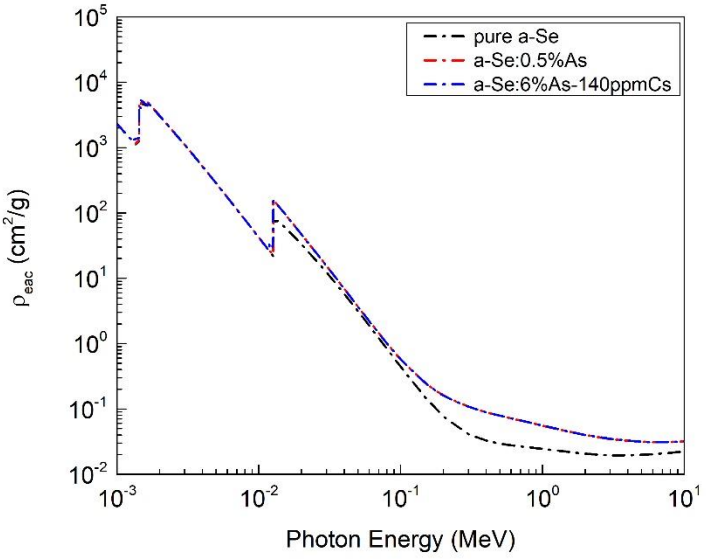

Figure A.2 Energy absorption coefficients of pure a-Se, a-Se:0.5%As, a-Se:6%As-140 ppm Cs.

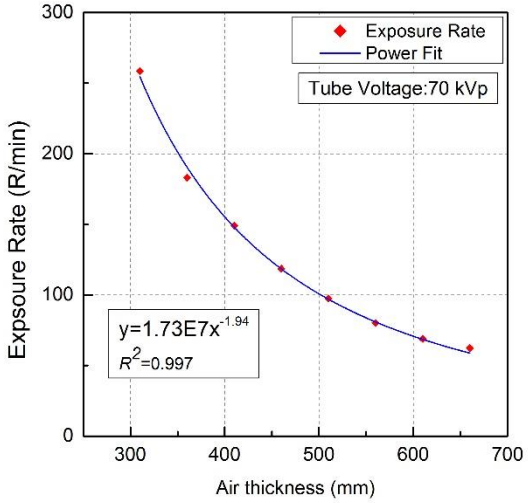

Figure A.3 Extrapolation of measured exposure rate (R/min) values to close sample to source distances.

APPENDIX B

The G-criteria that are considered in this thesis are algebraic combinations of the onset characteristic temperatures. Since each of these temperatures have a certain spread (standard deviation), the criteria will have an overall standard deviation, which is a combination of these standard deviations. In other words, the variance of the G-criteria is related to the onset temperature variances. The standard deviation for G-criteria can be found by referring to the law of combination of errors. [65]

Basically, this law explains how the standard deviation of a function is related to the standard deviations of each independent variable that defines the function. As an example, consider an arbitrary function that is dependent on multiple variables $V(a,b,\ldots,t)$. The quadrature sum of the errors of these variables will give the variance of the function, that is

$$\sigma_V^2 = \left(\frac{\partial V}{\partial a}\right)^2 \sigma_a^2 + \left(\frac{\partial V}{\partial b}\right)^2 \sigma_b^2 + \ldots + \left(\frac{\partial V}{\partial z}\right)^2 \sigma_z^2$$

σ_V^2 being the variance of the function $V(a,b,\ldots,t)$. The positive square root will give the mean standard deviation of this function. Therefore, this law can be applied to find standard deviation of all glass stability criteria. The variance and combination of errors for the glass stability criteria considered in this study can be observed in Table A.1 and Table A.2.

Table A.1 Variance and combination of errors of fundamental glass stability criteria.

Criterion	Variance Abbreviation	Combination of Errors
ΔT_{mg}	$\sigma(\Delta T_{mg})^2$	$\sigma_g^2+\sigma_m^2$
ΔT_{xg}	$\sigma(\Delta T_{xg})^2$	$\sigma_g^2+\sigma_x^2$
α	$\sigma(\alpha)^2$	$\frac{1}{T_m^2}\sigma_x^2+\frac{T_x^2}{T_m^4}\sigma_m^2$
K_T	$\sigma(K_T)^2$	$\frac{1}{T_m^2}\sigma_g^2+\frac{T_g^2}{T_m^4}\sigma_m^2$

Table A.2 Variance and combination of errors of advanced glass stability criteria.

Criterion	Variance Abbreviation	Combination of Errors
K_H	$\sigma(K_H)^2$	$\frac{1}{(T_m-T_x)^2}\sigma_g^2+\frac{(T_m-T_g)^2}{(T_m-T_x)^4}\sigma_x^2+\frac{(T_x-T_g)^2}{(T_m-T_x)^4}\sigma_m^2$
K_W	$\sigma(K_W)^2$	$\frac{1}{T_{mo}^2}(\sigma_{go}^2+\sigma_{xo}^2)+\frac{(T_{xo}-T_{go})^2}{T_{mo}^4}\sigma_{mo}^2$
K_{LL}	$\sigma(K_{LL})^2$	$\frac{1}{(T_g+T_m)^2}\left[\sigma_x^2+\left(\frac{T_x}{T_g+T_m}\right)^2(\sigma_g^2+\sigma_m^2)\right]$
ω	$\sigma(\omega)^2$	$\frac{T_g^2}{T_x^4}\sigma_x^2+\left(\frac{2}{T_g+T_m}\right)^2(T_m^2\sigma_g^2+T_g^2\sigma_m^2)$
β'	$\sigma(\beta')^2$	$\left(\frac{1}{T_m}-\frac{T_x}{T_g^2}\right)^2\sigma_g^2+\frac{1}{T_g^2}\sigma_x^2+\frac{T_g^2}{T_m^4}\sigma_m^2$

ϕ	$\sigma(\phi)^2$	$\left(\left(\frac{T_x}{T_g}-1\right)^{0.143}\left(\frac{T_x-T_m}{T_m-T_g}\right)\left(\frac{1}{T_m-T_g}-0.143\frac{T_x}{T_g(T_x-T_g)}\right)\right)^2\sigma_g^2$ $+\left(\frac{1}{T_m-T_g}\left(\frac{T_x}{T_g}-1\right)^{0.143}\left(1+\frac{0.143}{T_x-T_g}\right)\right)^2\sigma_x^2$ $+\left(\left(\frac{T_x}{T_g}-1\right)^{0.143}\frac{T_x-T_g}{(T_m-T_g)^2}\right)^2\sigma_m^2$
ω_2	$\sigma(\omega_2)^2$	$\left(\frac{T_x}{2(T_x-T_g)^2}-\frac{1}{T_m}\right)^2\sigma_g^2+\left(\frac{T_g}{2(T_x-T_g)^2}\right)^2\sigma_x^2+\frac{T_g^2}{T_m^4}\sigma_m^2$
β	$\sigma(\beta)^2$	$\left(\frac{T_x(T_m-T_g)+2T_xT_g}{(T_m-T_g)^3}\right)^2\sigma_g^2+\left(\frac{T_g}{(T_m-T_g)^2}\right)^2\sigma_x^2$ $+\left(\frac{2T_xT_g}{(T_m-T_g)^3}\right)^2\sigma_m^2$
γ_m	$\sigma(\gamma_m)^2$	$\frac{1}{T_m^2}\sigma_g^2+\frac{4}{T_m^2}\sigma_x^2+\frac{(2T_x-T_g)^2}{T_m^4}\sigma_m^2$
ξ	$\sigma(\xi)^2$	$\left(\frac{1}{T_x}-\frac{1}{T_m}\right)^2\sigma_g^2+\left(\frac{T_g}{T_x^2}\right)^2\sigma_x^2+\frac{T_g^2}{T_m^4}\sigma_m^2$

APPENDIX C

Error distribution of advanced glass stability criteria obtained in each experimental stage is presented below. Plots associated with pure a-Se and a-Se:0.5%As films are introduced separately.

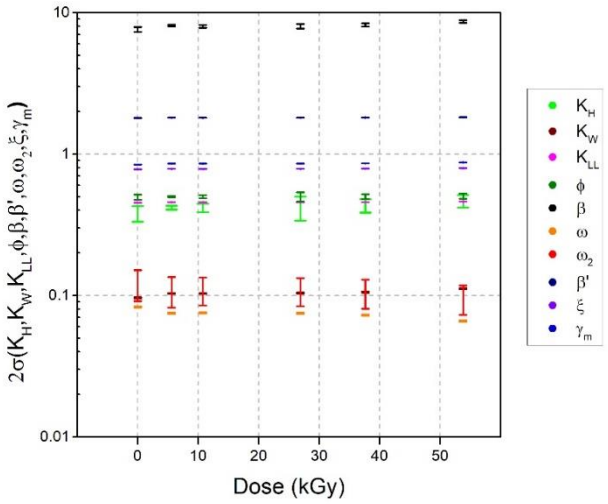

Figure C.1 2σ distribution of x-ray irradiated pure a-Se samples.

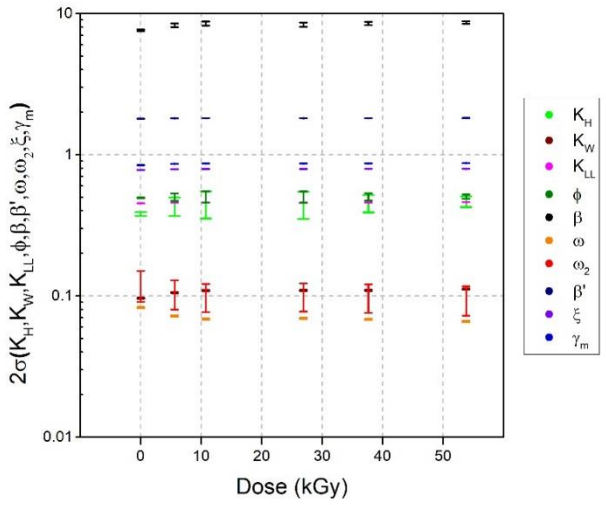

Figure C.2 2σ distribution of x-ray irradiated pure a-Se samples with 5-hour rest at 295 K.

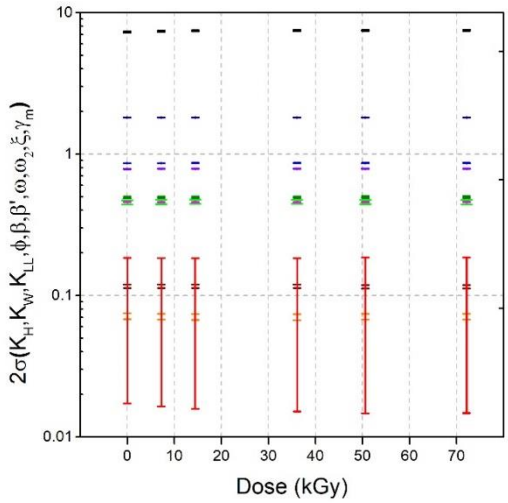

Figure C.3 2σ distribution of x-ray irradiated pure a-Se samples with 5-hour rest at 308 K.

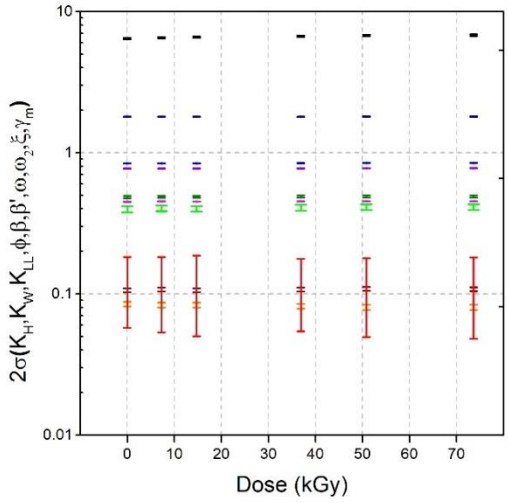

Figure C.4 2σ distribution of x-ray irradiated pure a-Se samples with 5-hour rest at 328 K.

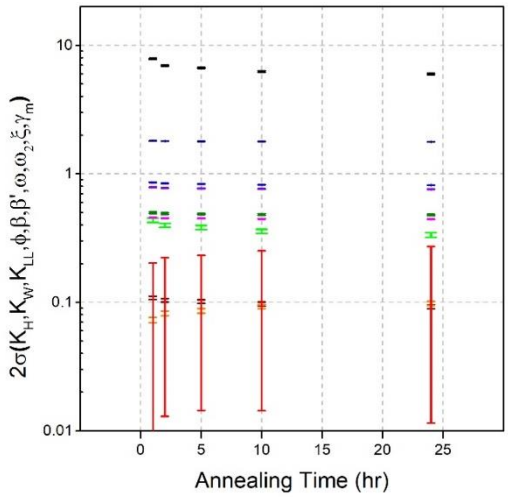

Figure C.5 2σ distribution of equally x-ray irradiated pure a-Se samples with extending resting periods at 308 K.

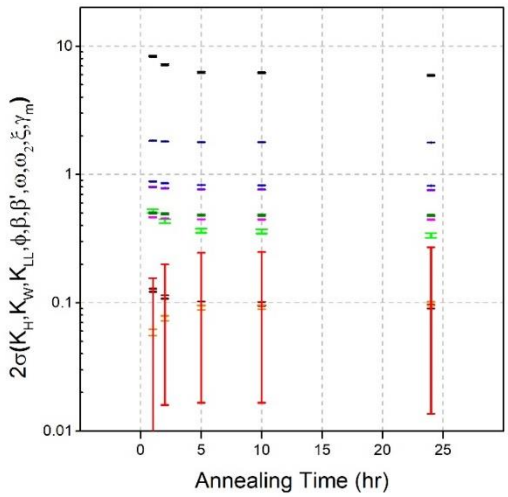

Figure C.6 2σ distribution of equally x-ray irradiated pure a-Se samples with extending resting periods at 328 K.

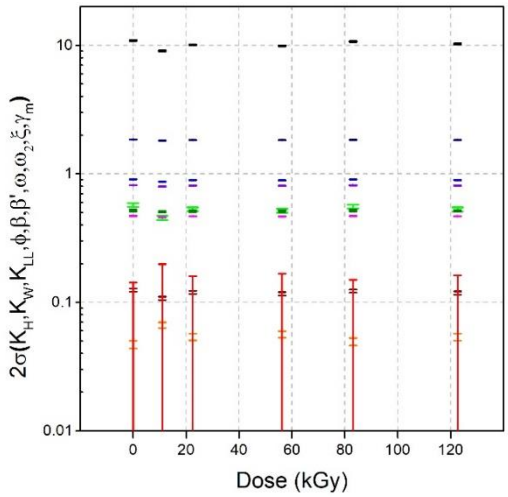

Figure C.7 2σ distribution of x-ray irradiated a-Se:0.5%As samples.

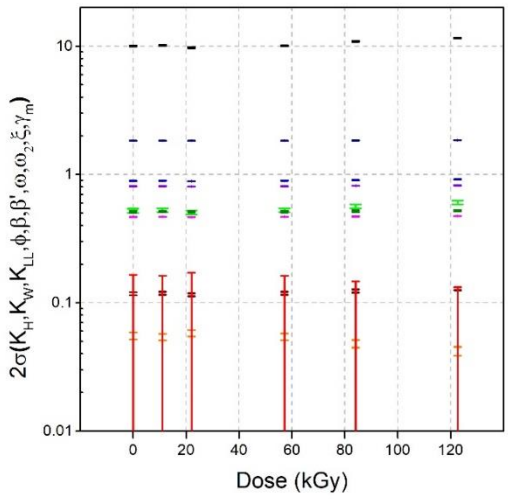

Figure C.8 2σ distribution of x-ray irradiated a-Se:0.5%As samples with 5-hour rest at 295 K.

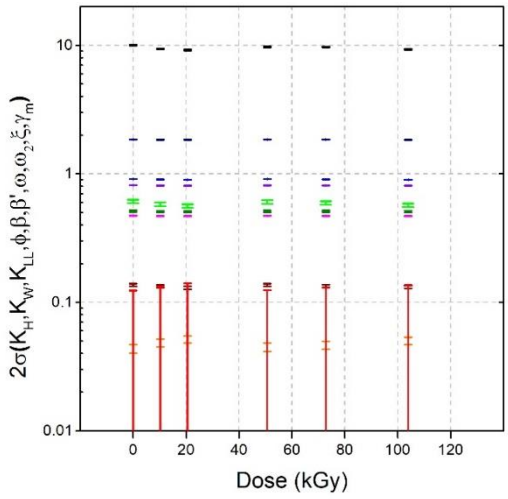

Figure C.9 2σ distribution of x-ray irradiated a-Se:0.5%As samples with 5-hour rest at 308 K.

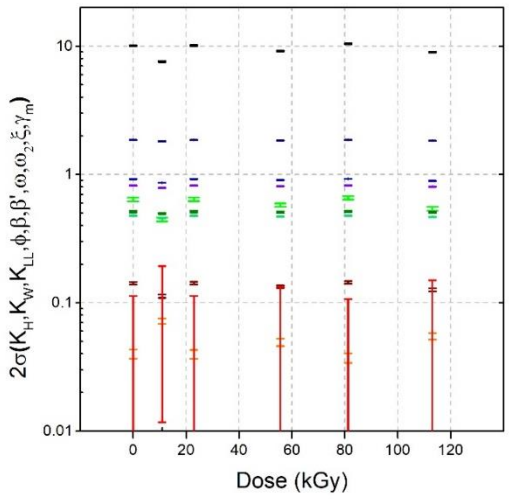

Figure C.10 2σ distribution of x-ray irradiated a-Se:0.5%As samples with 5-hour rest at 328 K.

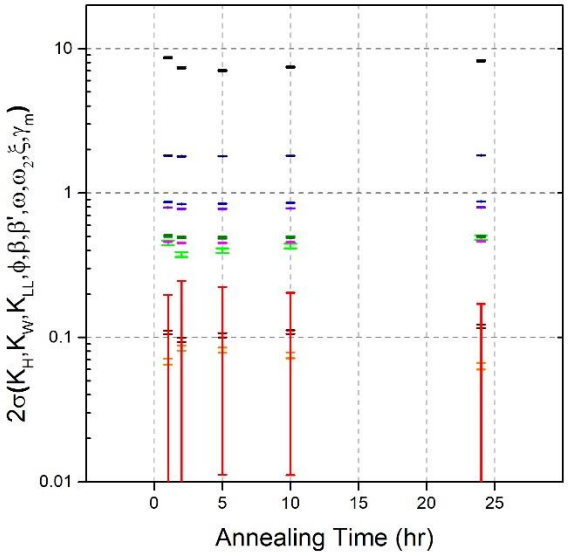

Figure C.11 2σ distribution of equally x-ray irradiated a-Se:0.5%As samples with extending resting periods at 308 K.

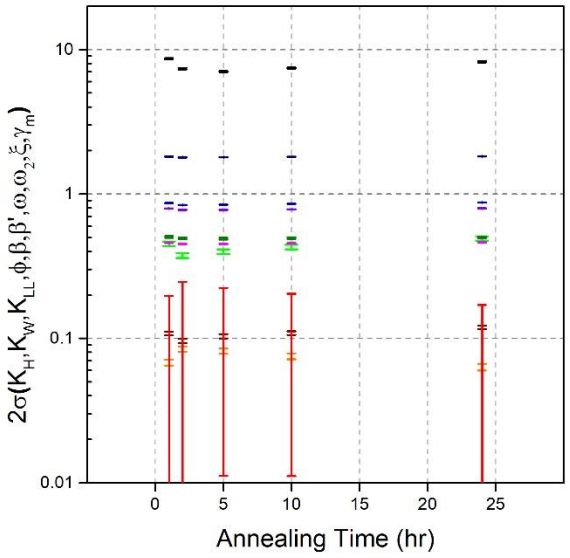

Figure C.12 2σ distribution of equally x-ray irradiated a-Se:0.5%As samples with extending resting periods at 328 K.